2024-01-19

Development of a Redox Functional Nucleic Acid Integrated Electrochemical Biosensors for Wearable Applications

Janghorban, Mohammad

UNIVERSITY OF CALGARY

Development of a Redox Functional Nucleic Acid Integrated Electrochemical Biosensors for Wearable Applications

by

Mohammad Janghorban

A THESIS

SUBMITTED TO THE FACULTY OF GRADUATE STUDIES

IN PARTIAL FULFILMENT OF THE REQUIREMENTS FOR THE

DEGREE OF MASTER OF SCIENCE

GRADUATE PROGRAM IN BIOMEDICAL ENGINEERING

CALGARY, ALBERTA

JANUARY, 2024

Abstract

The corrugated nature of biosensor surfaces holds paramount significance in increasing their efficiency. This investigation scrutinizes the electrochemical performance of wrinkled and flat sensor surfaces. The textured surface is embedded with wrinkles about 1 μm in thickness and a wavelength of 32 μm.

Testing the biosensors with a 1μM cortisol sample, the wrinkled electrode produced a fold change of 1.84±0.65 compared to the planar electrode, which produced a fold change of -0.11±0.07. Such observations underscore the heightened signal augmentation of the textured design. Additionally, specificity tests for the cortisol concatenated aptamer showed no false positive signal when tested with other interferent biomarkers.

Initial trials utilizing cortisol mixed artificial sweat and DI samples demonstrated its performance in cortisol detection with an LOD of 59 nM in artificial sweat. The assay's reusability was tested through multiple incubations with a standard cortisol solution, indicating consistent performance over three cycles. Stability trials in artificial sweat revealed a stable initial response, maintaining stability for up to six hours before a notable decline after 72 hours. However, further experiments may be required to prepare the device for more practical applications. Attempts to regenerate the biosensor using UV light were unsuccessful, and further on-body and human sweat tests showed reduced effectiveness compared to laboratory conditions.

While the initial development, optimization and testing of the biosensor achieved some successes, it also highlighted several areas requiring refinement, including but not limited to electrode design, standardization of testing procedures, and optimization of the heating process to enhance the functionality and reliability of the biosensor for its intended applications.

Acknowledgements

I would like to extend my heartfelt gratitude to my mentor, Dr. Richa Pandey, for opening the door to this incredible experience and continually guiding and supporting me throughout this venture. This dissertation and the entirety of my graduate studies would not have seen the light of day without the instrumental assistance and unwavering support from my supervisor.

I'd also like to express my gratitude to Irvyne Aradnas, Karem Malaeb, and Habiba Abuelazm. Their contributions as undergraduate students have been indispensable in progressing this thesis. Additionally, Dr. Aditya Nittala and Dr. Kartikeya Murari deserve a special mention for their expert guidance, particularly in the domains of electronics and app development.

I am also immensely grateful to our colleagues at Microsystems hub, for letting me use their incredible facility and work on my research. I must also acknowledge the insights and suggestions of my supervisory committee, Dr. Colin Dalton, and Dr. Jinguang Hu.

I am thankful to the entire team at the Department of Biomedical Engineering for their consistent understanding and support. Above all, my profound gratitude goes to my family for their unwavering faith in me, their constant backing, and their significant role in shaping who I am today.

Dedication

To my beloved parents,

For the countless times you've stood by me, the countless moments you've believed in my vision – my deepest gratitude. Your steadfast encouragement and love have been the pillars that propelled me forward, allowing me to pursue aspirations without restraint. You've given me the freedom to envision boundlessly. Thank you for letting me dream free.

Table of Contents

List of Figures

List of tables

List of abbreviations

ADC	analog to digital controller
ATP	adenosine triphosphate
Au	gold
CATCH	cortisol apta-watch
CAPTAIN PATCH	concatenated aptamer integrated skin patch
CONCAPTAMER	concatenated aptamer
CV	cyclic voltammetry
DAC	digital to analog controller
DNA	deoxyribonucleic acid
DPV	differential pulse voltammetry
EIS	electrochemical impedance spectroscopy
ELISA	enzyme-linked immunosorbent assay
FET	field effect transistor
GPIO	general-purpose input-output
GOx	glucose oxidase
MB	methylene blue
NA	nucleic acid
OPAA	organophosphorus acid anhydrolase

PEDOT-PAN NF	poly(3,4-ethylenedioxythiophene) polyacrylonitrile nanofiber
POC	point-of-care
PTFE	polytetrafluoroethylene
PVDF	polyvinylidene fluoride
RNA	ribonucleic acid
SELEX	systematic evolution of ligands by exponential enrichment
SWV	square wave voltammetry
UV	ultraviolet
VECARE	venous ulcer care device

Chapter 1 : Thesis Prelude - A Glimpse into Wearable Biosensor Innovations

Recent advances and growth in wearable tech have sparked a lot of attention in the healthcare and diagnosis fields. The variety of wearable health trackers is growing, including tools that can monitor many physical and chemical health markers, like pulse and blood sugar. One key focus in this landscape is keeping an eye on cortisol levels in our bodies, since it plays a big role in our daily activities and how we manage stress. If cortisol levels aren't balanced, it could lead to severe mental health issues, like depression, and anxiety.

The central goal of my thesis revolves around creating a new wearable tool to easily check cortisol levels. The study aims to design a special "redox modified concatenated aptamer integrated skin Patch," called the Captain Patch. This patch stands out as it's the first to use a redox modified concaptamer approach for cortisol tracking in wearable tools. The design for the utilized electrodes cues from the unique patterns of human skin. This design assists with cortisol detection, even if it's present in tiny amounts in synthetic sweat.

What makes the Captain Patch special is the unique combination of redox modified concaptamers and textured gold electrodes which has been made with a lot of attention to make the device work better. Its design, along with chemicals that can undergo redox reactions, looks to solve some of the current hurdles in wearable health trackers.

This new device has the potential to improve how we monitor health in real-time and could play a role in spotting and treating various health issues early on, marking a new era in wearable health tech. For context, much of the upcoming sections is drawn from a previous review article I authored, which played a pivotal role in preparing the themes and topics here. The necessary permissions were secured to repurpose content from this source [1].

1.1 Introduction

Wearable sensors are "on-body" devices that capture vital human health data (electrical, electrophysiological, and biochemical). Their popularity is evidenced in a recent increase in usage, driven by customers' growing desire to monitor their health and vital signs. These wearable devices have the potential to enable preventive, time-sensitive, and patient-centered decision-making, particularly in remote communities, by providing useful health data on the early onset and progression of infections, mental health and neurological disorders, rare and chronic diseases, and so on [2]. Wearable sensing offers a wide range of on-field uses, including monitoring the health of military troops in difficult-to-reach places, astronauts on space missions, concentrated people in distant areas, healthcare professionals, and the general public under endemic or pandemic conditions. The use of modern medical technology to generate a thorough biochemical profile of patient samples demands skilled personnel, complicated operations, expensive equipment, and availability to reliable energy. Many of these problems are mitigated by point-of-care (POC) diagnostic devices, which allow for quick and easy operation at the moment of need [3]. However, many applications, such as outbreak screening, monitoring during surgery, and biohazard detection, need continuous and aseptic monitoring to eliminate the chance of infection transmission or sample contamination [4]. Wearable biosensors have the potential in these cases to be swiftly adapted for a specific target, such as viruses or bacteria, and easily changed into "easy to wear" technology [4]. Most commercially feasible wearable devices may now evaluate physical indicators (e.g., temperature, activity, tension, and so on) as well as electrophysiological activities (e.g., electroencephalography, electrocardiography, electromyography, and so on) [5]. They do not,

however, give more detailed information on users' health state at the biomolecular level, such as nutrients, hormones, proteins, tiny molecules, enzymes, and so on [6]. As wearable technology becomes more common, the development of specialized applications to construct wearable devices with molecular diagnostics capacity is required. Using diverse sensing techniques, these biosensors can detect molecular analytes in bodily fluids such as perspiration [7], interstitial fluid [8], saliva [9], and tears [10]. The device must include biorecognition components that are sensitive, specific, stable, consistent, and easy to functionalize in order to act as a wearable biosensor. Wearable biosensors are now confined to protein-based (enzymes and antibodies), chemical sensing, or diabetes (glucose) control [11]. These sensors' wearable uses need their long-term continuous use in varying temperatures, pH, and environments. For example, enzyme-based wearable biosensors suffer from poor stability due to reaction byproducts and temperature change, making continuous reliable signal production difficult [12]. Nucleic acids (NAs) have lately acquired favour in wearable biosensors as biological recognition components. NA-based biosensors are capable of binding to and hybridizing with target biomarkers (strand hybridization, displacement). NAs are more scalable than protein-based biorecognition elements because their chemical synthesis does not require any host animals, can overcome multi-step processing requirements due to their programmability, are compatible with a wide range of conjugation chemistries, and have the structure switching ability to process reversible signal generation for continuous monitoring [13]. This procedure does not need prior understanding of the molecular target's interactions with the sequences. This streamlines molecular diagnostic assay development by combining biomarker identification and probe creation into a single stage [13]. To address some of these issues in protein-based biosensing approaches, there has been a growing interest in combining NA, particularly Aptamers, with wearable devices, which has encouraged wearable biosensor researchers to investigate novel NA-integrated assays for detecting non-

invasive health-related biomarkers [14]. When combined with other transduction mechanisms, NA-based biosensors have outstanding analytical performance, allowing the development of reagent-free and wash-free tests. However, comprehending their use in continuous and wearable applications remains difficult.

Commercial biowearables can already measure glucose [11], ketones [15], and lactate [16] utilizing protein-based biorecognition reagents such as glucose oxidase enzymes, lactate oxidase, and beta-hydroxybutyrate. To realize the full potential of biowearables, critical enabling technologies such as stable/reversible chemical or bioaffinity reagents , and building high surface-to-volume ratio electrodes to increase signal transduction must be developed [17]. Nonetheless, aptamers have showed tremendous promise in overcoming some of these issues. Aptamer-based wearable biosensors are emerging as strong candidates in offering better analytical and clinical performance for the non-invasive detection of cortisol. Aptamers, which are short strands of DNA or RNA, outperform protein-based biorecognition reagents in terms of cost, stability, and ease of production [18]. Furthermore, the ability to identify lower biomarker concentrations is hampered by strong background signal (noise) caused by the greater footprint of these protein-based biorecognition agents contributing to nonspecific absorption. Aptamers have low molecular weight and size. This results in a more accurate target interaction, resulting in higher molar target binding densities and lower background signals. They are easily modifiable using functional groups to improve sensitivity, selectivity, and stability [19–21]. Aptamers are used as affinity probes on electrochemical [22–24] or field effect transistor-based devices [25–27], where they interact with cortisol and generate a resistance change corresponding to passivation of the electrode surface that is proportional to cortisol concentration. However, there are obstacles to creating a direct redox-based aptamer assay for cortisol detection that is combined with a wearable biosensing motif.

Furthermore, the electrode surfaces on which the aptamer is immobilized play an important role in improving the efficacy of wearable biosensors [28–30]. It is possible to increase the overall performance of the biosensor by changing the surface of the electrode, increasing the loading density of biorecognition reagent on electrodes for enhanced interaction with analytes [29]. To obtain high analytical sensitivity in biosensors, many new solutions have been utilized, including the utilization of nanoparticles [21,31], hierarchical [17,29,30] or templated nanostructures or template based surface texture [32,33]. A two-step technique of merging high surface to volume ratio and redox active biorecognition reagents such as redox aptamers has the potential to ease wearable biosensor performance problems.

Delving into the intricacies of aptamer-enhanced wearable biosensors necessitates a solid grounding in the subject. With this perspective in mind, the following sections introduce fundamental concepts, paving the way for a comprehensive exploration of wearable technology enriched with NAs.

In the ensuing chapter, we will navigate through the advancements of bioreceptor-infused wearable biosensors. We'll traverse through their foundational methods, spotlighting the best practices and materials in the process. As we delve into NA receptors, their crucial role in elevating the device capabilities will be brought to the limelight, emphasizing the merit of NAs, specifically Aptamers. The mechanisms that turn biological signals into comprehensible data will also be expounded upon.

1.2 Essentials of Biomolecular Recognition

Wearable health-monitoring devices have become instrumental in the age of personalized medicine. Integrating various biorecognition agents – from traditional enzymes and antibodies to the innovative NAs – is the essence of these groundbreaking tools. Each of these recognition elements has its strengths and challenges when applied in real-world scenarios. For instance, while enzymes and antibodies have been the stalwarts of sensing, they come

with their own set of limitations, like stability and specificity concerns. This is where the versatility of NAs and aptamers shines, positioning them as formidable contenders in this arena. Their ability to be tailored for specific targets, combined with their relative ease of production, signifies a bright future for wearable health devices [13]. At the heart of a wearable biosensor's sensing layer is the bio-recognition component. This biological element, which interacts with the analyte of interest, plays a pivotal role in dictating key performance indicators like specificity and sensitivity. This biological interaction is then converted into a measurable signal by the transducers present in the sensing layer [34]. As mentioned before, traditional probes used in wearable biosensing research are enzymes and antibodies [11,35]. Antibodies are naturally occurring proteins whose "Y" structure allows them to bind specifically and sensitively to their target antigens. However, the processes of discovering, isolating, and purifying these antibodies involve slow and costly procedures, which includes injecting antigens into laboratory animals like rabbits, mice, and goats [36].

Monoclonal antibodies offer the advantage of binding specifically to a precise site on the target, which is key to highly specific and sensitive detection. However, when monoclonal antibodies are produced using hybridomas, there is a risk of genetic mutation, which can result in batch-to-batch variations over time. Specifically, these mutations may alter the binding site or paratope of the antibodies, affecting their specificity [35]. In addition, the orientation of the target site on a functionalized antibody within a wearable biosensing platform is crucial to the platform's performance, as incorrect orientation could prevent target binding and decrease sensitivity [37].

Enzymes, another type of naturally occurring protein, are also employed as bio-recognition elements in wearable biosensors [11]. Enzymes are catalytic proteins that have been widely used in wearable biosensors due to their longevity, ease of functionalization on the sensor, and target analyte specificity [38]. At present, microbial enzymes are most commonly

synthesized for wearable biosensing applications through controlled fermentation. However, long-term stability without loss of functionality due to degradation is a primary concern when working with enzymes. Hence, stabilizing the enzymes is necessary to extend the overall shelf life and operational stability of the biosensor. For instance, alcohol oxidase, which is used to detect alcohol concentrations in sweat or interstitial fluid when integrated with wearable biosensors, operates optimally at a basic pH (8–10) [39], while sweat and interstitial fluid are slightly acidic to neutral [40]. This pH mismatch can result in decreased enzyme activity in wearable biosensing applications. Similarly, body temperature fluctuations can affect enzyme activity by impacting their activation energy or thermal stability. An example of this is organophosphorus acid anhydrolase (OPAA), which is used to detect toxic organophosphorus compounds [41]. One of the main issues with OPAA is that its optimal operating temperature is 45 °C, significantly higher than human body temperature, thus limiting its practical use in wearable biosensors. Moreover, the sample environment must be considered to maintain the enzyme's optimal catalytic activity in biosensors. For example, the enzyme glucose oxidase (GOx), used in glucose wearable biosensors—one of the most clinically successful wearable biosensors for detecting interstitial fluid glucose levels [42] —is affected when co-produced hydrogen peroxide for oxidase-based enzymes weakens enzyme structures. These enzymes can deactivate if applied incorrectly [12].

For wearable biosensors to have clinical relevance, they must utilize biorecognition elements that are sensitive, specific, stable, consistent, and easy to produce [43]. Lately, the use of NAs as biological recognition layers in wearable biosensors has gained popularity [44]. These offer benefits like those of enzymes and antibodies, with the added advantage of versatility in customization and biological specificity [45]. NAs don't require a host animal for production but can be created in vitro by adding mononucleotides to a 3′-hydroxyl end of the polynucleotide chain [46]. This results in faster production times as it is not dependent on the

host animal's immune system, and it is easier to modify their structure without concerns about genetic drift [47]. Commonly used NAs in wearable biosensors are DNAs, RNAs, and aptamers [45].

1.2.1 Aptamers

Among the various NA-based biorecognition elements, aptamers are drawing considerable attention in the development of wearable biosensors [17,22,48–50]. Aptamers are short, single-stranded functional oligonucleotides that can bind to a wide range of targets, such as cells, proteins, nucleic acids, ions, and other molecules [18].

The process of developing aptamer sequences is carried out by systematic evolution of ligands by exponential enrichment (SELEX), a repetitive and in vitro selection method that sequentially optimizes random sequence libraries until a sequence with high affinity for a particular target is achieved [47]. This cost-efficient technique allows for the creation of an aptamer probe that exhibits high affinity and specificity for any analyte, with excellent batch-to-batch consistency, and without prior knowledge about the target. Aptamers can be readily chemically modified and integrated with various sensing mechanisms [45].

The interaction between an aptamer and its target involves a combination of non-covalent forces such as hydrogen bonds, electrostatic interactions, van der Waals forces, and hydrophobic interactions. These forces facilitate a snug fit between the aptamer and its biomarker, leading to stable complex formation. This binding is not just a physical alteration; it often leads to functional changes. For instance, in therapeutic applications, this change might activate or inhibit a biological pathway. In biosensing applications, the conformational change can be used to generate a measurable signal, such as a change in fluorescence or electrical conductivity. Moreover, the conformational change enhances the selectivity and specificity of the aptamer-biomarker interaction. The unique three-dimensional structure formed by the aptamer upon binding ensures that it interacts strongly with its specific target

while minimizing non-specific interactions with other molecules. This specificity and selectivity are fundamental to the effectiveness of aptamers in various applications, including therapeutic interventions and biosensing technologies.

Dissimilar to DNA/RNA-based sensors, which rely on partial or full hybridization with the target, aptamers undergo a three-dimensional structural shift when binding to their target through intermolecular interactions [34]. This makes the aptamer-target interaction akin to that of antibody-antigen. As the aptamer field continues to evolve, a noteworthy innovation has emerged in the form of concatenated aptamers (concaptamers). Essentially, these are sequences of aptamers lined together, designed to have numerous recognition sites for their respective targets. By utilizing the inherent advantages of concaptamers, it's theorized that we can achieve a greater density of target engagement than what's typically seen with the singular attachment points of traditional aptamers [51]. This potential increase in detection precision and clarity could be a game-changer for wearable biosensor technology.

In general, for wearable biosensors, aptamer-based bioreceptors are the preferred capture probes over antibodies because of their smaller size, allowing for a high surface density. Furthermore, the interaction with the target may alter the distance between the target and the sensing platform, resulting in a stronger detection signal due to their conformational change [51].

Wearable technologies are often subject to harsh temperatures and mechanical forces. Therefore, sensing probes must maintain their structural integrity. Aptamers offer better chemical, thermal, and structural stability than antibodies [23,52]. Moreover, aptamer-target affinity remains more consistent over the storage period, leading to longer shelf lives for aptamer-based wearable biosensors [23,53].

Specifically, in wearable biosensing, aptamers are most commonly used to measure cortisol concentrations in biological fluids such as saliva or sweat [22–24,54–56]. Wang et al. in a recent study found a new DNA aptamer sequence for cortisol binding that had a detection limit of 1 pM and a dissociation constant of 500 nM. The aptamer, discovered from an N36 random oligonucleotide library by SELEX, was based on the elution of cortisol-bound sequences versus capture strand binding. The aptamer was able to detect physiologically relevant cortisol concentrations in saliva and sweat and demonstrated selective binding to cortisol over other biologically relevant non-target molecules such as corticosterone, testosterone, and aldosterone. Combined with the wearable biosensor's ability to detect physiological range fluctuations in cortisol concentration, the sensor shows potential for real-time monitoring of cortisol levels in saliva and sweat [54]. Other analytes that wearable aptamer-based biosensors detect using structure switching and surface charge alteration-based transduction include cytokines [53], serotonin [52], and dopamine [52].

In addition to aptamers, other functional NAs like DNAzymes [57] and ribozymes [58] hold promise to be incorporated into wearable biosensing, following their success in in-vitro and precision diagnostics. Importantly, the binding of aptamers to their targets can be reversed, making aptamer-based sensors reusable and more cost-effective [59].

Table 1:Summary of studies incorporating aptamers as bioreceptors into a wearable platform.

Sensing material	**Target analyte**	**Transduction method**	**Limit of Detection***	**References**
In_2O_3 FET on polyamide with tape-based microfluidics	Cortisol	FET	1 pM	[54]
Gold modified electrodes with Graphene-gold nanoparticles with SU-8 microfluidics	IL-6,	Electrochemical	10 ng mL^{-1} (4.76×10^{-1} nM)	[60]
	IL-8,		10 ng mL^{-1}(1.18 nM)	

	TGF–β1,		50 pg mL $^{-1}$(1.13 pM)	
	Staphylococcusaureus		1 ×10^{8} CFU mL^{-1}	
Graphene—Based FET on ultrathin Mylar	TNF-α	FET	2.75 pM	[48]
	IFN-γ		2.89 pM	
Graphene-Based FET on SiO_2 Coated PEN	TNF-α	FET	26 pM	[49]
Graphene-Nafion composite film	IFN-γ	FET	740 fM	[53]
ZnO on microporous hydrophilic membrane	Cortisol	Electrochemical	0.11 μM	[23]
ZnO coated nano-porous polyamide	Cortisol	Electrochemical	2.7 nM	[22]
PDMS@CNC/CNT	Cortisol	Electrochemical	5 nM	[24]
In_2O_3 nanoribbons on PET	Serotonin	FET	10 fM	[52]
	Dopamine			
PEDOT-PAN nanofibers FET on PET	Cortisol	FET	10 pM	[27]
MeHA functionalized hydrogel microneedles	Glucose	Optical	1.1 mM	[19]
	ATP		0.1 mM	
	L-tyrosinamide		3.5 μM	
	thrombin		25 nM	
*To determine the molarity, first divide the concentration (in g/ml) by the molecular weight for cortisol (362.46 g/mol). Next, multiply the result by 10^{3}. The resulting value represents the molarity in M (moles per liter).				

1.2.2 Concatenated aptamers

Concatenated aptamers, a particularly intriguing type of aptamer-based structures, have garnered significant interest. Initially conceptualized by Shi et al., this concept was demonstrated with a pentavalent RNA aptamer targeting the splicing regulatory protein B52 [61]. Based on the first patent's definition, a concaptamer aptamer is a construct comprising two or more aptamer motifs, which may be identical or different, and may include additional structural elements or functional groups. With their inherent versatility, Nucleic acid aptamers

lend themselves to being used as modular building blocks. These can be assembled in various configurations to create structures with specific functions [61]. Aptamers can be chemically modified and conjugated using numerous methods, providing a comprehensive toolkit for designing customizable aptamer-based constructs tailored to specific applications. Simply linking identical aptamer motifs can significantly enhance a construct's avidity through multiple binding sites [61]. Conversely, combining different aptamer motifs opens up possibilities for creating multifunctional molecules. These molecules can form the foundation for biosensors capable of detecting multiple analytes, targeted therapeutics for specific proteins or cells, cell-specific immunomodulators, or theranostic (therapeutic and diagnostic) agents. Over the past decade, the field of aptamer research, particularly in the development of concatenated aptamers, has seen growing interest [61].

In designing concatenated aptamers, a crucial aspect is how individual aptamer units are linked together. The specific method of connection depends on the nature of the aptamer-target interaction and the intended function of the multi-aptamer construct. Typically, aptamer domains are covalently joined, though end-to-end fusion without linkers is less common. The use of oligonucleotide linkers is a standard approach, given the nucleic acid nature of aptamers. By altering the length and sequence of these linkers, one can manage the spacing between aptamers and their interactions. For independent functioning of each aptamer unit, 'neutral' linkers like oligo(A), oligo(U), or oligo(T) are employed. The length of these neutral linkers can range from 3 to 50 nucleotides, with 15–20 nucleotides being typical.

An alternative, albeit more complex, method for designing linkers involves additional SELEX of the linker sequence. The SELEX process involves various combinations of aptamer domains and randomization of the linker. After multiple rounds of selection, the resulting molecules retain the binding activities of all individual components within the multivalent

construct. Initially developed for bivalent aptamers, this strategy could theoretically be extended to create more complex multivalent molecules with specific sets of activities [61].

In discussing concatenated aptamers, it's important to consider their avidity when binding to multivalent targets, such as multimeric proteins or proteins with high surface density on cells. Avidity refers to the cumulative strength of multiple binding interactions, as opposed to affinity, which describes the interaction of one aptamer domain with its binding site. Avidity, measured by the dissociation constant of the fully bound aptamer-target complex, can significantly surpass the affinities of individual aptamers, especially when the target has multiple binding sites for aptamers.

For certain applications, it's necessary to activate aptamer modules sequentially rather than simultaneously. In such cases, structure-switching aptasensors are designed. This involves incorporating one aptamer sequence into another, connecting two aptamer domains with a short unstable stem. Alternatively, aptamers sharing a linker sequence can undergo structural rearrangements upon binding, enabling the second aptamer to adopt an active conformation.

1.2.3 Aptasensors using concatenated aptamers

A common application for aptamers in analytical contexts is the combination of two aptamers: one for capturing an analyte and the other for binding to a reporter group. The critical aspect of these bifunctional aptamer designs is that the reporter group only binds after the analyte has been captured. Typically, these aptameric sensors, also known as structure-switching aptasensors, are designed by connecting two independent aptamer units with a short, unstable stem. The binding of the analyte stabilizes the stem, thereby enabling the signaling aptamer to bind to a dye or other molecule crucial for detection.

An example of this approach was the development of sensors for three different targets (ATP, theophylline, FMN) as demonstrated in a specific study. These sensors included an aptamer

for the malachite green (MG) dye, which significantly enhances its fluorescence upon binding with the aptamer. All aptamers maintained their original target affinities. Notably, the ATP sensor was chimeric, combining a DNA aptamer for ATP with an RNA aptamer for MG, while the other two sensors were entirely RNA-based, suggesting their potential for expression within living cells [62].

1.2.4 Redox molecules as reporters

Linking electrochemical signaling with alterations in aptamer conformation offers multiple benefits in analytical sensing. Primarily, as the redox-active molecule is covalently bonded to the nucleic acid aptamer, the variation in the electrochemical signal is exclusively due to the target-induced structural transformation of the aptamer. Such a signaling method is more resistant to signals generated from non-specific interactions between elements in the matrix and the electrode surface.

E-AB sensors predominantly utilize reversible redox couples like methylene blue or ferrocene as their redox-active tags, with each molecule presenting its own set of pros and cons. The binding of methylene blue to a nucleic acid, typically one with a 3′-amine terminus, is achieved through a reaction with n-hydroxysuccinimide ester-activated methylene blue. On the other hand, ferrocene is attached using a similar approach with its carboxylic acid n-hydroxysuccinimide ester [63].

Both molecules are appealing for signaling due to their reversible electrochemical behaviors and straightforward conjugation chemistry. Methylene blue, which undergoes a reversible two-electron, one-proton reduction, is extensively used. Nevertheless, its redox reaction is pH-sensitive, necessitating caution in environments with variable or unknown pH levels. Ferrocene, conversely, partakes in a one-electron oxidation to become ferrocenium. However, ferrocenium is susceptible to nucleophilic attacks, even from mild nucleophiles like chloride, potentially leading to detachment from the nucleic acid. This poses a limitation in

physiologically relevant solutions, which can be mitigated by using buffers free of strong nucleophiles. Additionally, Ferapontova et al. highlighted challenges in using ferrocene in physiological matrices. Their findings indicate that the oxidation of ferrocene occurs at a positive potential relative to the electrode's point of zero charge, which can encourage nonspecific protein adhesion [63].

1.3 Requirements for a Transduction Mechanism

In wearable biosensors, a transducer is employed to transform the biorecognition occurrence into a legible signal and information relevant to clinical practice using a variety of physical techniques. Broadly, the transduction mechanisms in a wearable biosensor can be classified into optical, electrical, and electrochemical (Figure 1a–c) [22,60,64].These techniques offer the advantages of straightforward operation via miniaturization, immediate results, and low energy consumption [65–67]. The biochemical signal generated from the interaction between the biorecognition element (NA) and the target analyte is typically quite weak. Therefore, an effective signal transduction strategy is crucial for converting this faint signal into amplified strength with a high signal-to-noise ratio [68].

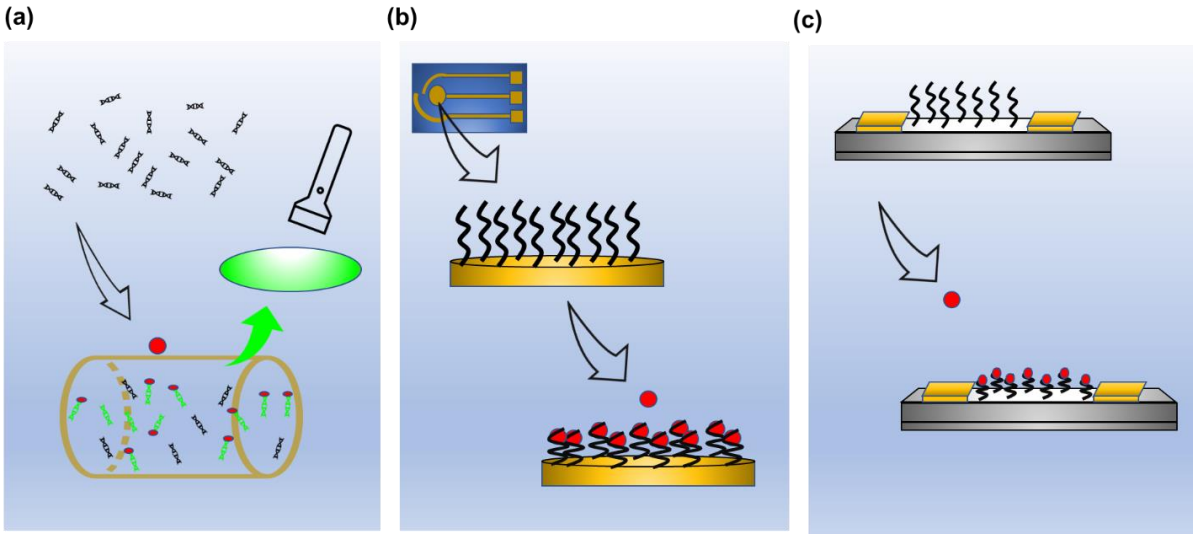

Figure 1:Schematic illustration of various transduction mechanisms, (a) optical, (b) electrochemical, and (c) electrical. (Reprinted with permission from ref [1] Copyright 2022 The Authors).

1.3.1 Optical

A large number of wearable biosensors incorporating nucleic acid assays depend on optical techniques for biosensing [65]. In such scenarios, an optical transducer records shifts in optical properties to yield a signal output manifested in forms like colorimetry, fluorescence, and luminescence [69–71]. A distinctive fluorescence assay utilizing an aptamer attached to a cross-linked methacrylated hyaluronic acid hydrogel microneedle patch biosensor facilitated the quick detection of several biomolecules, such as glucose, adenosine triphosphate (ATP), L-tryosinamide, and thrombin [19]. The transduction mechanism employed in this assay stands out for allowing signal detection on-needle. After the minimally invasive application of the microneedles into the skin, an adequate amount of interstitial fluid (ISF) was extracted. The aptamer, connected with a Cy3-fluorophore, is hybridized with a quencher-conjugated DNA competitor strand, thereby reducing the fluorescence intensity. A method without reagents is utilized, where in the absence of the target in the extracted ISF, the quencher and fluorophore remain close, resulting in no fluorescence output. When the target binds, the competitor strand, along with the quencher, detaches from the fluorophore-conjugated aptamer, leading to the observation of fluorescence. The detection limit was 1.1 mM, 0.1 mM, 3.5 uM, and 25 mM for glucose, ATP, L-tryosinamide, and thrombin, respectively, with high selectivity against non-specific targets. The biosensor patch was also successfully applied to the skin of diabetic rat models. A significant limitation is that fluorescence was recorded using a bench top fluorescence microscope, negating the ease-of-use aspect of wearable platforms. Continuous measurement can be achieved by using a linker that prevents the complete removal of the quencher-conjugated DNA from the aptamer upon target binding. Miniaturizing optical detecting strategies could also improve this device . Furthermore, optical wearable biosensors enhance ease of use, with qualitative data being easily interpreted by untrained individuals. However, the primary drawback limiting optical

signaling methods in wearable biosensing schemes is the complex conversion of qualitative data into quantitative data, thus reducing its potential for integration into wearable biosensors for thorough, real-time monitoring and analysis.

1.3.2 Electrical

The dominant transduction mechanism for wearable biosensors incorporating NAs is the field effect transistor (FET)-based biosensors within the electrical realm. FETs are semi-conductive devices consisting of three electrodes: a source, a drain, and a gate. Biorecognition elements are primarily immobilized on the gate [66]. Detection is achieved by observing target-induced changes in the conductivity of the semiconductor channels, which provides quantitative electrical measurements [66]. FETs display extraordinary sensitivity, with detection limits reaching into the zeptomolar range and even the ability to detect single molecules [7,54,72,73]. Nonetheless, the sensitivity of receptor-modified FETs is limited by the Debye length [74]. Specifically, the repulsive forces between NA targets are shielded by the high ionic strength of the solution under physiological conditions[75]. The high ionic strength of the electrolyte leads to a short Debye length, which is the electrostatic screening effect of charges in solution. This restricts the crucial length of the probe immobilized on FETs, as charges are electrically screened beyond the Debye length, which is measured starting from the electrode [74,75]. Under physiological conditions, the critical Debye length is less than 1 nm. Therefore, the use of NAs that change conformation upon target recognition can generate significant signals since structural changes are likely to occur within the Debye length, leading to considerable electric changes [73,76].

Significant progress has been made in the development of FET wearable biosensors. One of the most extensively researched NA-based strategies is the development of cortisol-detecting FETs, with aptamers immobilized on novel materials such as ln_2O_3 thin nanofilm sensing channels [7]. Interestingly, the cortisol sensing array was integrated into a watch, enabling it

to both collect and analyze real-time cortisol levels in sweat at specific points in time. When cortisol interacts with the aptamer, conformational changes in the phosphodiester backbones of the aptamers cause surface charge perturbations, which are measured as electrical signals correlating with varying cortisol concentrations [7]. When tested using artificial sweat, this biosensor achieved a limit of detection of 1 pM and a detection range of 1 pM to 1 μM. The biosensor demonstrated high specificity, as insignificant responses were measured against non-relevant targets such as testosterone, progesterone, corticosterone, and aldosterone. The device was also tested in saliva samples from participants in a Trier Social Stress Test, and measurements were consistent with cortisol level trends obtained from standard laboratory assays. Furthermore, the device was used to determine cortisol level changes according to ciconcaptamerdian rhythm and showed consistent results from ELISA analysis of the samples used. Prior to performing on-body sweat measurements, the assembled device was attached to the wrist skin of a healthy individual with double-sided tape, and FET sensor baselines were recorded in artificial sweat for calibration. The target stimulation region of the skin was first cleansed with deionized water and ethanol before five minutes of iontophoretic sweat gland stimulation. Precipitation is then transferred from the skin to the sensor array with the aid of the microfluidic layer. In addition to the developments described above, various studies have explored the use of FET as the sensing strategy, trying to detect cortisol at physiologically relevant concentrations using aptamer-cortisol binding, which enabled signal change. For instance, one study utilized a liquid-ion gated field effect transistor comprising an aptamer conjugated poly(3,4-ethylenedioxythiophene) polyacrylonitrile nanofibers (PEDOT-PAN NFs) as its sensor channel [27]. The PEDOT-PAN NFs FET biosensor had a limit of detection of 10 pM of cortisol with a response range between 1 pM to 10 μM. To test the wearable applicability of the device, the sensor was placed on human skin while participants exercised. In this test, the wearable sensor was able to detect and discriminate

between various levels of cortisol from human sweat measured at different times of day. The aptamer-functionalized graphene layer on a platinum gate electrode of an extended field effect transistor to detect cortisol was also investigated. The device had a detection limit of 0.2 nM and a detection range between 1 nM and 10 μM [27]. Despite their efficiency and sensitivity in cortisol detection, this research has not utilized the full potential of aptamer chemistry and regeneration for continuous long-term use.

One study aimed to detect IFN-γ, a cytokine biomarker, by developing a FET flexible biosensor with a regenerative aptamer-functionalized graphene-nafion composite film as its sensing channel [53]. The negatively charged IFN-γ-aptamer complex and its compact conformation move close to the sensing channel, inducing a change in current detected upon target binding. The limit of detection was 740 fM in undiluted human sweat and 880 fM when mounted onto an artificial hand. At equal concentrations, the change in signal for IFN-γ is five times greater compared to non-specific targets, such as TFN-a, interleukin-002, and interleukin-6. After biomarker detection, the biosensor was dipped in ethanol to dissolve the Nafion film and displace the bound aptamers. Nafion and aptamers were then drop-casted and functionalized, respectively, back to the FET sensor. Regeneration was successful for 80 cycles, with sensor response consistent with the first cycle. Previously, Z. Wang et al. developed a wearable graphene-based FET functionalized with aptamers for detecting cytokines including IFN-γ, which demonstrated a limit of detection of 2.89 pM [53]. This new finding indicates an improvement in the design and development of wearable biosensors for detecting IFN-γ with FET as its sensing component. Multiplex analysis of biomarkers using FET has also been achieved and offers more information on one's health. For instance, a multiplexed ln_2O_3 nanoribbon FET functionalized with aptamers to detect serotonin and dopamine was developed, with a limit of detection of 10 fM and a detection range between 0.1 pM and 1 μM [52].

1.3.3 Electrochemical

Electrochemical-oriented wearable biosensors are emerging as highly promising due to their benefits such as reagent integrated assessment, sensitivity, and simple manufacturing process. An electrochemical sensor combines an electrochemical transducing component with immobilized biorecognition components capable of interacting with a target [22,55]. When the target binds, the subsequent chemical reaction is converted into an electrical signal which can be measured to indicate target concentrations. However, they come with a few challenges including sensitivity to sample matrix effects, a narrow temperature range for optimal operation, and limited shelf life [77,78].

Continuing the development of aptamer-based wearable biosensors for detecting sweat cortisol, a watch named **C**ortisol **A**pta-Wa**tch** (CATCH) was developed. This device uses a sensor surface coated with ZnO and functionalized with an aptamer, built on a nano-porous polyamide substrate, for cortisol detection [67]. The binding of the target leads to an increase in charge transfer resistance which is then quantified using electrochemical impedimetric spectroscopy. As a complementary technique, chronoamperometry was also used to verify the performance of the sensing platform. The sensor was able to detect cortisol concentrations as low as 1 ng/mL within a range of 1–256 ng/mL. The aptasensor was also able to track the rise and fall of cortisol levels, in line with the ciconcaptamerdian rhythm.

In order to overcome the common requirement of chemical reagents for device regeneration in aptamer-based sensors, the researchers modified their analytical approach. They tracked changes in cortisol concentrations based on the change in the slope of the previous concentration. A change in slope would indicate a change in impedance response, offering a novel method to extend the on-body operation of the device. The sensor showed a strong response to cortisol but negligible responses to non-targets at concentrations of 200 ng/mL.

To validate its performance, the device was tested by healthy human participants and was able to detect cortisol levels in sweat between 1–12 ng/mL. Comparable studies on electrochemical-based sensors for cortisol detection in wearable formats have yielded similar results. Ganguly et.al. demonstrated a limit of detection of 4 ng/mL, while Mugo et al. showed a limit of detection of roughly 1.8 ng/mL [67].

A unique electrochemical-based flexible immunosensor was developed that used functionalized aptamers on a nanocomposite of graphene-gold nanoparticles and modified electrodes. This enabled simultaneous detection of TNF-α, IL-6, IL-8, TGF-1, S. aureus, pH, and temperature, making it valuable for monitoring wound conditions [60]. Named as the venous ulcer care device (VeCare) platform, this biosensor, which can be applied directly to a wounded skin, incorporates a wound contact layer, a microfluidic collector to gather target analytes, and a breathable barrier within the sensor complex. In the absence of analytes, the redox probe of the bound aptamers is close to the electrodes, enabling charge transfer. After the target binds, conformational changes in the aptamers move the redox probe away from the electrode, resulting in a reduction in the redox current. The sensor integrates a portable wireless analyzer that can carry out and measure electrochemical tests, and the data can be wirelessly transmitted to a mobile device. Intriguingly, the wireless analyzer is connected to a clinical management system, facilitating quick clinical care in diagnostic and treatment scenarios. This sensor design allows for on-body sampling, reagentless transduction, and analysis. The sensor proved its ability to detect target concentrations within physiologically relevant ranges, showed selectivity against similar non-targets, and demonstrated specificity and reproducibility. Furthermore, clinical application of VeCare was evident from correct analyses of wound exudate obtained from patients with venous ulcers [60]. Moreover, in situ wound monitoring was also tested in mice models, demonstrating the potential of wearable applicability of the device.

1.4 Electrochemistry basics for electrochemical biosensors

To comprehend the functioning of electrochemical biosensor measurements, it is essential to first delve deeper into the fundamentals of electrochemistry. Electrochemistry, a method to study electron transfer reactions, connects electron flow to chemical changes, especially the oxidation or reduction of metal complexes in inorganic chemistry [79]. To illustrate, consider the reduction of ferrocenium (Fc+) to ferrocene (Fc), either through a chemical reducing agent or an electrode. In the simplest terms, an electron moves from one molecule to another because the energy level of the electron in the donating molecule is higher than that in the receiving molecule, making the transfer thermodynamically favorable. In electrochemical reduction, the electron transfer is driven by an energy difference between the electrode and the molecule. Unlike chemical reductions, where changing the reductant alters the driving force, electrochemistry allows easy control of the reaction's driving force and the measurement of thermodynamic and kinetic parameters [79].

In understanding a basic CV profile, the graphs presented are known as voltammograms or cyclic voltammograms. The x-axis indicates a parameter applied to the system, such as the applied potential (E), while the y-axis shows the corresponding current (i) response (Figure 2).

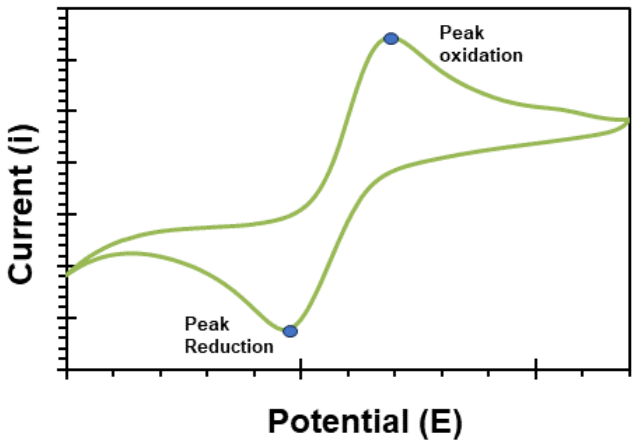

Figure 2: Representation of a CV graph.

1.4.1 Explaining the Peak Shapes in Cyclic Voltammetry

The presence of peaks in a cyclic voltammogram can be understood through the equilibrium between ferrocenium (Fc+) and ferrocene (Fc), described by the Nernst equation. This equation links the electrochemical potential to the activities of the oxidized (Ox) and reduced (Red) forms of an analyte in equilibrium. The equation involves constants like Faraday's constant (F), the universal gas constant (R), the number of electrons involved in the reaction (n), and the temperature (T) [79].

$$E = E^0 + \frac{RT}{nF}\ln\frac{(Ox)}{(Red)} = E^0 + 2.3026\frac{RT}{nF}\log_{10}\frac{(Ox)}{(Red)} \quad \text{(Equation 1)}$$

The Nernst equation is crucial in predicting how a system reacts to changes in concentration or electrode potential. Applying a potential equal to E°′ (approximate E1/2) to an Fc+ solution, the equation predicts an equilibrium where Fc+ is reduced to Fc until their concentrations equalize. During a CV scan, the concentration of species near the electrode fluctuates according to the Nernst equation. Scanning a solution of Fc+ to negative potentials reduces

Fc+ conversion to Fc at the electrode, changing the local concentration and resulting in the characteristic cyclic voltammogram shape (the duck-shape) [79].

As the potential moves negatively to reduction values, [Fc+] near the electrode decreases as it's converted to Fc. At the peak cathodic current, Fc+ diffuses from the bulk solution to the electrode. This diffusion layer grows, slowing the transport of Fc+ to the electrode, and leads to a current decrease as the scan progresses. When switching to positive potentials, the concentration of Fc at the electrode, which had increased, satisfies the Nernst equation. The Fc is then oxidized back to Fc+ as the potential becomes more positive. The two peaks result from the diffusion of the analyte to and from the electrode [79].

If the reduction is both chemically and electrochemically reversible, the peak-to-peak separation (ΔE_p) is 57 mV at 25°C. Chemical reversibility refers to the analyte's stability upon reduction and subsequent reoxidization, while electrochemical reversibility concerns the kinetics of electron transfer between the electrode and analyte. Fast electron transfers (electrochemical reversibility) quickly establish Nernstian equilibrium with potential changes. Conversely, a high barrier to electron transfer (electrochemical irreversibility) requires more extreme potentials for reactions, resulting in larger ΔE_p. Electrochemically reversible processes, where electron transfers are rapid and follow the Nernst equation, are termed "Nernstian" [79].

The scan rate in an experiment determines how quickly the applied potential changes. Higher scan rates result in smaller diffusion layers and, consequently, larger currents. For electrochemically reversible processes involving redox species that diffuse freely, the Randles-Sevcik equation explains that the peak current (i_p) increases linearly with the square root of the scan rate (υ). This equation involves various factors: n (the number of electrons transferred in the redox event), A (the electrode surface area, usually considered as the

geometric surface area), D_o (the diffusion coefficient of the oxidized analyte), and C_0 (the bulk concentration of the analyte).

$$i_p = 0.446nFAC^0(\frac{nF\upsilon D_0}{RT})^{1/2} \text{ (Equation 2)}$$

The Randles-Sevcik equation is useful for determining whether an analyte freely diffuses in solution. Since analytes can adsorb to the electrode surface, it's crucial to confirm that the analyte remains uniformly distributed in solution before analyzing its reactivity. Additionally, the equation can be employed to calculate diffusion coefficients, a process detailed in an experimental module focusing on the cyclic voltammetry of ferrocene and the measurement of diffusion coefficients [79].

1.5 Setting up an electrochemical cell for experiments

The following sections will delve into the functions of each CV component and the assembly process for an electrochemical cell to gather data in CV experiments.

1.5.1 Preparing the Electrolyte Solution

Electron transfer in CV experiments necessitates maintaining electrical neutrality, which is achieved through ion migration in the solution. As electrons move from the electrode to the analyte, ions shift to balance the charge and complete the electrical circuit. A supporting electrolyte, usually a salt, is dissolved in the solvent to reduce solution resistance, forming what is commonly called the "electrolyte solution".

A good solvent exhibits several key characteristics that are crucial for its effective use in experiments. Firstly, it must remain liquid at the temperatures utilized during the experiment, ensuring consistent behavior and interactions. Secondly, it should have the capacity to fully dissolve both the analyte and high concentrations of the supporting electrolyte, which is essential for accurate and reliable results. Additionally, a good solvent resists oxidation and

reduction within the potential range employed in the experiment, maintaining its stability and effectiveness. It is also important that the solvent does not react adversely with the analyte or the supporting electrolyte, as such reactions could compromise the integrity of the experiment. Finally, ensuring that it is free from impurities that could affect the experimental outcomes [79].

Qualities of an effective supporting electrolyte include high solubility in the chosen solvent, chemical and electrochemical inertness under experimental conditions, and the capability of being purified. This quality is vital to remove any impurities that could potentially affect the experiment's outcome, thereby ensuring the accuracy and reliability of the results [79].

To enhance the conductivity of a solution, it is essential to incorporate high levels of supporting electrolytes. This is because, during electron transfers at the electrodes, the movement of the supporting electrolyte is necessary to maintain charge balance, thereby completing the electrical circuit. The overall conductivity of the solution is directly linked to the concentration of the dissolved salt. In cases where the electrolyte concentration is inadequate, the solution tends to resist the transfer of charge.

Additionally, high electrolyte concentrations are needed to limit the movement of the analyte. Analyte migration to the electrode surface occurs through convection (movement due to mechanical forces like stirring), migration (movement under an electric field), and diffusion (movement due to concentration gradients). To minimize convection and migration, high electrolyte concentrations are employed, ensuring the electrolyte, rather than the analyte, migrates to the electrode for charge balancing [79].

Ferrocyanide ($[Fe(CN)_6]^{4-}$) and ferricyanide ($[Fe(CN)_6]^{3-}$) solutions are frequently employed in electrochemical experiments due to their unique properties. In aqueous solutions, these complexes are chosen for their stability and specific electrochemical characteristics.

Potassium ferrocyanide and potassium ferricyanide are common choices, often used in cyclic voltammetry and other electroanalytical techniques. These cyanide complexes provide distinct redox peaks, making them ideal for studies involving electron transfer processes [79].

1.6 Electrode Selection for Cyclic Voltammetry

1.6.1 Three-Electrode Setup

For CV experiments, a three-electrode system is usually required. This arrangement is standard in electrochemical studies. The working and counter electrodes facilitate current flow, while the reference electrode provides a stable benchmark for measuring the applied potential.

1.6.2 Reference Electrode

In electrochemical cells, the role of a reference electrode is crucial as it establishes a stable and precise equilibrium potential, essential for the accurate measurement of potentials of other electrodes within the system. This benchmarking is particularly important in aqueous solutions, where the commonly utilized reference electrode is the AgCl/Ag electrode. This electrode is typically separated from the main solution by a porous frit. Ensuring that the solvent and electrolyte within the reference compartment are consistent with those used in the main experiment is crucial in reducing junction potentials, which can otherwise impact measurement accuracy [80].

1.6.3 Counter Electrode

The counter electrode plays a crucial role in completing the electrical circuit during the application of potential to the working electrode. To avoid limiting reaction kinetics at the working electrode, the counter electrode typically has a larger surface area. Common

materials for the counter electrode include platinum, gold or carbon-based materials. The counter electrode should be as inert as possible, sometimes isolated from the system by a fritted compartment to prevent byproduct generation [80].

1.6.4 Working Electrode

The working electrode is where the electrochemical reaction of interest occurs. Its potential is controlled by a potentiostat, based on the reference electrode's potential. The working electrode must be composed of materials that are redox-inert within the desired potential range. Different materials can be chosen for the working electrode to suit specific experimental needs. This will be discussed in the coming sections.

Maintaining a clean, well-defined surface area of the working electrode is critical. Cleaning methods vary based on the electrode type and may include mechanical polishing followed by ultrasonic cleaning in ultrapure water. To remove residual particles from polishing, it's common to perform several CV scans in a basic electrolyte. This "pretreatment" process is repeated until consistent scan results are achieved with no observable peaks [80].

Changing electrode materials can affect electrochemical responses, making it a useful approach to diagnose various issues like differing electron transfer kinetics or electrode-specific reactivities.

1.7 Squarewave voltammetry for electrochemical analysis

In recent times, square wave voltammetry (SWV) has become increasingly popular in creating sensitive electrochemical sensors and biosensors. The performance of these sensors is largely dependent on their sensitivity and selectivity to specific analytes. Enhancing this sensitivity can be achieved through using methods such as SWV, which is a more sensitive electrochemical technique. Additionally, enhancing electrode design or material, such as

boron-doped diamond film electrodes, carbon paste electrodes, gold-based nanowires/nanotubes, and carbon nanotubes, can improve sensor sensitivity. These modifications have been extensively studied, highlighting the role of both modified and unmodified electrodes in SWV-based methodologies [81].

The majority of voltammetric methods rely on continuously changing the potential applied to a solution via an electrode and measuring the resultant current. The most commonly used technique is CV, which helps identify the nature of redox reactions occurring in a solution. While CV is not as sensitive as pulse-based methods, it is widely used for various purposes beyond just detecting trace amounts of an analyte. CV is primarily employed to gather essential information, such as oxidation/reduction mechanisms, establishing formal potentials, and studying electron transfer and kinetics [81].

Figure 3 illustrates waveforms for different voltammetric methods and the timing of current sampling. CV's waveform is linear, meaning the potential changes linearly over time. Among electroanalytical techniques, pulse-based methods are generally more sensitive. Techniques like differential pulse voltammetry (DPV), normal pulse voltammetry (NPV), and SWV are highly effective. These techniques modify the potential of a sample by switching between potentials, unlike CV, which sweeps through different potentials. In DPV, current is sampled at points S_1 and S_2, with typical values of T ranging from 0.5 to 5.0 seconds and pulse period (t_p) around 50 milliseconds. The current difference (I_2 - I_1) reflects the impact of the pulse. The SWV waveform, a variant of the DPV waveform, has equal durations for pre-electrolysis period (T) and t_p, appearing as a symmetrical square wave on a staircase. Current is sampled twice per cycle at the end of each pulse, as depicted in Figure 3. The forward sample S_1 is taken from the first pulse per cycle, and the reverse current at the end of the second pulse. The calculation is based on the difference between the forward and reverse currents (S_1 - S_2). It is important to consider that the peak current in SWV is about four times greater than that in

DPV. The frequency of the square wave, which is determined by the application of the square wave on the staircase potential, dictates the sampling rate of the analyte. Each pulse leads to a slight increase in potential, so a higher pulse frequency results in a faster potential scan rate. Like in CV, an increased sweep rate results in a rise in peak current. However, this also leads to an elevation in peak potential, which, unlike in CV, is proportional to the logarithm of the square wave frequency. The advantages of SWV are significant, overshadowing any potential drawbacks. This reinforces its status as an effective and adaptable technique. SWV has found extensive applications in various fields such as medical diagnostics, environmental testing, food science, and in measuring enzymatic kinetics [81].

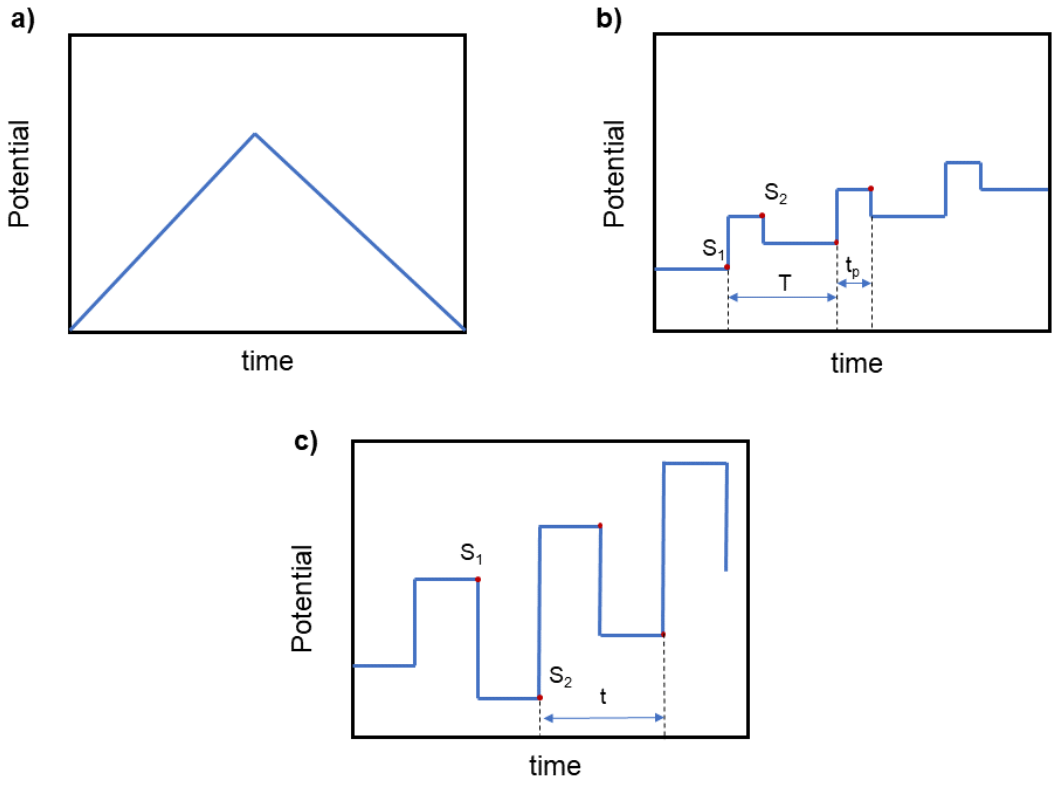

Figure 3:Waveforms for a) Cyclic Voltammetry, b)Differential Pulse Voltammetry, and c) Square Wave Voltammetry including the time for current sampling.

1.7.1 Utilizing SWV in Diagnostic Biosensors

The rapid and sensitive detection of disease-related biomarkers using SWV is of significant interest and importance for diagnostics and monitoring pharmacological treatment responses.

Various methods have been used in the sensing/biosensing of disease biomarkers, including immunoassays, antibody-functionalized magnetic beads, and DNA-decorated electrodes. There's a wide array of studies on electrochemical sensing/biosensing of different analytes for diagnostic purposes using SWV. For example, Reisberg et al. developed an electrochemical DNA hybridization sensor capable of detecting single nucleotide polymorphisms (SNPs) with high precision. This sensor uses a peptide nucleic acid (PNA) probe attached to a quinone-derived electroactive polymer. Changes in the polymer-solution interface's electrochemical properties are observed upon hybridization of the PNA probe with a target DNA strand, as indicated by an increased quinone peak current in SWV, but not with a non-complementary sequence. This sensor shows promise for genetic disease diagnosis involving SNPs. Liao et al. created an electrochemical genosensor for detecting Escherichia coli O157:H7, a pathogen causing serious illnesses. They used gold nanoparticle screen-printed electrodes modified with thiol-capped single-stranded DNA. The genosensor works on a competitive assay principle, measuring current changes related to the amount of E. coli present. Liu et al. devised an immunosensor for interferon gamma (INF-γ), which plays a role in treating certain diseases. The sensor uses a thiolated DNA hairpin with an INF-γ binding aptamer and a redox tag, changing the redox current when INF-γ binds to the aptamer [82].

1.7.2 Electrode material for the electrodes

The choice of electrode materials is paramount in all electrochemical systems, including voltammetric biosensors. Factors like electron transfer properties, surface texture, porosity, and the ability for chemical functionalization are critical in designing a biosensor. Various materials and configurations can be used to create these sensors. Gold, platinum, and carbon are commonly used, with popular configurations being disc electrodes, interdigitated

electrodes, microelectrodes, and nanoelectrodes. Gold is a preferred substrate as the working electrode due to its ability to easily form bonds with thiolated molecules, a process occurring spontaneously between gold and thiols [83]. This adaptability makes it possible to create a variety of biosensors, as thiols can be incorporated into a range of biomolecules, from proteins to nucleic acids. For instance, gold electrodes can be coated with self-assembled monolayer (SAM) of thiolated DNA for detecting small molecules, or enzymatic activity. Similarly, thiolated antibodies or antigens can be attached to gold to develop immunosensors capable of identifying specific biomarkers. SAM is a key component in biosensing, particularly when used with gold electrodes [83]. Besides using single-component electrodes like gold and platinum, it's also typical to enhance electrode materials, particularly carbon, with conductive polymers, nanomaterials, and anti-biofouling layers. The traditional methods used in the semiconductor industry, like photolithography, are highly precise for producing biosensor electrodes and are well-suited for mass-producing integrated circuit chips. However, these techniques become overly complex or even impractical when it comes to creating 3D, high-aspect-ratio, and hierarchically structured materials optimized for biosensing across multiple scales. Therefore, to develop such advanced multiscale and 3D materials for electrochemical sensing, new miniaturization and fabrication strategies need to be explored [84].

Before electrochemical diagnostic systems are market-ready, they must undergo extensive iterative design, implementation, testing, and validation. This process is essential to optimize the system, conduct clinical trials, and gain regulatory approval. Rapid prototyping methods that can scale from producing a few devices for demonstration to thousands for validation and millions for distribution are especially valuable. Polymers are an excellent choice for device substrates in rapid prototyping due to their stability, versatility in form factors, compatibility with various rapid fabrication methods, and cost-effectiveness compared to other substrates [84].

To address the requirements for rapid prototyping and materials engineering for electrochemical biosensing systems, a specific production strategy was adopted to produce surface modified electrodes by using the corrugation phenomenon. This phenomenon is commonly encountered in situations where films or sheets are subjected to compressive forces, leading them to adopt constricted geometrical shapes, resulting in folds, creases, ridges, or crumples. To alleviate mechanical stress, these films or sheets often form periodic structures or buckles perpendicular to the applied force.

1.8 Theory of wrinkling

Studies on corrugation formation predominantly utilize polymers, such as polydimethylsiloxane (PDMS), as the elastic substrate, with a rigid, thin film, often metallic such as gold, on top [85].

A mathematical model for the corrugation formation for these bilayer structures was introduced in order to predict their 3D topography. In the case of uniaxial strain, where shrinking happens in one direction, the wrinkle wavelength can be calculated using specific a formula (refer to equation 3 in chapter 3), taking into account the elastic moduli and Poisson's ratios of the film and substrate. The wrinkle size is influenced by these material properties and the thickness of the film [86].

Conversely, the wrinkles' amplitude heightened with the rise in heating temperature, suggesting greater compressive stress. Thus, altering the mechanical characteristics of materials allows for the artificial creation of wrinkles with specific wavelengths and amplitudes, suitable for a range of applications. With advancements in understanding and predicting the dimensions of corrugated features, research has shifted towards controllably fabricating corrugated materials and incorporating these unique structures into functional devices [86].

1.8.1 Creating corrugated devices

Fabricating corrugated thin-film structures on various substrates typically involves a series of steps. First, the substrate is stretched, followed by the application of the thin film. Finally, the process concludes with either compressing or releasing the substrate. A common method uses thin metal films on PDMS substrates. The PDMS is either heated or stretched to expand its volume or surface area, followed by coating it with a metal layer using sputtering or evaporation. Once the thin film is applied, the substrate is cooled or released, applying compressive force on the film and causing it to wrinkle [87].

This xurography-based method offers a fast way to create shadow masks without requiring cleanroom facilities, and is economical in terms of materials and equipment. Using this technique, we can produce parallel line cuts with a minimum spacing of 100 μm and circular features with diameters as small as 200 μm in the vinyl mask. After applying the metallic electrode material, the sputtered PS-PS is heated, allowing the PS-PS sheets to shrink to about 40% of their original size [85].

Polymer-gold electrodes are also utilized to fabricate flexible biosensors such as immunosensors for their unique properties. For instance, a flexible immunosensor was fabricated with a nanolayer of gp120 antigen immobilized on a flexible PET substrate. Other types of polymers such as Polystyrene (PS), Polypropylene (PP), or Polyethylene (PE) can also be used in the fabrication of flexible biosensors [88].

These polymers offer several advantages as supports for biosensing platforms, including flexibility, weight, conformability, portability, cost, disposability, and scope for integration.

These polymers are chosen for their flexibility, weight, conformability, portability, cost, disposability, and scope for integration. They are also lightweight, ultra-conformable (bendable, stretchable, foldable), portable, disposable, and inexpensive. Furthermore, they

offer extended scope for a high degree of functional integration and can accommodate additional functionalities such as wireless transmission modules, control and data acquisition instrumentation, and in-built power units.

1.8.2 Polyvinylidene fluoride as a substrate for surface modified gold electrodes

Polyvinylidene fluoride (PVDF) can also be used as a highly non-reactive and pure thermoplastic fluoropolymer. PVDF has been used in the development of fiber biosensors. A study [89] demonstrated a high-sensitivity fiber biosensor based on PVDF-excited surface plasmon resonance (SPR) in the terahertz band. The PVDF layer was used to excite the surface plasmon wave on the metal surface, enhancing the sensitivity of the sensor by utilizing its piezoelectric properties. The development of PVDF-based biosensors for breast cancer detection has also been reported. For example, a piezoelectric microcantilever sensor was developed to detect HER2 biomarker levels present in human blood samples of patients with breast cancer [90].

Moreover, PVDF's non-piezoelectric state has excellent chemical resistance, good thermal stability, and low dielectric constant, making it suitable for use in harsh environments. These characteristics make PVDF a promising material for use in biosensors and similar devices.

1.9 Conclusion

The advancement of personalized healthcare has been greatly boosted by the rise of wearable health-monitoring tools. These devices, at their core, use a range of biological agents – from the longstanding enzymes and antibodies to the emerging NAs – to detect specific molecules. Traditional elements like enzymes and antibodies, although dependable, face challenges regarding their stability and specificity. This has paved the way for NAs, especially aptamers, to become game-changers due to their adaptability and simpler production. Current research has already showcased aptamers' potential in monitoring biological markers like cortisol in

bodily fluids. Furthermore, for wearable sensors to translate the biological interactions into understandable signals, various transduction mechanisms come into play. These mechanisms are fundamental in amplifying and interpreting the weak biochemical signals generated from the interactions. While traditional biomolecular agents have served wearable biosensors well, the rise of NAs, particularly aptamers, hints at a new possibility for more efficient, stable, and customizable health-monitoring devices. This evolution, paired with appropriate transduction mechanisms, signifies a promising trajectory for wearable health-monitoring systems.

Chapter 2 : Thesis Rationale, Objectives, and Outline

2.1 Rationale

The evolving landscape of health technology, particularly wearables, is ushering in a transformative era of modern healthcare and personal monitoring. Devices designed for close contact with the human body are increasingly facilitating non-invasive, real-time insights into physiological conditions. Within this field, aptamer-based sensors emerge as one of the promising innovations. Aptamers, as specialized molecular structures, have a unique capability for selective molecular target recognition. Yet, their singular binding site often posed a limitation, compromising the desired sensitivity essential for real-time detection. To overcome this limitation, the concaptamer was proposed. These molecular structures, endowed with multiple binding sites, can potentially augment their capabilities for target interactions, resulting in significantly heightened sensitivity. Nevertheless, translating this molecular interaction into a detectable signal remains challenging. This gap is bridged by Methylene blue (MB), a redox molecule. Connected to concaptamers, methylene blue not only amplifies the interaction but also renders it apt for signal detection.

Surface alterations in biosensing platforms are believed to potentially elevate their interaction capabilities with targets. The idea of binding a concaptamer to a redox compound and aligning it with a surface-modified gold electrode suggests a possible boost in the electrochemical signal output. The idea behind such a design is to potentially improve detection sensitivity and maintain an unwavering functionality under varying scenarios.

The projected advantages of these surface modifications are worth considering. Enhanced sensitivity is one key expectation, but along with it, the right substrate, harmonized with the customized aptamer structure, might promise stable and reliable outcomes. This can lead to an elevated specificity of the biosensor, thereby promoting swift and pinpointed feedback.

Sweat, as an easily accessible and rich source of biomarkers, particularly cortisol, offers valuable insights into various physiological states, such as stress. The orientation of the concatenated aptamer biosensor towards sweat cortisol detection epitomizes the convergence of molecular tech advancements with real-world applications. Thus, the main rationale for this work is to combine the new concaptamer technology with practical use to improve health monitoring.

2.2 Hypothesis

It is hypothesized that by employing MB-modified concaptamers, which have several binding sites in comparison to the traditional aptamers with a singular active site, there will be a notable enhancement in analytical performance. This enhancement, combined with surface modified electrodes made from flexible Au-PVDF will manifest in terms of heightened sensitivity, improved specificity, and a more precise limit of detection.

2.3 Specific Aims

2.3.1 Specific Aim 1

Our first aim is to design and fabricate flexible gold electrodes using non-piezoelectric PVDF as the substrate by magnetron sputtering. We then heat-shrink the electrodes to further investigate the feasibility of these devices for wearable applications by characterizing their electrochemical properties.

2.3.2 Specific Aim 2

Our second aim is to utilize an MB conjugated concaptamer on corrugated gold - PVDF electrodes and optimize the assay parameters such as concaptamer concentration, concaptamer surface density, assay time, buffer concentration, etc.

2.3.3 Specific Aim 3

We will evaluate the analytical sensitivity, specificity, limit of detection, and reproducibility of the prepared biosensor in spiked buffer, artificial sweat and human sweat. Different concentrations of cortisol and similar non-target biomarkers will be prepared in artificial and real perspiration to validate the practicality of the wearable biosensor.

2.4 Novelty

The novelty of this work delineates as follows:

1. Our wearable biosensor utilizes a new concaptamer conjugated with a redox molecule, a combination previously unexplored in the field of wearable biosensors. The purpose of this new approach is to provide a more efficient and accurate detection of sweat cortisol. Most existing biosensors rely on traditional assays, which might not be as precise. By introducing this new assay, our work not only pushes the boundary of what's possible in cortisol detection but also lays the groundwork for future research in this field.

2. The choice of material is crucial for the performance, durability, and efficiency of wearable biosensors. This thesis takes a divergent path from previously utilized materials, choosing PVDF as the substrate material for the electrochemical wearable sensor. PVDF brings a lot of benefits - it's durable and can be potentially used to produce textured electrode surfaces. Its use in developing the electrochemical wearable sensing motif is novel, setting this work apart from other similar endeavors. By adopting PVDF, the thesis aims to create a wearable sensor that's effective and also practical for utilization.

Chapter 3 : Device design, fabrication, and characterization

3.1 Contribution

The acknowledgment of collaboration and support is fundamental to the progression of this research project. I wish to extend my profound appreciation to Microsystems hub, whose assistance played a crucial role in advancing this study. Their state-of-the-art facility facilitated not only the production but also the characterization process of our gold electrodes. Their contribution has been instrumental in shaping the outcomes of this work.

3.2 Key research questions

Moving on to our experiments into the device design, fabrication, and characterization, we're confronted with a series of questions. Firstly, we examine the role and effectiveness of the cleaning techniques employed, particularly how oxygen plasma cleaning might eclipse other methods in cleaning the gold electrodes' surface. Then, we characterize the electrodes' electrochemical and mechanical traits: how do these elements ensure that our biosensors remain flexible, and consistently transmit electricity even under stress?

The surface structure of the electrodes becomes a focal point, prompting us to investigate its potential influence on the overall electrochemical capabilities. Simulated models offer insights into how structured surfaces might differ from real electrode performance. We also look into the heat treatment parameters; specifically, which heat conditions are ideal for creating the most effective surface corrugation that boost electrode reactions?

We are drawn to the potential of a wrinkled electrode, specifically cortisol detection. We are focused on the question of how much wrinkled electrodes can improve cortisol detection compared to planar electrodes.

3.3 Introduction

This chapter delves into the methodology employed in constructing cortisol-sensing electrochemical biosensor electrodes, an important part that might improve our ability to measure and monitor stress biomarkers.

The process commences with the production of the gold electrode. As mentioned in Chapter one, Gold was chosen for its compatibility with biological substances, high conductivity, and inertness. It also helps with the utilization of SAMs for biosensor production, making it suitable for biosensor applications [83,84].

In the creation of the sensor, PVDF films were utilized, and the process encompassed several stages. These included preparing a mask with the electrode design inspired by the University of Calgary logo, which would be applied on the PVDF surface, sputtering 100nm gold on the PVDF, removing the mask, and cleaning the electrode surface. Since the biosensor's transduction mechanism is based on an electrochemical reaction involving CV and SWV, a three-electrode system was chosen for the biosensor. The working, counter and reference electrode were made from gold.

An integral aspect of crafting electrochemical biosensors is the preparation and cleansing of the gold electrode surface. This significance arises from the highly sensitive nature of these sensors towards surface contamination as electrochemical interrogations are highly sensitive to surface contamination and obstruction. Consequently, it is essential to apply an optimized technique that can efficiently clean the gold surface.

For this matter, we experimented with various cleaning techniques and compared their outcomes to discern the most efficient method [91]. We gauged the effectiveness of each cleaning process by conducting CV on each treated electrode. CV served as a reliable indicator of a cleaned surface since it measured the development of current in an electrochemical sensor under changing voltage conditions which signifies the potential presence of any remnants or impurities on the electrode. Ideally, a fully cleaned electrode should show a uniform duck-shaped voltammogram, devoid of unexpected spikes or shifts. Any inconsistencies in the CV patterns can point to remaining contaminants that may disrupt the electrode's electrochemical reactions. For our investigation, achieving consistent and predictable voltammograms is vital, ensuring the electrode's top-tier sensitivity and precision for further tests. For a well cleaned electrode, the variation in the potential between the oxidation and reduction peak should be close to the theoretical value of 59 mV at room temperature. Also, the oxidation to reduction peak ratio should be close to 1:1, implying that the oxidation and reduction processes are reversible. The oxidation and reduction potentials for the CV were set at 0.8V and -0.4V, respectively, to ensure clear visibility of the relative peaks. Additionally, the scan rate for the CV was chosen to be 50 mV/s to balance the time efficiency of the measurement and the clarity of the electrochemical signals. The electrolyte solution was prepared using a mixture of ferrocyanide and ferricyanide, with concentrations exceeding 1mM. This composition was chosen to supply enough redox species essential for the electrochemical analysis of the electrodes [79].

Different cleaning methods inspired by other research projects working on this matter were evaluated to determine the most effective approach [91].

For our first fabrication process, the electrodes were submerged in IPA and then subjected to sonication for fifteen minutes. Sonication created ultrasonic waves, leading to pressure changes and the formation of tiny vacuum bubbles within the liquid. These vacuum bubbles

can remove most organic and inorganic compounds. The abrupt bursting of these bubbles acts like a brush on the electrode surface, helping to dislodge any foreign particles. The IPA combined with the sonication would further assist in removing any organic impurities.

For our second cleaning procedure, we performed CV in a solution of 0.1 M sulfuric acid with a scan rate of 50 mV/s, repeating this process for a total of 50 cycles. Sulfuric acid, serving as the electrolyte, has a significant impact on the cleaning process's effectiveness due to its concentration. The application of potential triggers oxidation and reduction reactions on the electrode's surface. This alternating potential in sulfuric acid facilitates both types of reactions, thereby clearing various contaminants from the electrode surface.

For our third cleaning method, we utilized oxygen plasma at 0.5 Torr pressure for one minute. In this cleaning strategy, high-energy charged particles are directed to the electrode surface, removing any contaminations on the electrode.

Following the fabrication and cleaning process, the electrodes were once more evaluated for their electrochemical characteristics. This stage is vital for validating the performance and suitability of the electrodes within our biosensor application. In the previous steps the electrochemical evaluation was done with the standard Ag/AgCl reference electrode and platinum counter electrode to carefully assess the electrochemical behaviour of the PVDF-Au after cleaning. However for this step, the gold counter and reference electrodes were used to fully assess the electrochemical behaviour of three-electrode based setup.

In addition, the endurance of the electrode material in an electrochemical testing environment can influence the sensor's performance over extended periods. If the material is susceptible to deterioration under its operational conditions, the electrode may not consistently deliver reliable results [92,93].

Therefore, the physical characteristics of electrodes are also crucial. These devices must be both sturdy and adaptable, able to withstand the physical strains of regular use or the physiological conditions within the body.

To examine how mechanical strain might impact the performance of the biosensor, we used Ossila four-point probe. By measuring the sheet resistances of the electrodes after subjecting them to physical strain, like completely bending the electrodes in the middle and 180º twisting them along their axis, for a duration of ten minutes. The results were then compared with the resistances of electrodes that had not undergone mechanical loading.

In wearable applications, shear stress, though less frequent, can be more mechanically intense when it occurs. This is important for the PVDF-Au electrode, where twisting can lead to significant material deformation, such as gold flaking. Bending stress, in contrast, is a more common occurrence during regular use when the material flexes. This flexing can result in material fatigue, and over time, may lead to cracks or breakage. For testing, shear stress is simulated by twisting the electrodes, while for bending stress tests, electrodes are completely bent to monitor changes in sheet resistance [94].

A critical part of the procedure was the heat-treating process, which contributed to forming a textured surface on the cleaned sensors. As mentioned before in chapter one, a quick way to improve the electrochemical performance of electrodes is the introduction of 3D structures such as corrugation on the electrode surface. Considering the prepared PVDF-Au electrode, the heat-treatment is crucial as it allows the adjustment of sensor characteristics, such as its surface and subsequent performance, by modulating the heat treatment variables, namely temperature and duration. The temperature was chosen close to the melting temperature of the PVDF film (165 ~170℃) [95], giving the pre-stretched film enough thermal energy to release the stress and shrink through its lowered viscosity. Based on the mechanical properties of the film and the substrate, in order to achieve wrinkling with the 1µm wavelength, 100 nm

of gold was deposited on the PVDF substrate. By using equation 3 and the mechanical properties provided in table 2, a wavelength of 1.28μm is calculated for the corrugated electrode.

$$\lambda = 2\pi h_{f0}\left(\frac{(1-\nu_s{}^2)E_f}{3(1-\nu_f{}^2)E_s}\right)^{\frac{1}{3}} \qquad \text{(Equation 3)}$$

Table 2: Parameters used for wavelength (λ) calculation equation.

Symbol	Description	Value	Unit	Reference
h_f	Thickness of sputtered gold	100	nm	N/A
ν_s	Poisson's ratio for PVDF	0.4	N/A	[95]
ν_f	Poisson's ratio for gold	0.415	N/A	[96]
E_s	Elastic modulus for PVDF	3	GPa	[95]
E_f	Elastic modulus for gold	76	GPa	[96]
λ	Calculated wavelength	1285	nm	N/A

Wavelengths in the range of nanometers to micrometers, are commonly investigated in research for various applications involving wrinkled electrodes. For electrochemical applications, typically 1μm wavelength is generally considered to strike a balance between enhancing sheet resistance and surface area, and not limiting the electrochemical reaction through diffusion [17,97,85,30].

The electrodes are thermally processed within a convection oven as they can provide more uniform heat application to the electrodes compared to other instruments (i.e. hotplates) [98]. The electrodes were set between two polytetrafluoroethylene (PTFE) felts to make sure they freely shrink without sticking to any surface or crumbling on their own surface. After the oven

reaches the target temperature, the electrodes are loaded and heated with different time durations, and then taken out of the oven right after the specific heating duration. Following the optimization of the heating temperature and duration, the study focused on investigating the impact of the vinyl mask's orientation on the electrode's electrochemical behaviour. This was done due to the PVDF's tendency to shrink uniaxially.

Subsequently, while maintaining the same electroactive surface area of the electrodes, modifications were made to the design of the connecting arms. These arms were lengthened and thickened with different dimensions, to assist in facilitating easier handling and testing in subsequent steps as the small size of the electrodes after shrinking was hard to handle during experiments. The thickness of the connecting arms was modified to address the issue of crack propagation observed during heat treatment in the extended electrodes. This adjustment aimed to determine whether altering the thickness could reduce cracking. This experiment was done in a batch of 10 for electrode design to investigate the number of occurrences of this issue.

In the next step, the effect of a heating regimen was also investigated compared to the previous method, in which the PVDF-Au samples would be loaded in the oven at the target temperature without preheating. This adjustment was necessary because the previous heat treatment resulted in cracks forming in the electrodes, leading to disconnections.

In the heating regimen, the electrodes were placed in the oven, and sandwiched between layers of PTFE felt. A slow heating rate, within the capabilities of the oven, was adopted, and the heat treatment was conducted in accordance with the previously optimized heating process.

It's important to note that this procedure isn't universally applicable and necessitates further calibration.

The surface morphology of the heat-treated electrodes was subsequently examined using Scanning Electron Microscopy (SEM). This analysis aimed to measure the wavelength of the

surface patterns formed and compare these measurements to the theoretically calculated values.

The objective of this process is to discern the ideal conditions that result in the most effective corrugation, thereby optimizing the performance of the electrodes. The outcomes from these varying heat treatment conditions, along with their influence on the electrochemical behaviour of the biosensor, will be detailed and analysed in the subsequent sections.

For the next step, under optimized heating conditions, the effect of heating on reference and counter electrodes was studied. A wrinkled working electrode was connected to the Emstat4S potentiostat. Two sets of electrodes, wrinkled and planar, were used for both the reference and counter electrodes. The oxidation and reduction peaks of these electrode sets were compared using the CV graphs acquired. This comparison aimed to understand the influence of electrode surface morphology for reference and counter electrode on electrochemical behavior while the working electrode is already surface modified.

We then proceed to commence with the computational modeling and study of a corrugated electrode surface, employing the multifunctional capabilities of COMSOL Multiphysics.

This section covers the investigation of the CV responses of electrodes, undertaken via computational modeling using COMSOL Multiphysics. The analysis involved two distinct models: a 2D planar electrode and a corrugated electrode, enabling a deeper understanding of the influence of surface morphology on electrochemical characteristics.

By doing so, we evaluated the electrochemical behaviour of these surfaces, thereby facilitating a comparison between the planar and corrugated models.

In the upcoming sections, the minimum sample size of three was used for calculating averages and standard deviations. The mean and standard deviation derived from these samples provided an initial understanding of the data. Though not incorrect, it is recognized that such

a small sample size might limit the statistical power and increase the potential for errors [99]. Consequently, the findings are viewed as exploratory, laying the groundwork for future research with larger samples to validate and expand upon these initial observations.

3.4 Materials and methods

3.4.1 Device design and fabrication

The fabrication of wrinkled electrodes begins with a vinyl masking (Permanent Cricut® Premium Vinyl™) covering the PVDF substrate (25.3-micron thickness, acquired from PROFESSIONAL PLATICS) with the required electrode patterns imprinted on it using a Cricut Explore Air 2®. The design of the vinyl mask was applied to the PVDF in both vertical and horizontal orientations to evaluate its uniaxial shrinking behavior. The vinyl mask is removed, and the electrodes are cut out after a 100 nm thin layer of gold is sputtered onto the substrate (Figure 4). The gadget is made up of three gold electrodes: a working electrode, a reference electrode, and a counter electrode. The electrodes are created so that the surface area of the counter electrodes is $25mm^2$ (5 times the surface area of the working electrode) and the surface area of each working and reference electrode is $5mm^2$.

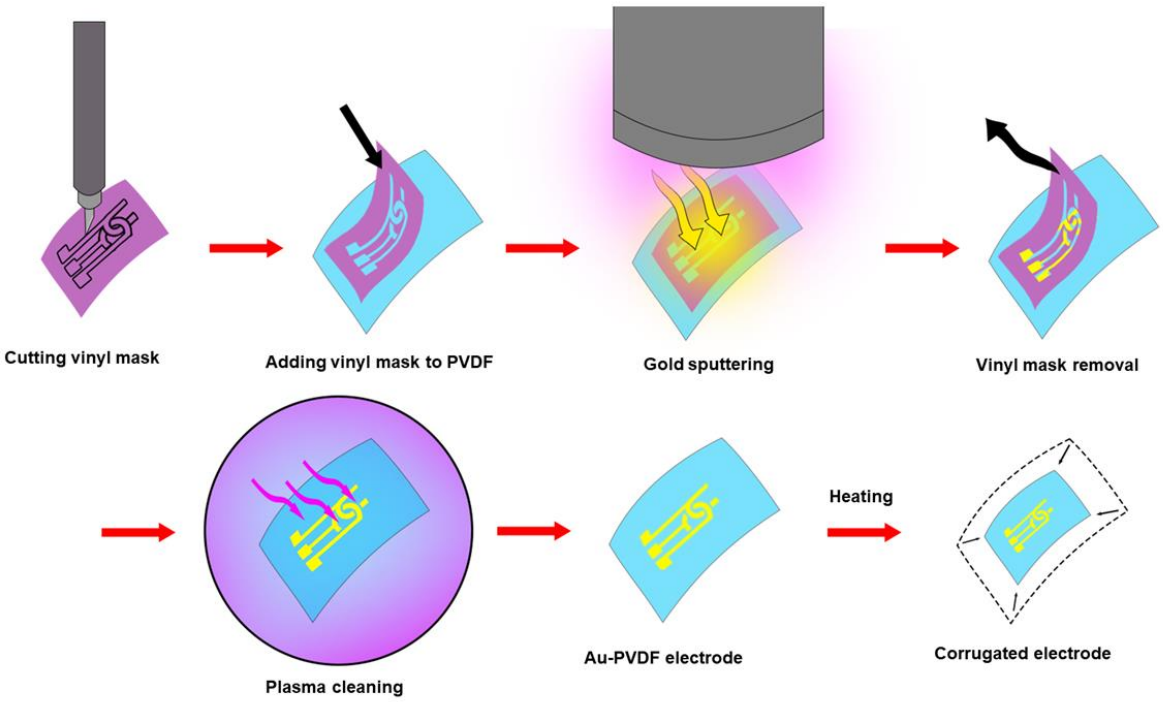

Figure 4:Step-by-step process of PVDF-Au electrode production.

3.4.2 Device cleaning procedures

The initial methodology involved subjecting the electrodes to sonication (VWR Symphony Ultrasonic Cleaner) in IPA (ULINE Model No S-17477) for a duration of 15 minutes. In our second technique, we performed CV (Emstat4S potentiostat) in a solution of 0.1 M sulfuric acid (Sigma, CAS No. 7664-93), setting a scan rate of 50 mV/s and repeating the procedure for 50 cycles. Our third method employed an oxygen plasma cleaner for one minute, at an oxygen pressure of 0.5 Torr (Harrick Plasma PDC-001-HP).

To evaluate the cleaning process, CV was done from -0.4V to 0.8V with a scan rate of 50 mV/s in a solution composed of 25 mM PBS (Sigma 10X PBS, Product No. 6505-OP), 25mM NaCl (Sigma, CAS No. 7647-14-5), 2mM Potassium ferrocyanide (Sigma, CAS No. 14459-95-1).

3.4.3 Device characterization

Post-cleaning, we gauge the electrochemical behavior of our electrodes using an Emstat4S potentiostat. A standard Ag/AgCl electrode (Saturated AgCl/Ag electrode R0302) is employed as the reference electrode, while platinum (0.5*37mm 99.99% purity platinum wire electrode) acts as the counter electrode.

We further scrutinize the gold working electrode's functionality by performing CV. This technique measures the electrochemical system's current response under varied potential, from -0.4V to 0.8V with a scan rate of 50 mV/s in a solution composed of 25 mM PBS (Sigma 10X PBS, Product No. 6505-OP), 25mM NaCl, 10 mM Potassium ferricyanide (Sigma, CAS No. 13746-66-2), and 10 mM Potassium ferrocyanide (Sigma, CAS No. 14459-95-1). In addition, we performed Electrochemical Impedance Spectroscopy (EIS) (Emstat4S potentiostat) in the same solution. EIS measures the electrochemical system's impedance across a wide frequency range, from 50 KHz to 1 Hz, with a potential amplitude of 0.01 V.

We then evaluated the electrodes' electrical quality post-application of mechanical stress using a 4-point probe (Ossila). This tool measures the sheet resistances of the electrodes after they have undergone 10 minutes of 180º twisting along the electrode axis and full bending in the middle of the electrode.

3.4.4 Electrode corrugation procedure and characterization

To induce corrugated structures on gold electrodes, we utilized Teflon felt (7836 Felt 1.65mm thick, Pelegrina Medical), and gold electrodes were encased between two layers of this material. To optimize the heating process, we administer the heat treatment in a convection oven (Binder Standard Series) across diverse durations and varying temperatures (150°C, 160°C, 170°C, 180°C, and 190°C, each temperature for 5, 10, 15, and 30 minutes), enabling us to assess the impact of these variables on the corrugation formation. After optimizing the

heating temperature and duration, a heating regimen was adopted. The electrodes were loaded and heated to the target temperature with a heat-rate of $3^{\circ C}/_{min}$ before being heat-treated with optimized conditions. The electrodes were then left in the oven to be cooled slowly as the oven was turned off. The surface morphology of heat-treated and unheated samples is then observed using Quanta FEG scanning electron microscopy in secondary and backscattered modes with electron-accelerating energy of 20 KeV. The cracks on the wrinkled electrodes were presented using a 10X Olympus CH30RF100 optical microscope.

3.4.5 COMSOL Multiphysics Simulation of a corrugated electrode surface

For the planar model, its dimensions were set at 100µm x 100µm (width x height), representing an unmodified, flat electrode surface. This offers a standard of comparison with the textured model.

In the case of the textured or corrugated model, the same overall dimensions were retained but with the inclusion of five parametric curves to simulate the surface's corrugated geometry with 1µm wavelength. These curves symbolize individual wrinkles, each spanning between 3 to 18µm in height and 1µm in width, thereby imitating the irregularities present on the corrugated electrode surface.

The electroanalysis module within the COMSOL Multiphysics software was used to define the textured surface as the electrode surface (Table 3).

In order to set distinct concentrations for our reactants, the reduced form was Set at $2*10^{-3}$ $^{mol}/_{l}$, while the oxidized version was initialized at a zero concentration to imitate the same environment for CV setup with 2mM potassium ferrocyanide solution.

Both the reduced and oxidized forms were set to have a consistent diffusion rate set at $1*10^{-9}$ m^2/s, ensuring that any differential outcomes in redox activities were predominantly a result

of the design alterations, keeping molecular diffusions constant and similar to the diffusion of ferrocyanide in water [100–102].

The oxidation and reduction potentials were set at 0.8V and -0.4V, respectively. The scan rate was set to 50mV/s. All parameters are similar to the experimental values used for CV experiments. The values for the reference exchange current density and electrical double layer capacitance were adopted from other setups assessing the electrochemical behaviour of surface models in COMSOL Multiphysics [100–102].

Table 3: Parameters used in the COMSOL Multiphysics TM Model

Name	Value	Description
cRed	2E-3[mol/l]	Reduced entities concentration
cOx	0[mol/l]	Oxidated entities concentration
height1	3 - 6 - 12 - 18	Wrinkle height
DcRed	1e-9[m^2/s]	Diffusion coefficient for Reduced entities
DcOx	1e-9[m^2/s]	Diffusion coefficient for Oxidated entities
SR	50[mV/s]	Scan rate for CV
NC	1	Number of cycles for CV
VP1	0.8[V]	Vertext potential 1
VP2	-0.4[V]	Vertext potential 2
RCD	1000[mol/(m^2*s)]*F_const	Reference exchange current density
Cdl	0.2[F/m^2]	Electrical double layer capacitance

3.5 Result and discussion

3.5.1 Effect of different cleaning procedures on the electrode's electrochemical performance

To identify the best cleaning process, we tested various procedures and evaluated their efficacy based on the results from CV tests on the treated electrodes.

Our first method involved immersing the electrodes in IPA and subjecting them to sonication for a quarter of an hour.

Our final attempt involved utilizing an oxygen plasma cleaner for one minute at an oxygen pressure of 0.5 Torr.

From our experiment, it became clear that oxygen plasma cleaning was the most dependable technique for preparing our gold electrodes for biosensor development.

This was evident in the shape of the CV as well as the oxidation to reduction peak ration (figure 5). The IPA sonication proved to be ineffective on the electrodes and partially removed some of the gold from the PVDF (Figure 5b). Additionally, there are no clear oxidation and reduction peaks, implying the surface of the electrode is obstructed by impurities, hindering further electron transfer (Figure 5c). In the second strategy, although the CV graph demonstrated a more distinct duck-shape, the oxidation peak to reduction peak ratio was 41 µA:27 µA, deviating from the ideal 1:1 ratio. This highlights that the electrochemical reaction was not sufficiently reversible for optimal biosensor application.

The third cleaning strategy emerged as a more reliable cleaning method, as the CV graph exhibited a clear duck-shape, as well as an oxidation peak to reduction peak ratio of 50µA:41 µA. Even though this ratio is not ideal as well, the peak-to-peak potential separation in the third strategy was 0.5V smaller than in the second process. This implies that the third cleaning method produced electrodes with more reversible redox reactions.

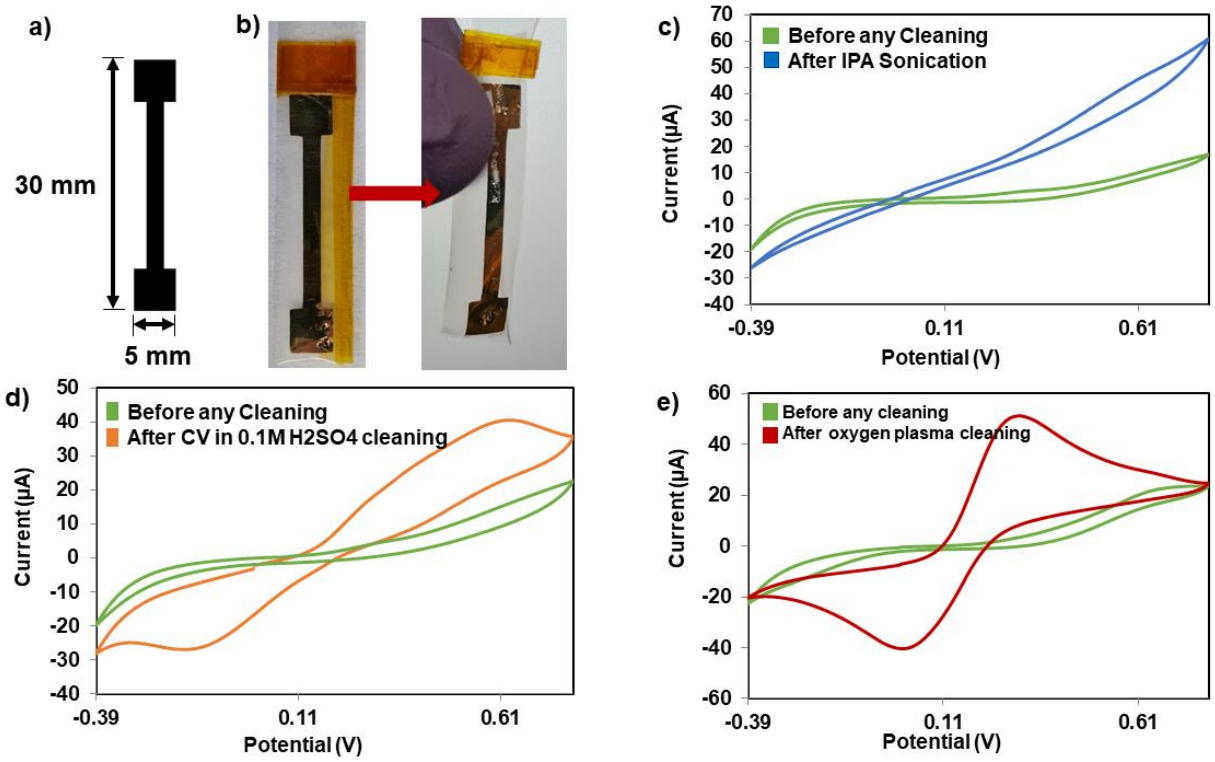

Figure 5: a) Electrode design used as the working electrode for cleaning process optimization. b) IPA sonication effect on gold electrodes. This method severely damaged the electrodes contrary to other methods. c) CV graph of the electrode cleaned through IPA sonication. d) CV graph of the electrode cleaned through 0.1M H_2SO_4 CV cleaning. e) CV graph of the electrode cleaned through oxygen plasma cleaning. The CV "duck" shape in this method is more pronounced, emphasizing a successful cleaning process.

3.5.2 Electrochemical and electromechanical characterization of electrodes

Our observations revealed that the electrodes exhibited resilience to mechanical strain, with the sheet resistance remaining steady at approximately 11 ohms per square (Figure 6). This finding underscores the electrodes' flexibility and their capacity to maintain their electrical characteristics despite being subjected to physical stress, a crucial feature for biosensors intended for wearable applications where the device will inevitably face frequent movement and physical strain.

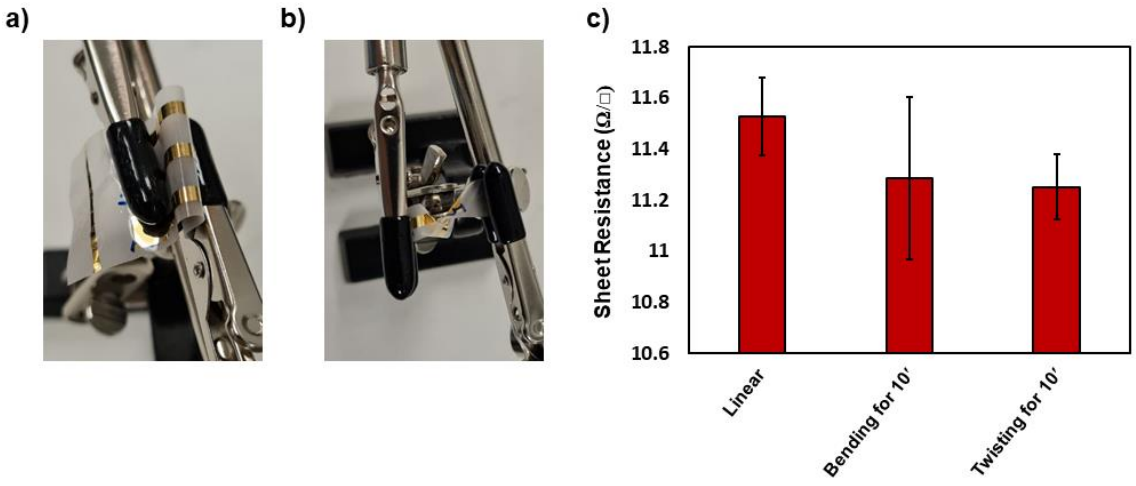

Figure 6:a) Electrodes bent for 10 minutes. b) Electrodes twisted for 10 minutes. c) Sheet resistance measurement of the electrodes after each mechanical deforming.

An analysis was conducted on the cleaned electrodes to check their electrochemical characteristics, utilizing tools such as CV and EIS. For these tests, in order to fully assess the three electrode system, the device's internal gold electrodes were employed, contrasting previous Ag/AgCl and Platinum electrode assisted electrochemical interrogations (figure 7a). From the EIS examinations, a charge transfer resistance (R_{CT}) was recorded at 473.68 Ω. This specific resistance metric is in harmony with the values previously documented for thin film gold electrodes (figure 7b) [103,104].

Looking into the CV evaluations, when probed at a scan rate of 50 mV/s, a distinct oxidation peak was observed, measuring at 100 μA at the 0.1V potential. On the other hand, the reductive surge was detected at -99.4 μA when a -0.08V potential was achieved.

The measured gap in potential between the oxidative and reductive peaks spanned 180 mV. Moreover, the near-equivalent magnitude of these peaks — with their proportion almost mirroring a 1:1 ratio — underscores a back-and-forth redox activity on the electrode's surface (Figure 7c). This balanced activity reaffirms the consistent electrochemical events on these electrodes, making them suitable for readings in wearable sensor platforms.

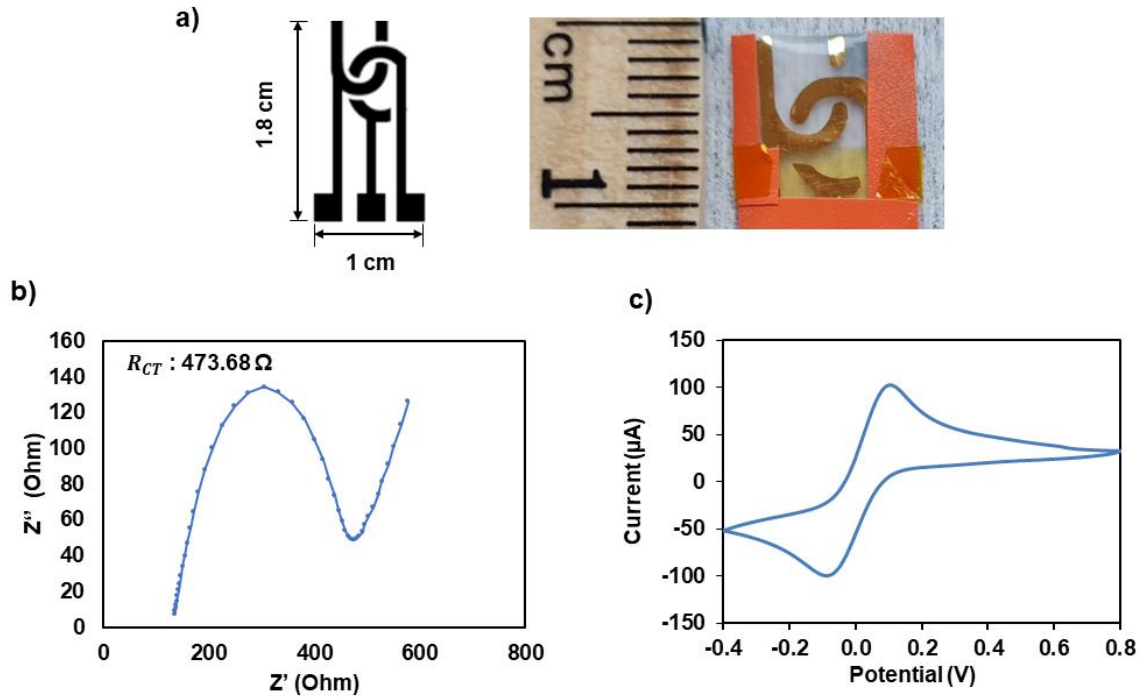

Figure 7:a) Electrode design based on the University of Calgary Logo. b) EIS measurement of the three-electrode based design. c) CV graph of the three-electrode based setup with the gold internal electrodes.

3.5.3 Corrugated electrode morphology and performance

Our investigation demonstrated that the sensors treated with heat for 15 minutes at 170℃ outperformed those treated at other temperatures in terms of electrochemical reactions, with average oxidation current peak of 2.94 ±0.097 µA/mm^2. (Figure 8 and table 4)

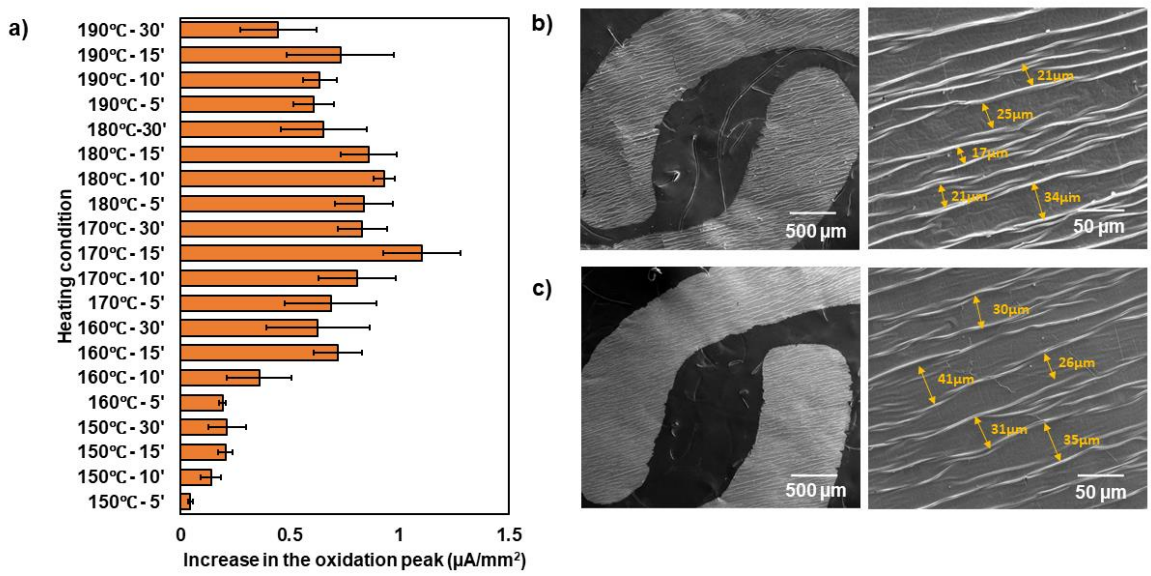

Figure 8: a) The CV performance of 170℃ to 190℃ heated electrodes after heating duration. (n=3) b) SEM images of 190℃ heated electrodes for 15 minutes. c) SEM images of 170℃ heated electrodes for 15 minutes.

The discrepancy in these performances can be tied to the extent of surface corrugation formation each sensor presented. The sensors treated for 15 minutes at 190℃, 180℃, 170℃, 160℃, and 150℃ exhibited a decrease in total geometric area by 42%, 38%, 35%, 11%, and 2% respectively. Interestingly, the sensors subjected to 190℃, despite possessing corrugated surface patterns, didn't perform as well as their 170℃ counterparts in electrochemical testing. The samples treated at 190℃ exhibited a surface wavelength of approximately 23.6±6.4µm, whereas those treated at 170℃ displayed a wavelength of 32.6±5.6µm. These observed values significantly deviate from the theoretically calculated wavelength of 1 µm.

Table 4: Current oxidation peak for 1mm^2 samples for each heating condition (n=3).

Heating condition	Average	STDEV
150℃ - 5'	0.0473	0.0096
150℃ - 10'	0.1406	0.0446
150℃ - 15'	0.2066	0.0316
150℃ - 30'	0.2146	0.0854
160℃ - 5'	0.1946	0.015
160℃ - 10'	0.3606	0.1497
160℃ - 15'	0.7193	0.1089
160℃ - 30'	0.628	0.236
170℃ - 5'	0.687	0.2104
170℃ - 10'	0.8086	0.1773

170℃ - 15'	1.1033	0.175
170℃ - 30'	0.8316	0.1127
180℃ - 5'	0.8393	0.132
180℃ - 10'	0.9306	0.0477
180℃ - 15'	0.861	0.1289
180℃-30'	0.6546	0.1967
190℃ - 5'	0.6083	0.0921
190℃ - 10'	0.6376	0.0769
190℃ - 15'	0.731	0.2461
190℃ - 30'	0.4486	0.1727

The cause for this can be associated with the diffusion effect induced by the intense surface patterns. The distinct wrinkling on the surface may have limited the ionic movement during electrochemical analyses, leading to a lower oxidation peak. A similar effect is seen with the heating duration as well. Electrodes heated in multiple temperatures but for 30 minutes, do not show the same increment in the oxidation peak, and the 15-minute heating durations seems to be optimal (Figure 9).

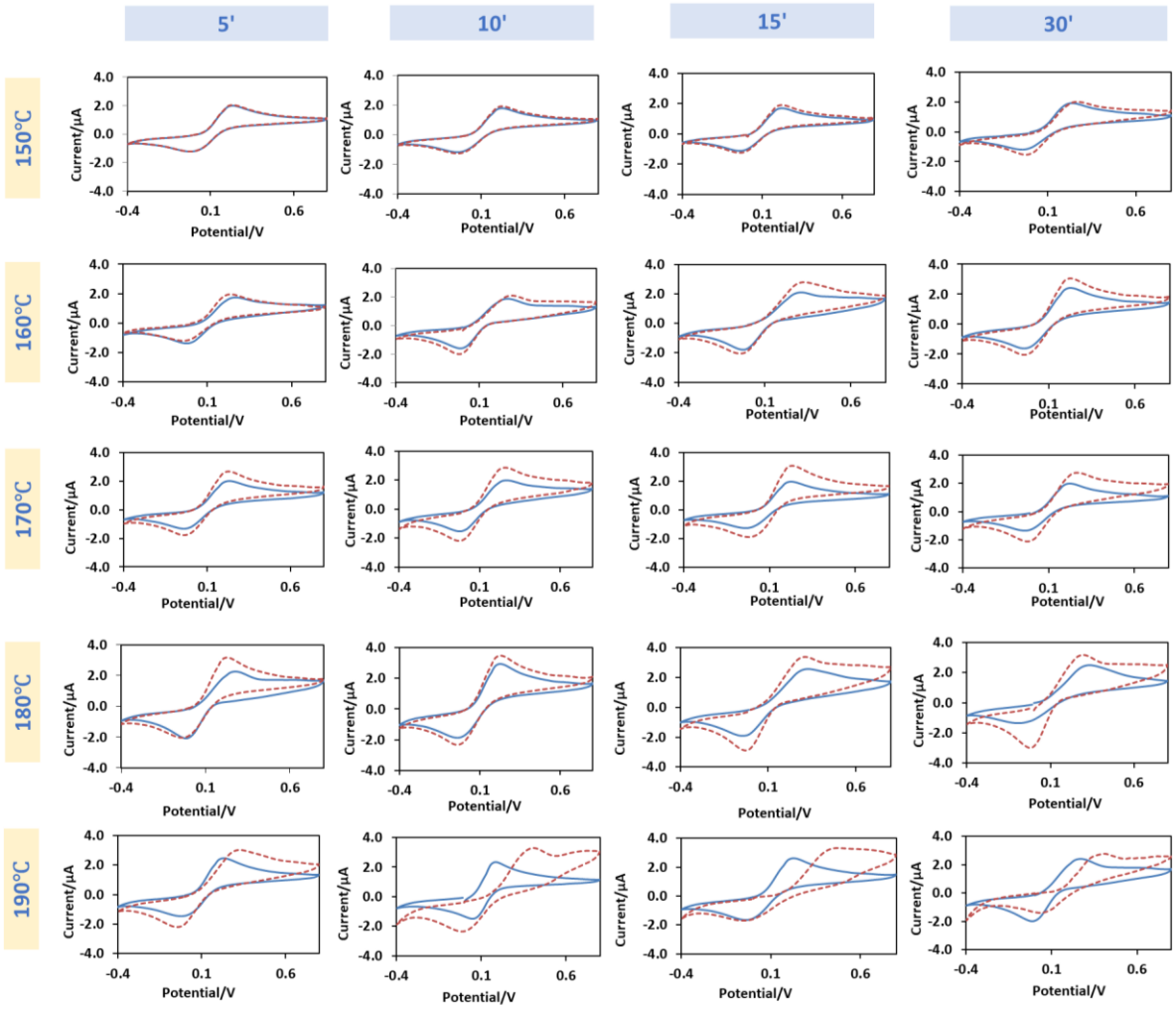

Figure 9: Comparison of all CV graphs before (blue line, representing planar sample group) and after (red dotted line, representing wrinkled sample group) heating with different conditions. Each graph is the average of three samples.

Figure 10 presents a comparison between the morphology and electrochemical behavior of an electrode heat-treated in optimized conditions versus a planar electrode. The study focused on the effect of corrugation on reference and counter electrodes. This was done by maintaining a corrugated working electrode and alternating between modified (corrugated) and non-modified (non-corrugated) versions of the reference and counter electrodes. Analysis of the oxidation peaks revealed that the peak current for the non-corrugated reference and counter electrodes was 5.77±0.19, whereas it was 5.83±0.10 for the corrugated counterparts. Comparing these oxidation peaks indicates that the increased surface area for the corrugation

of the reference and counter electrodes does not significantly impact the peak current (Figure 10d).

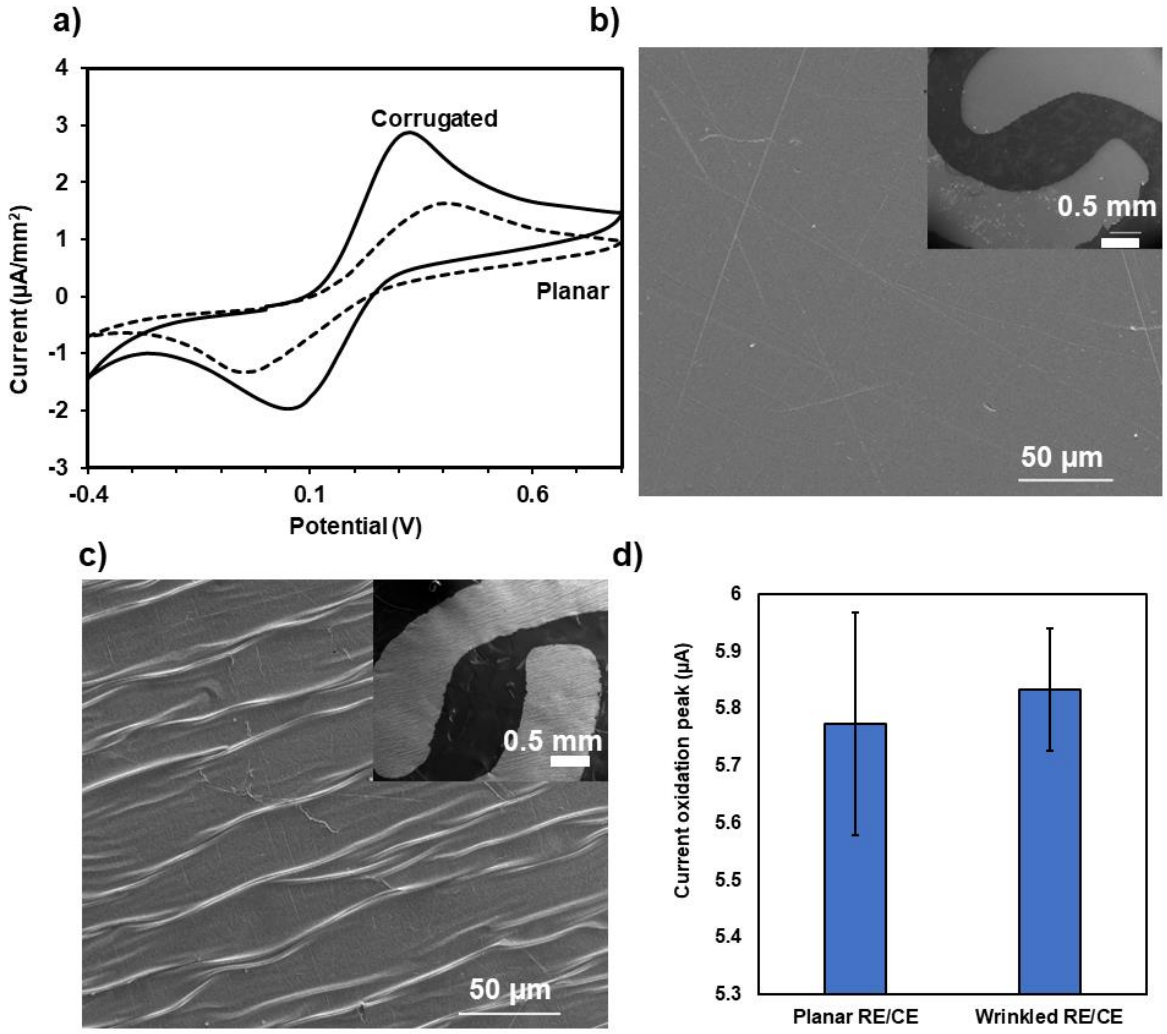

Figure 10:a) Electrochemical cyclic voltammetry study of the planar and corrugated sensors. b) SEM images of planar sensors (inset: the working electrode area), c). SEM images of corrugated sensors (inset: the working electrode area). d) comparison between the planar and corrugated reference and counter electrode.

Another observation was the influence of the PVDF roll's initial orientation on the direction of contraction. This behavior can be attributed to PVDF's unique manufacturing process, where it's first stretched and then rolled up. Due to this process, the material would contract in a specific direction. The orientation of the vinyl masking during its placement on the PVDF influenced whether the final electrode contracted sideways or lengthwise. However, when

both configurations were tested through CV, there was no discernible difference in their operational outputs, as they both show similar gaps in the potential peaks and similar oxidation to reduction peaks (5µA: 4.5µA for horizontal shrinking and 5.3µA:4 µA for vertical shrinking). (Figure 11)

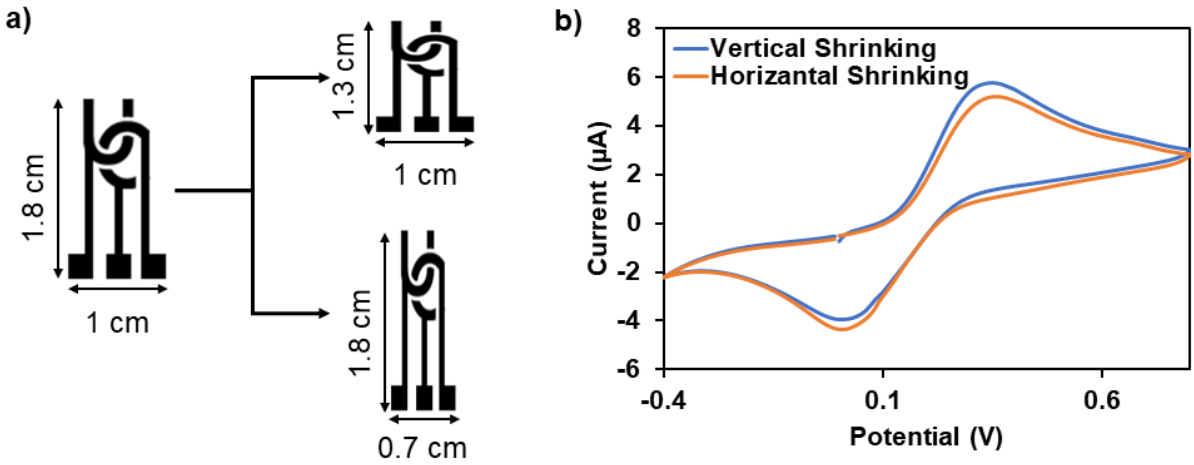

Figure 11:a) Horizontal and vertical shrinking of the electrodes after the heating process. b) CV performance of each shrunk electrode.

In testing various logo electrode designs for the Captain Patch biosensor, we observed distinct outcomes tied to their dimensions, especially during the heat-treating process. As illustrated in Figure 12, the longer electrodes were prone to complications, notably cracks after wrinkling. Increasing the thickness of the connecting arms was not effective since the number of non-functional electrodes was also high. In contrast, the unmodified design measuring 1.8 cm by 1 cm presented the lowest non-functional electrodes. This design yielded more consistent functional wrinkle-induced electrodes.

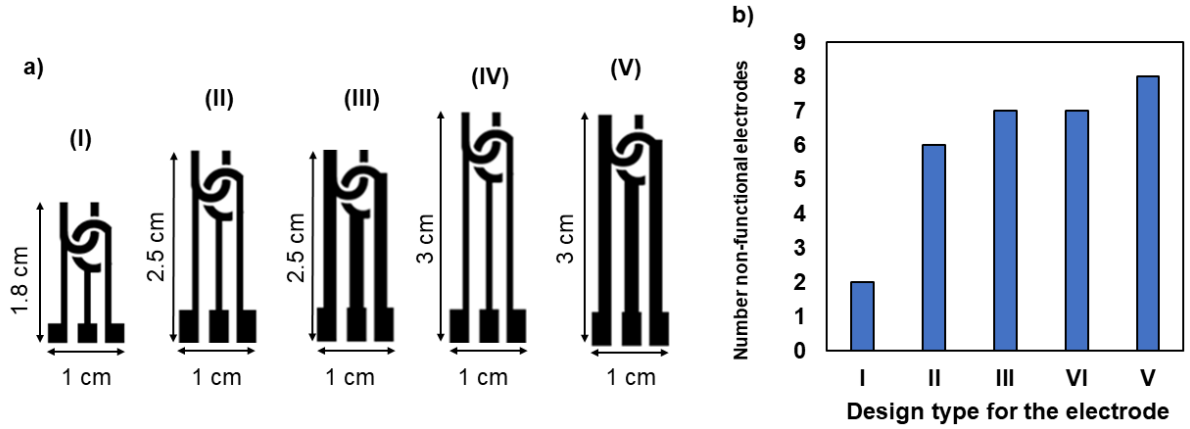

Figure 12: a) Different logo electrodes designed for the Captain Patch biosensor. During the heat-treating process, longer electrodes showed crack production and induction after wrinkling. b) Number of dysfunctional electrodes after heat-shrinking due to crack production in a batch of 10.

Following the observation of crack propagation in the longer electrodes, a heating regimen was adopted to determine if it could reduce the number of dysfunctional extended electrodes compared to the previous experiment where heat shrinking was not applied. As illustrated in Figure 13a, there was a slight decrease in the number of non-functional electrodes across all designs, though the proportion of functional electrodes remained low in a batch of 10 for each electrode type. Furthermore, Figure 13a demonstrates that the original electrodes, measuring 1.8 by 1 cm, resulted in a higher number of functional electrodes. This suggests that these dimensions are more conducive to heat shrinking and subsequent applications.

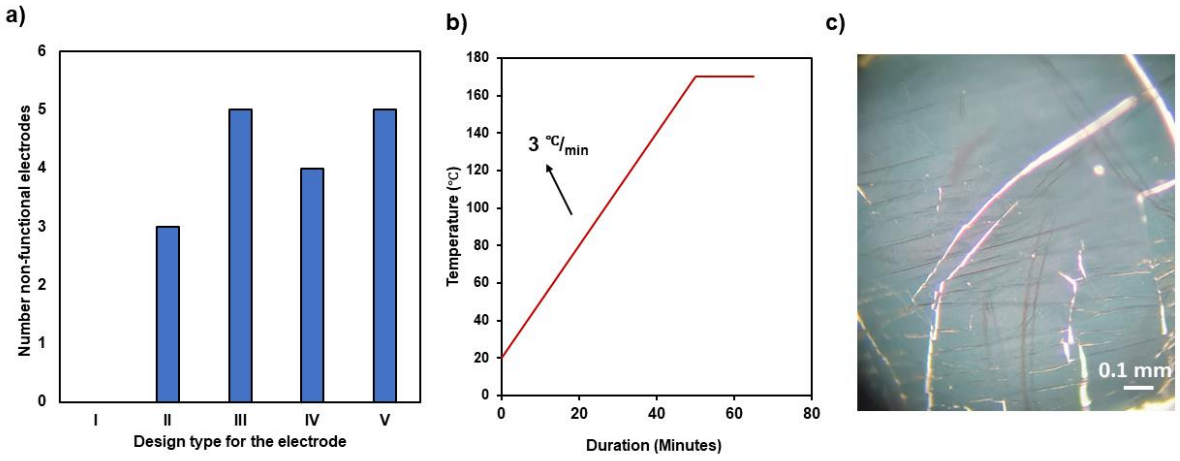

Figure 13: a) Number of dysfunctional electrodes after heat-shrinking with a heating regimen in a batch of 10.b) Heating-regimen graph used for the heating process. c) Picture of a crack in a wrinkled electrode under a 10X Olympus CH30RF100 optical microscope.

3.5.4 Corrugated surface simulation

The software program COMSOL Multiphysics™ was utilized to create a model of a structure with similar surface wrinkling, providing valuable insights into how such surface features influence the available reactive surface area.

The output of this model reinforced our initial observations, indicating that the textured sensor could enhance the surface-to-volume ratio and, therefore facilitate redox reactions more efficiently. Also, with the increase in the height of the corrugation, simulated CV shows greater redox activity. It is observed by inducing wrinkles with 18 µm height and comparing it to the planar model, the oxidation peak alternates from 0.376µA to 0.482 µA (Figure 14).

Our simulation outcomes further underscore our primary findings, emphasizing that a corrugated sensor layout can effectively increase the ratio between surface and volume, improving redox activities more effectively.

Variances in the wrinkle's height or amplitude introduced in the model led to changes in its electrochemical activity. As an illustration, using an amplitude of 18 µm to compare with a basic design showed pronounced shifts in the oxidation peak. Yet, even at a subtle height

change of 3 µm, there was an evident deviation when contrasted with a completely flat contour.

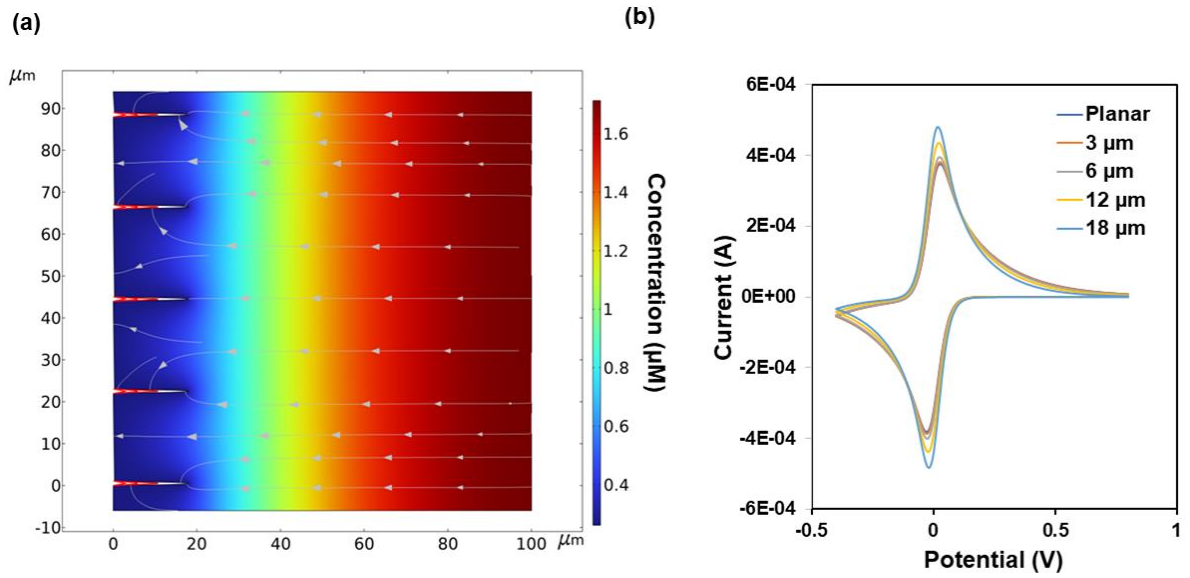

Figure 14: a) 2D model of the cross section of a corrugated electrode with their relative concentration gradient of the oxidated and reduced species during the CV process. b) A demonstration of the current peak increment due to the increase in the corrugation height.

3.6 Conclusion

In light of the experimental results and analyses provided, it can be concluded that the optimization of both physical and electrochemical properties is vital for the performance of biosensors. The cleaning procedure employed is critical, and our results showed that oxygen plasma cleaning was more dependable, as evidenced by the CV graph displaying a distinct duck-shaped curve, along with an oxidation to reduction peak ratio of 50µA to 41µA. Although this ratio is still not optimal, the potential gap between the peaks in this cleaning method was 0.5V less than that observed in the sulfuric acid cleaning process.

In addition to the cleaning process, the characterization of electromechanical properties of the electrodes were maintained stable, even under mechanical strain. Electrochemical characterization revealed a clear oxidation peak at 100 µA at a 0.1V potential, while a

reduction peak was observed at -99.4 μA at -0.08V, indicating a close to 1:1 ratio of oxidative to reductive activities. This balance suggests a consistent back-and-forth redox process on the electrode's surface and confirms the suitability of these electrodes for use as biosensors.

Simulation played a key role in better understanding the potential effects of a textured surface on the electrode. The computational study suggested that a corrugated surface could considerably enhance the surface-to-volume ratio, and therefore the biosensor's electrochemical properties. This was confirmed in our subsequent experiment, where we found that heat-treated sensors displayed ripple-like surface patterns, improving their performance.

The study found that sensors heat-treated for 15 minutes at 170℃ displayed superior electrochemical reaction performance, with an average oxidation current peak of 2.94 ±0.097 μA/mm², compared to other electrodes. This enhanced performance is attributed to a balance between surface corrugation and diffusion effect. Sensors treated at temperatures ranging from 150℃ to 190℃ showed a reduction in the total geometric area by 2% to 42%, with those treated at 190℃ having corrugated surfaces yet underperforming in electrochemical tests compared to the 170℃ group.

Furthermore, a similar effect was observed with the duration of heating. Electrodes heated at various temperatures for 30 minutes did not exhibit the same increase in oxidation peak as those heated for 15 minutes, suggesting that a 15-minute heating duration is optimal for achieving the best electrochemical response. This finding underscores the importance of both temperature and duration in balancing the effect of corrugation and diffusion.

The orientation of the vinyl mask applied to the PVDF dictated whether the final design for the electrode contracted sideways or lengthwise. When these configurations were evaluated using CV, their operational outputs were similar, regardless of the contraction direction. Both

configurations exhibited comparable potential peak gaps and nearly equivalent oxidation to reduction peaks (5µA: 4.5µA for horizontal shrinking and 5.3µA: 4 µA for vertical shrinking). This finding suggests that the direction of PVDF contraction does not significantly influence the electrochemical performance of the electrodes.

The length of the logo electrode designs is important, particularly during heat treatment. Longer electrodes tended to develop cracks following wrinkling. Attempts to increase the thickness of the connecting arms did not prove effective, as the number of dysfunctional electrodes remained high. The original electrode design, measuring 1.8 cm by 1 cm, exhibited the least number of non-functional electrodes. This suggests that longer electrodes are not suited for wrinkling. Similar results were also observed when a heating regiment was adopted, however the number of dysfunctional electrodes was reduced in all electrode designs.

Using COMSOL Multiphysics™ to model a wrinkled surface structure, it was found that textured sensors with an increased surface-to-volume ratio could enhance redox reactions more efficiently. Simulations showed that higher corrugation, like wrinkles of 18 µm height, led to a significant increase in redox activity, evidenced by a change in the oxidation peak from 0.376µA to 0.482 µA. It is important to note that the simulation does not outline the effect of diffusion on the electrochemical behavior of the CV since the diffusion coefficient for the model was set to constant. Therefore, deviating from the experimental results where higher corrugation was causing lower electrochemical activity.

Chapter 4 : Assay design, optimization, and validation

4.1 Contribution

Within this chapter's progression, Irvyne Aradnas (Undergraduate Summer student) supported the assay design and its subsequent evaluation, giving valuable assistance to the overall process.

4.2 Key research questions

At the outset of our study into improving biosensors, especially those directed by aptamers, we had a set of guiding inquiries. We aimed to grasp the role of the buffer makeup in ensuring that concaptamers fold correctly and remain stable, leading to better analyte binding. Specifically, we looked at how the amount of $MgCl_2$ in this buffer might change the results when comparing cortisol-treated samples with control ones. We also wanted to know how long cortisol should be in contact with the sensor to get a clear reading, and if altering this duration might compromise accuracy. When evaluating the design of electrodes, we wondered if those with a textured surface might work better than smooth ones because of the potential for more interactions due to the increased surface area. We also hoped to determine the best amount of concaptamer to place on the sensor, aiming for a mix of good results, sensitivity, and affordability. Although many might assume that textured surfaces would offer better molecular binding due to their increased area, we asked if this was true when working with concaptamers compared to other aptamers. These central questions directed our comprehensive examination into making biosensors more effective and trustworthy.

4.3 Introduction

Developing a successful biosensor requires a sequence of procedures, including design, fine-tuning, and validation. These stages ensure that the biosensor operates efficiently and accurately and is sensitive to the analyte of interest, making it fit for practical usage.

As previously noted, when the aptamer comes into contact with its biomarker, it undergoes a conformational change. This change can be harnessed to develop a transduction mechanism that generates an electrochemical signal, aiding in biomarker detection. The conformational shift alters the distance between the head of the concaptamer, modified with an MB redox reporter, and the electrode surface. Such a variation is detectable through changes in the intensity of the MB reduction signal in SWV. As the distance between the electrode surface and the redox reporter decreases, the SWV signal intensifies, which can be effectively utilized for biomarker detection (Figure 15).

It is essential to highlight that only those aptamers capable of undergoing a hairpin conformational change are suitable for this mechanism. This specific structural transition results in a reduced distance between the 3’ end of the concaptamer and the electrodes. The original, non-concatenated aptamer, which possesses a B-DNA type structure, is apt for this purpose due to its ability to exhibit such conformational changes [105].

Therefore, it is essential to determine whether the concatenation of the aptamer has altered its conformational mechanism. To achieve this, circular dichroism (CD) is performed on the concaptamers, and the results are compared with those of the original aptamer to identify any significant differences.

Circular Dichroism is a spectroscopic technique used to analyze the binding affinity of an aptamer to a specific biomarker and to observe conformational changes in the aptamer upon

target binding. CD measures the differential absorption of left and right-handed circularly polarized light by chiral molecules. This method is particularly sensitive to the secondary and tertiary structures of biomolecules, such as nucleic acids and proteins [105].

For the original aptamer, the CD spectra displayed a negative peak around 237 nm and positive peaks at 220 nm and 268 nm, confirming the stem-loop B-DNA structure. The CD analysis further indicated that upon cortisol binding, there was a noticeable change in molecular ellipticity, suggesting target-induced structural changes in the aptamer. CD profile for the concaptamer is expected to exhibit behavior similar to that observed in the original aptamer [105].

CD's utility is especially pronounced in studying aptamer-biomarker interactions. Binding induces a notable conformational change in the aptamer, detectable through variations in the CD signal.

Biosensor development begins with the assay design phase, where the assay solution, is prepared. Part of this process is choosing a suitable binding buffer, a solution that retains the concaptamer’s stability and functionality, thereby promoting the concaptamer’s interaction with the target. The selection of the buffer depends on several factors, such as pH, ionic strength, and the presence of stabilizing agents.

Tris(hydroxymethyl)aminomethane Hydrochloride, often referred to as Tris-HCl, is a frequent ingredient used in binding buffer mixtures. It's predominantly utilized to sustain and regulate the solution's pH. It exhibits buffering capabilities within the pH window of 7.0 to 9.0, a spectrum suitable for the concaptamer’s redox component. A suitable pH range is integral to the stability of methylene blue since the redox reaction is highly sensitive to pH alternation [63,106,107]. Consequently, a consistent Tris-HCl concentration is instrumental

in maintaining the correct pH values for the concaptamer and the effective operation of other buffer constituents.

Another binding buffer component is Sodium Chloride (NaCl). NaCl enhances the ionic potency of the solution, affecting the bonding interactions between the concaptamer and the molecule it targets. This is particularly noteworthy if the target molecule is electrically charged, with Na+ and Cl- ions serving to counterbalance the charges and promote bonding. Additionally, NaCl aids in stabilizing the buffer and preserving the solubility of biological molecules. [80,81].

Magnesium chloride ($MgCl_2$) in the binding buffer is also crucial for supporting the structural integrity of concaptamers. In the case of concaptamers, $MgCl_2$ assists in preserving their three-dimensional form.

In unison, these ingredients formulate a buffer that sustains a consistent environment in pH and ionic strength, while also establishing the necessary conditions for effective concaptamer function. This is vital for yielding dependable and uniform results in your investigative studies.

Concaptamers exhibit a strong affinity for their target molecules, such as proteins, and bind with a high degree of specificity. Their binding capacity hinges largely on their distinct three-dimensional conformation, a feature that $MgCl_2$ helps maintain, enabling effective binding of the aptamer to its target [80,81].

However, it's crucial to apply the correct $MgCl_2$ concentration. Insufficient amounts may fail to provide ample concaptamer structure stabilization, while excessive quantities could potentially disrupt other buffer constituents. In a biosensor, this 3D structure of the concaptamer is instrumental as it facilitates the identification and quantification of

biomarkers. As is the case with all binding buffer components, the optimal $MgCl_2$ concentration should be ascertained, considering the specific demands of the assay.

Consequently, the composition of the binding buffer closely aligns with that used in other research, maintaining identical concentrations of NaCl and Tris-HCl, while exploring the optimal concentration of $MgCl_2$ for the buffer. The binding buffer constituted 50mM Tris-HCl and 137mM NaCl, with $MgCl_2$ concentrations tested at 1, 5, 10, and 15 mM. The $MgCl_2$ concentration selected is in line with the ranges commonly used in similar studies [22–24,27,49,108,109].

Following the design stage is assay functionalization, where the prepared assay is attached to the sensor surface. The functionalization techniques can differ depending on the material of the sensor, the nature of the assay, and the required orientation of the biorecognition component for optimal analyte binding [82].

To functionalize the electrodes, the concaptamer solution mixed with binding buffer is heated for 5 minutes at 90°C. Warming up the concaptamer mixture at elevated temperatures like 90°C is known as "Refolding." This heating process straightens out the folded concaptamers, ensuring they don't have any folds that might limit their effectiveness. This step is essential for maintaining consistent results when embedding concaptamers on surfaces like electrodes [18].

After the refolding process, the concaptamer solution, is mixed with a 1mM Tris(2-carboxyethyl) phosphine (TCEP) solution. TCEP is crucial for reducing the thiol group attached to the concaptamer, thereby activating the thiol groups for the subsequent concaptamer functionalization step. This activation is essential for their effective attachment to the gold surface. To ensure the complete activation of all thiol groups linked to the concaptamer assays, the concentration of TCEP is maintained at a level a hundred times

higher than that of the concaptamers. Once prepared, the solution undergoes incubation, after which it is drop-cast onto the surface area. This step is pivotal in forming a SAM through thiol-gold chemistry. The amount of solution drop-casted on the working electrode, depends on the size of the electrode. In this case, 10µL was enough to cover the entire surface of the working electrode with the concaptamer solution to produce a SAM. It is worth mentioning that only the working electrode surface needs to come in contact with the prepared concaptamer solution for the biosensing application. The SWV needs to measure the methylene blue reduction peak from the surface of the working electrode only [30,110].

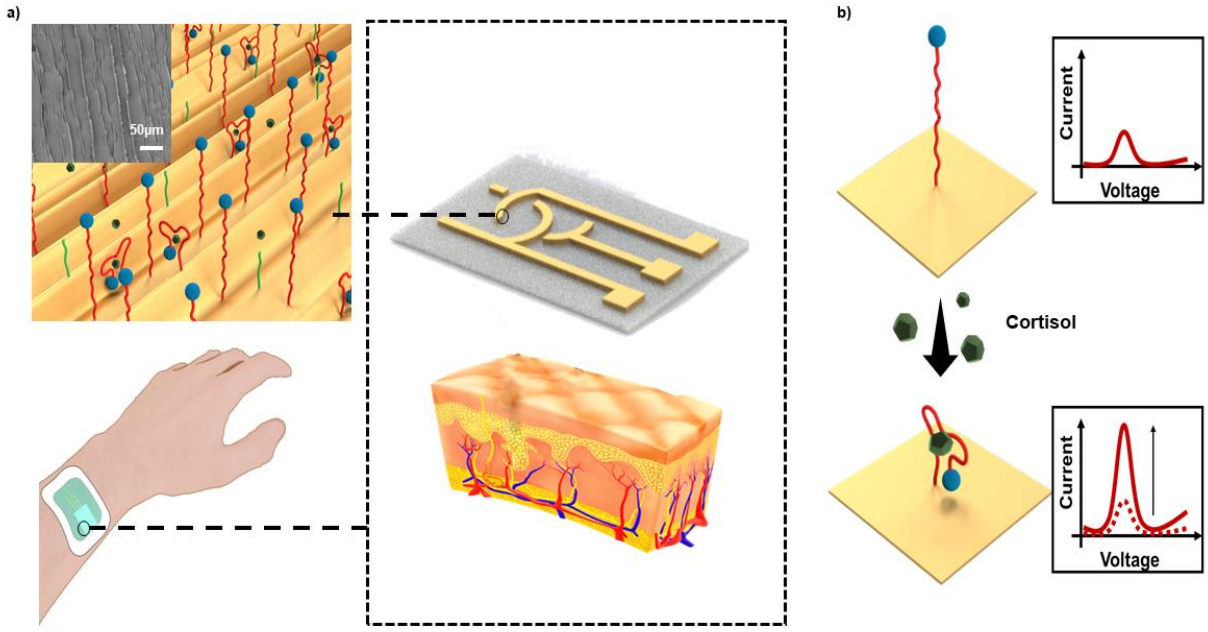

Figure 15: a) General scheme of Captain Patch that can detect cortisol in human sweat. A schematic of the functionalized corrugated sensor surface (inset: an SEM image of the corrugated sensor surface). b) A schematic of the biosensor before and after analyte introduction.

In the next step, 6-Meconcaptamerptohexanol (MCH) is added to electrodes that have already been functionalized with the concaptamer. MCH plays a crucial role in orienting the concaptamer molecules upright, thereby enhancing their three-dimensional structure which is key for effective biosensing. Additionally, MCH acts as a covering agent for the remaining gold surface on the electrode. This is important because it minimizes the exposure of any

excess gold surface, which could otherwise interfere with the SWV readings. A concentration of 100 µM MCH is used, as this amount is generally sufficient to adequately cover most of the gold surface and is widely adopted by other studies for similar applications [17,21,77,82,84,111].

The next step after functionalization, is assay optimization, where the operating conditions of the biosensor are adjusted to ensure the highest efficiency and reliability. This stage involves tweaking various parameters such as the concaptamer's concentration, and incubation duration. The goal here is to identify the conditions that yield the best performance in terms of signal detection for 1µM cortisol solution made with DI through SWV. A 1µM concentration in DI was selected as it represents a high potential cortisol level detectable in sweat, while limiting other chemical compound interference by using DI [112–114]. This elevated concentration was chosen to ensure a pronounced signal compared to the blank, facilitating the observation of effects resulting from modifications in parameters like binding buffer composition, concaptamer concentration, or incubation duration. This approach simplifies the identification of parameter impacts on biosensor performance.

As the next optimization process, the density of the concaptamer on the electrode's surface was studied as it is a critical determinant of the performance of concaptamer-guided sensing. The concaptamer concentration impacts the detection signal of the biosensor.

Packing the electrode's surface excessively with bioreceptors can lead to steric hindrance, a situation where the physical limitations of the sensor obstruct the efficient binding of the analyte to the bioreceptor and limit the 3D conformational change in the concaptamer after binding to the analyte. This could deteriorate the functionality of the biosensor. [83,84].

Therefore, it is indispensable to make a balance in the number of bioreceptors structured onto the electrode surface. This process of optimization ensures that the biosensor is adequately

equipped with bioreceptors to effectively detect the target analyte without creating a scenario of overcrowding leading to steric hindrance. In previous studies, bioreceptor concentrations have ranged from 0.5 µM to 10 µM, depending on the available surface area *[21,52,115–117]*. Consequently, this study explores the effects of concaptamer concentrations at 0.5 µM, 1 µM, and 1.5 µM on the detection signal for 1 µM cortisol. This approach aims to determine the optimal concaptamer concentration for effective cortisol detection. The number of concaptamers attached is then evaluated using chronocoulometry to ascertain whether the concaptamer density is sufficient for detecting 1 µM cortisol and to confirm the availability of adequate binding sites for cortisol at these concentrations *[118]*.

In order to quantify the concaptamer concentration on an electrode surface, a strategy was used to quantify immobilized concaptamers on gold involved leveraging the electrostatic attraction between specific redox cations, in this case 1mM ruthenium(III) hexaammine (RuHEX) concentration in Tris-HCl and the concaptamer's phosphate backbone. The coverage of probe concaptamer on an electrode surface is determined by the number of cationic redox molecules that electrostatically bind to the anionic concaptamer backbone. These cations compensate for the concaptamer's anionic phosphate groups. In a solution, these cations are unstable, easily exchanging with other solution cations. The strength of the association between concaptamer phosphates and cations increases with the cation's charge. When concaptamer-modified electrodes are placed in a low ionic strength electrolyte with a multivalent redox cation, these cations replace the native compensation cations and become trapped at the interface. This amount is measured using chronocoulometry [118]. Chronocoulometry can differentiate between charges from surface-bound reactions and those from diffusing redox molecules, allowing for accurate surface-confined species measurements. The surface excess of the redox marker is calculated from the chronocoulometric intercept differences in experiments with and without the redox marker.

For meaningful concaptamer surface density calculations, saturation conditions, where redox markers completely compensate concaptamer charge, are essential. The saturated surface excess of the redox marker is then converted to concaptamer surface density, taking into account the concaptamer's molecular characteristics and Avogadro's number:

$$Q = \frac{2nFA\sqrt{D_0 C_0}}{\sqrt{\pi}}\sqrt{t} + Q_{dl} + nFA\Gamma_0 \quad \text{(Equation 4)}$$

In chronocoulometry, the key parameters include n (number of electrons per molecule during reduction, which is one in our case), F (Faraday constant, in Coulombs per equivalent), A (electrode area in square centimeters), D_0 (diffusion coefficient in square centimeters per second), and C_0 (bulk concentration in moles per square centimeter). The capacitive charge, Q_{dl} (in Coulombs), and $nFA\Gamma_0$ the charge from the reduction Γ_0(mol/cm^2) of adsorbed redox marker are also crucial. The Γ_0 represents the surface excess, indicating the amount of redox marker confined near the electrode surface. The chronocoulometric intercept at time zero includes the double-layer charging and surface excess. Surface excess is determined by comparing chronocoulometric intercepts with and without the redox marker. Accurate conversion of surface excess to concaptamer surface density relies on saturation conditions, ensuring complete charge compensation of concaptamer by the redox marker, as determined from adsorption isotherms. This saturated surface excess is then translated into concaptamer probe surface density, considering the number of bases in the concaptamer, the charge of the redox molecule, and Avogadro's number [118].

$$\Gamma_{DNA} = \Gamma_0(\frac{z}{m})(N_a) \quad \text{(Equation 5)}$$

Γ_{DNA} represents the surface density of the probe in molecules per square centimeter, m denotes the number of bases in the concaptamer, z refers to the charge on the redox molecule, and N_A stands for Avogadro's number [118].

The surface area for the working electrode (A) was determined through a CV analysis, scanning from 0 to 1.5 V in a 0.1 M H_2SO_4 solution at a scan rate of 50 mV/s. The electrochemical charge associated with the redox reaction was calculated by integrating the area under the reduction peak. This value was then divided by the charge density required to form a single layer of AuO_x, which is 386 µC/cm².

In equation 4, the electrodes are subjected to testing under conditions where they exhibit similar diffusion effects. These effects, in comparison to the impact of double layer capacitance and the binding of RuHEX, are minimal. Thus, by analyzing the chronocoulometry graphs both with and without RuHEX, parameters such as Q_{dl} and Γ_0 can be accurately determined (Figure 16).

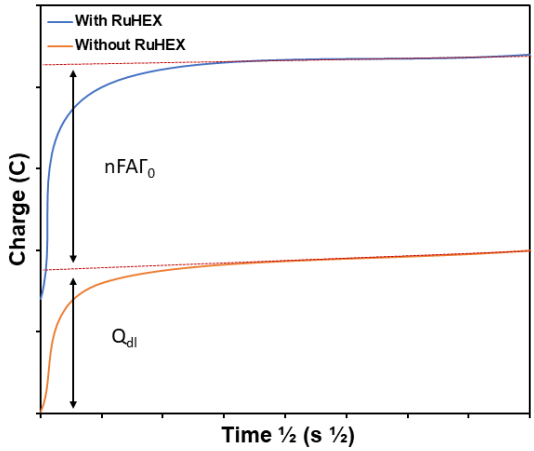

Figure 16:Representation of chronocoulometry graphs before and after testing functionalized electrodes with RuHEX. Q_{dl} and Γ_0 can be determined through the graphs interception with the Y axis.

In CV, the area under the reduction peak is directly proportional to the electroactive surface area of the electrode (Equation 2). This charge is represented by the integrated area under the peak, reflecting the total charge involved in the reduction process. By using a known electroactive species in a controlled setting, the relationship between the charge (as indicated by the area under the peak) and the surface area can be quantitatively established. This allows the electroactive surface area of the electrode to be calculated based on the measured CV

curve in sulfuric acid. It is worth mentioning that the parameters used for the chronocoulometry analysis were taken from previous studies that employed this technique [118].

For the cortisol detection transduction mechanism, our primary objective was to discern the ability of the instrument to detect cortisol levels through SWV Signal. To do this, we utilized SWV, choosing a span from 0V to -0.6V. The reduction of methylene blue is expected to be seen at -0.2V potential [63]. The preset parameters were a 0.025V amplitude and a frequency fixed at 60Hz (anodic negative). The frequency for the SWV was set in a way that did not remove functionalized concaptamers [119,120]. The SWV tests were conducted in a blended solution of 25mM PBS with 25mM NaCl, both before and after the introduction of cortisol to the functionalized electrode. This quantity of electrolyte has previously been established as sufficient for conducting the SWV test. To evaluate the relative variation due to cortisol exposure or controls, the earlier SWV peak current (before cortisol was added) was deduced from the SWV readings seen after cortisol introduction. This derived value, when divided by the first SWV peak current, offered us a normalized perspective on signal variation:

$$\text{Fold Change} = \frac{\text{SWV signal post target deposition - SWV signal pre target deposition}}{\text{SWV signal pre target deposition}}$$

Each stage of the biosensor development process is critical in determining the device's overall effectiveness. Thus, careful attention to each aspect, from assay design to optimization and validation, is vital in fabricating reliable and efficient biosensors.

4.4 Materials and methods

4.4.1 CD Experiment

The secondary structures of both the concaptamers, as well as their interaction with 10µM cortisol solution in 1X PBS (Sigma 10X PBS, Product No. 6505-OP), were assessed using Circular Dichroism (JASCO J-815). In summary, the CD spectra for 250µL of 10µM concaptamer (IDT), prior to and following cortisol binding (European Pharmacopoeia Hydrocortisone CRS, CAS No. 50-23-7), were obtained using a quartz cuvette. A minimum concentration of 10 µM is required for CD analysis. Additionally, the CD spectroscopic readings were taken ranging from 340 to 200 nm, at a scanning speed of 50 nm/min.

4.4.2 Assay preparation and binding buffer

Multiple binding buffers with different concentrations of $MgCl_2$ (Sigma, CAS No. 7786-30-3) were prepared in 50mM Tris-HCl (Sigma, CAS No. 1185-53-1) and 137mM NaCl (Sigma, CAS No. 7647-14-5). The binding buffer was prepared in DI. These concentrations were 1mM, 5mM, 10mM, and 15mM. Each separate buffer was prepared and employed for functionalization.

4.4.3 Assay functionalization on the device

To functionalize the electrodes, the concaptamer solution (IDT) is heated for 5 minutes at 90°C. We then reduce the disulfide group attached to the 5' end of the concaptamer with a reducing agent, i.e. TCEP (1:100 ratio) (Sigma, CAS No. 51805-45-9) to break the disulfide link and avoid dimer formation. The reduced concaptamer was then combined in a binding buffer required for structural conformation (50 mM Tris-HCL; 137 mM NaCl; 1 mM $MgCl_2$) ($MgCl_2$ concentration was optimized previous to this experiment) to make a 1 µM solution, which was drop cast on the working electrode. The electrodes are placed in a humid incubation

chamber at room temperature for sixteen hours. Following incubation, the electrodes were rinsed with binding buffer, backfilled with 100µM MCH (Sigma, CAS No. 1633-78-9), and kept in the humid incubation chamber for another 20 minutes. The electrodes were then rinsed in binding buffer once more before being used to detect the target analyte.

Utilizing SWV, a voltage range from 0V to -0.6V was selected for the tests. The parameters were preset to an amplitude of 0.025V and a frequency fixed at 60Hz (anodic negative). The SWV tests were conducted in a mixed solution of 25mM PBS (Sigma 10X PBS, Product No. 6505-OP) and 25mM NaCl (Sigma, CAS No. 7647-14-5), both prior to and following the introduction of 1µM cortisol solution in DI to the functionalized electrode.

4.4.4. Assay optimization and testing

To figure out the concaptamer (IDT) concentration on the modified electrodes, we turned to chronocoloumetry. For this, a mixture containing 1mM of RuHEX (Sigma, CAS No. 14282-91-8) combined with 10mM of Tris buffer (Sigma, CAS No. 77-86-1) was employed. Functionalized electrodes were dipped in the Solution. Chronocoloumetry was done in two stages (Emstat4S Potentiostat) with standard Ag/AgCl reference electrode (Saturated AgCl/Ag electrode R0302) and platinum counter electrode (0.5*37mm 99.99% purity platinum wire electrode). Once before dipping the functionalized electrode in only 10mM Tris buffer, and second with the RuHEX solution. The parameters for the chronocoulometry were set as follows: time interval at 0.005 seconds, first potential step at -0.4V for 0.5 seconds, followed by the second potential step at 0V for another 0.5 seconds.

The working electrode's surface area (A) was measured using CV analysis, which involved a scan from 0 to 1.5 V in a 0.1 M H_2SO_4 solution (Sigma, CAS No.7664-93-9) with a scan rate set at 50 mV/s. The electrochemical charge linked to the redox process was determined by

calculating the integrated area beneath the reduction peak. Subsequently, this charge was divided by the charge density necessary to establish a monolayer of AuO_x, quantified as 386 μC/cm².

The matter of establishing the a suitable incubation time for cortisol detection was experimented. Tests were carried out with three distinct incubation lengths - a 5-minute, a 15-minute, and a 30-minute time period.

4.5 Result and Discussion

4.5.1 CD spectra testing

Circular dichroism was used to examine how the aptamer's structure was altered by concatenation and interaction with the analyte. CD on the original aptamer identified a negative peak at 250 nm and two positive peaks at 214 nm and 274 nm in the non-concatenated aptamer, indicating a stem-loop B-DNA structure [121,122]. The concaptamer also exhibited a negative peak around 237 nm and positive peaks at 220 nm and 270 nm, mirroring the stem-loop B-DNA structure observed in the parent aptamer (Figure 17). Furthermore, the CD analysis revealed that the presence of cortisol led to a change in molecular ellipticity and in the intensity of the CD signal, signifying target-induced structural modifications in the concaptamer [105,121,122].

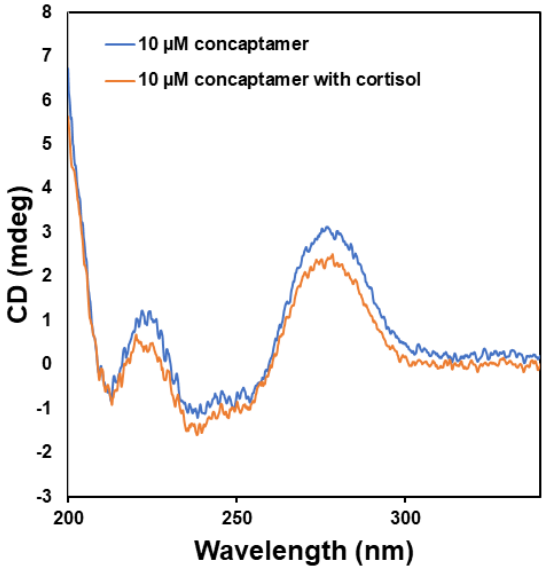

Figure 17: CD spectra of the 10uM concaptamer with and without 10uM cortisol. The concaptamer exhibited a negative peak around 237 nm and positive peaks at 220 nm and 270 nm similar to the original aptamer.

4.5.2 Optimizing the binding buffer composition.

Our investigative procedures have led to the finding that a 1mM concentration of $MgCl_2$ in the binding buffer yields a better signal-to-blank ratio. This conclusion is drawn from a comparative study involving cortisol-treated samples and control electrodes. The application of $MgCl_2$ concentrations apart from 1mM, exhibited a disparity in terms of the observed fold change, with the control samples demonstrating a positive fold change compared to the cortisol-treated ones. This indicates that the anticipated signal, expected to arise from the concaptamer's conformational change, is influenced by the initial 3D structure of the concaptamer. This initial structure is impacted by the concentrations of $MgCl_2$ attached to the concaptamer's negative backbone, subsequently affecting the signal detection. However, this difference was absent when the binding buffer was prepared with a 1 mM $MgCl_2$ concentration. The ratio of the cortisol signal to the blank was higher compared to other concentrations, indicating that the initial structure of the concaptamer prior to interacting with cortisol was favorable. Upon contact with cortisol, the MB redox reporter moved closer to the

electrode, resulting in an increased fold change in the SWV signal. Hence, based on the evidence from our studies, it's crucial to maintain a 1 mM $MgCl_2$ concentration in the binding buffer to ensure precise and dependable outcomes. (Figure 18a)

4.5.3 Optimizing the cortisol incubation time

The results highlight that an exposure window of 30 minutes is most advantageous, yielding a clear 'signal on' response.

Upon assessing cortisol samples with reduced exposure timeframes such as 5 and 15 minutes, the results demonstrated a 'signal off' effect, rather than the anticipated 'signal on'. This implies that the fold change seen in the cortisol-incubated samples, when compared to the fold change in the blank samples, showed minimal difference. This insight suggests that these short exposure durations may not provide the necessary timeframe for the effective cortisol-concaptamer binding and their conformational change, thereby impacting the acquired signal for detection.

However, extending the exposure duration to 30 minutes brought about an improvement in the fold change, resulting in an increased 'signal on' fold-change. This indicates that the extended timeframe facilitated the cortisol-concaptamer binding effectively, thereby enhancing the detection signal. (Figure18b)

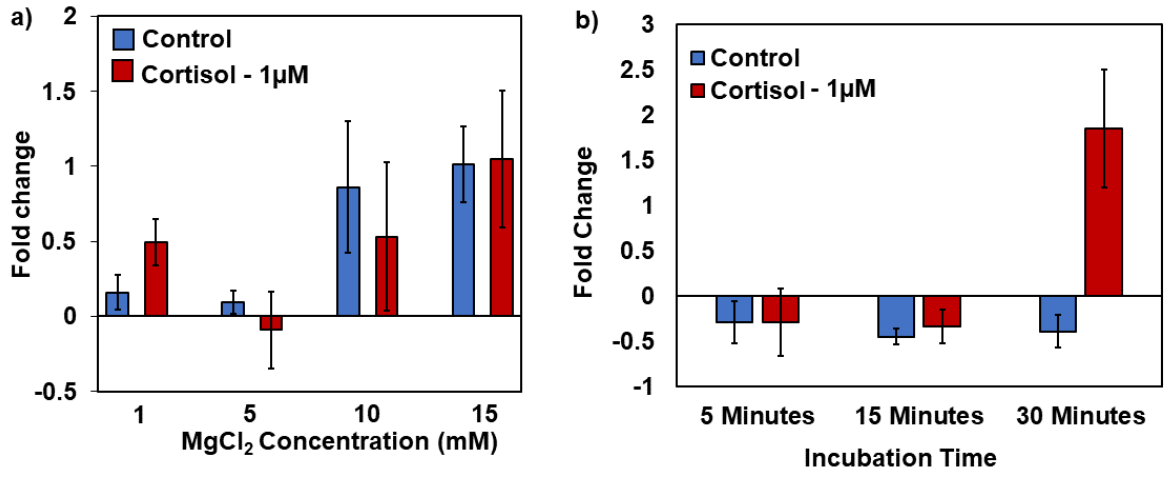

Figure 18: a) Effect of MgCl2 concentration in the binding buffer. b) Effect of cortisol incubation time on analyte detection.

4.5.4 Effect of concaptamer concentration during functionalization

The influence of different quantities of functionalized bioreceptors on the electrode's surface was inspected. Three distinct bioreceptor concentrations were employed – 0.5, 1, and 1.5µM – for surface application on the electrodes.

Evaluating the difference in fold change between control electrodes and those treated with a 1µM cortisol coating yielded an insightful discovery. With a 1µM bioreceptor concentration, the fold change for control samples proved lower than for other concentrations tested. For 1µM concaptamer deposition, the control showed a fold-change of -0.39 ± 0.17. While for 0.5µM and 1.5µM concaptamer deposition, the control showed a fold-change of -0.04 ± 0.09, and-0.05 ± 0.24 respectively. The ratio of the cortisol signal (1.84 ±0.65) to the blank (-0.39 ± 0.17) in samples deposited with 1 µM concaptamer was notably higher than in those with 0.5 µM and 1.5 µM. This indicates that the conformational change of the concaptamers at the 1.5 µM concentration, and thus the transduction mechanism, was hindered by steric effects. Conversely, the 0.5 µM concentration was insufficient and not optimally configured to yield an improved signal-to-blank ratio. (Figure 19a)

4.5.5 Assay functionalized corrugated electrode.

The process of cortisol detection was implemented on two distinct sensor types: those with a planar electrode, and those with a corrugated design.

When the cortisol detection process using SWV signal before and after incubation with cortisol was done, the results revealed that the corrugated sensor, which was functionalized with the assay, presented a higher fold change of 1.84 ±0.65.

Contrastingly, the planar functionalized sensor exhibited a lower fold change of -0.11±0.07. This increased fold change readings in the corrugated biosensor compared to the cortisol signal acquired with the planar electrode, suggests an improvement in the binding or interaction that took place between the assay and cortisol on the corrugated surface. These results are consistent with those obtained in earlier tests using only non-functionalized gold electrodes and ferrocyanide. This suggests that the increased surface area contributed to enhancing the electrochemical detection of cortisol, compared to using a planar electrode. (Figure 19b)

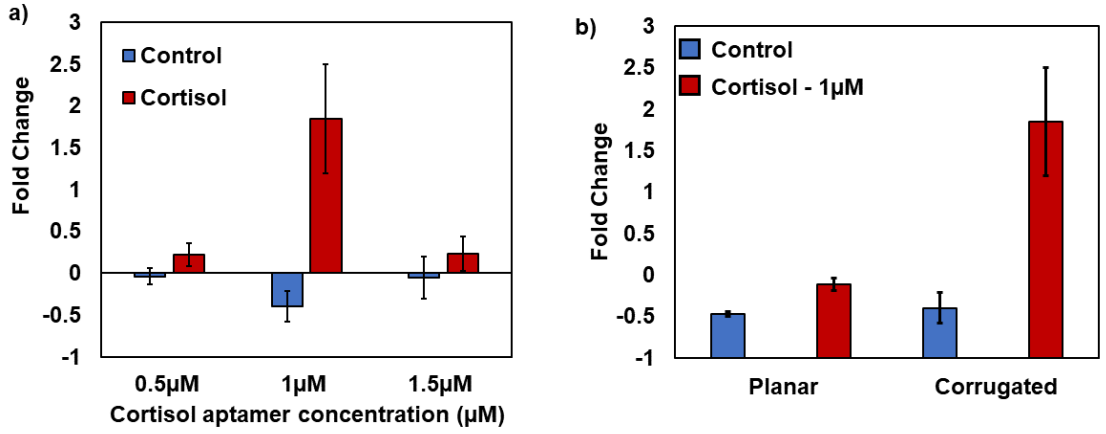

Figure 19:a) Effect of concaptamer concentration on electrodes and cortisol detection b) Comparison between functionalized planar and corrugated electrode for cortisol detection.

4.5.6 Functionalized aptamer quantification for corrugated and non-corrugated electrode.

An investigation into the number of the concaptamers bound to different electrode surfaces was undertaken (all functionalized with 1μM concaptamer). This involved comparing the planar electrodes with corrugated sensor surfaces. These data were acquired by analyzing the electrodes using chronocoulometry. (Table 5)

Table 5: Chronocoulometry data acquired and used for the probe quantification step (n=3).

Sample	$nFA\Gamma_0$ (μC)	reduction charge (μC)	Area (cm2)	Γ_0	Molecule /cm2
Planar electrodes	1.683± 0.076	20.66 ± 1.15	0.054 ± 0.003	$3.23*10^{-10} \pm 0.31*10^{-10}$	$1.42*10^{+13} \pm 0.13*10^{+13}$
Wrinkled electrodes	1.806± 0.050	27.50 ± 2.88	0.072 ± 0.007	$2.6*10^{-10} \pm 0.29*10^{-10}$	$1.15*10^{+13} \pm 0.11*10^{+13}$

The outcomes pointed to a similarity in the number of concaptamers adhered to each of these differing surfaces. More specifically, it was noted that the concaptamer density was approximately $1.4 * 10^{13} \pm 0.1 * 10^{13}$ on the flat sensors, and $1.1 * 10^{13} \pm 0.1 * 10^{13}$ on those with a corrugated layout. In this instance, the surface area of the corrugated electrode (0.072 ± 0.007 cm^2) was found to be larger than that of the planar electrode (0.054 ± 0.003 cm^2). This was determined by evaluating the reduction charge in the CV analysis for the generation of AuO_x species (386 μC/cm^2). This implies that the physical layout of the sensor doesn't significantly affect the adhesion capacity for concaptamers. A general assumption was that substrates with larger surface areas, like those with corrugated designs, should naturally offer

more locations for molecular attachment, thereby improving the overall adhesion potential. Yet, our observations indicate that for cortisol concaptamers anchoring to detection platforms, this might not always hold true.

4.6 Conclusion

CD was employed to investigate structural changes in the aptamer due to concatenation and its interaction with the analyte. CD analysis of the original, non-concatenated aptamer displayed a negative peak at 250 nm and two positive peaks at 214 nm and 274 nm, indicative of a stem-loop B-DNA structure. Similarly, the concaptamer showed a negative peak near 237 nm and positive peaks at 220 nm and 270 nm, closely resembling the stem-loop B-DNA structure of the parent aptamer. This result indicated that the concatenation does not affect the structural behaviour of the aptamer, therefore making it still effective in detecting cortisol levels. Additionally, the CD results indicated that cortisol interaction caused a change in molecular ellipticity and an alteration in the CD signal's intensity, reflecting the target-induced structural changes in the concaptamer.

Our research has determined that a 1 mM concentration of $MgCl_2$ in the binding buffer produces a more favorable signal-to-blank ratio. This finding emerged from a comparative analysis of cortisol-treated samples against control electrodes. Utilizing $MgCl_2$ concentrations other than 1 mM led to variations in fold change, with control samples showing a more positive fold change than those treated with cortisol. This suggests that the concaptamer's initial 3D structure, influenced by the $MgCl_2$ concentration on its negative backbone, significantly affects signal detection.

The findings indicate that a 30-minute exposure window is effective as it increases the fold change for cortisol deposited samples. In contrast, shorter exposure times of 5 and 15 minutes led to a lower fold change for cortisol. This outcome suggests that the fold change in cortisol-

incubated samples, compared to blank samples, was not significantly different with these reduced exposure times.

The study explored the impact of varying concentrations of functionalized bioreceptors on electrode surfaces, using concentrations of 0.5, 1, and 1.5µM for application. The cortisol signal-to-blank ratio in the 1µM concaptamer-deposited samples was higher than those with 0.5µM and 1.5µM. This suggests that a 1.5µM concaptamer concentration might be impeded by steric effects, while a 0.5µM concentration is too low and suboptimal, affecting the potential for an enhanced signal-to-blank ratio. By measuring the number of concaptamers attached to the surface of both corrugated and planar electrodes, it was observed that the number of concaptamers adhering to each type of electrode was quite similar. Although this number falls within a suitable range for biosensor functionality [21,123,124], the reason behind the enhanced fold change is still the increased area. Despite the similar number of concaptamers on each electrode, the corrugation process increased the electrode's surface area. This implies more space for the concaptamers to disperse and a larger area for cortisol to diffuse and interact with the concaptamers.

It should also be noted that the negative fold change observed in some blank samples may be linked to the difference in NaCl and $MgCl_2$ concentrations between the cortisol/blank solutions and the binding buffer, as all formers were prepared in DI water only. Since blank electrodes are incubated in these solutions for 30 minutes without these specific concentrations of salts to stabilize the concaptamer's negative backbone, some deterioration in the 3D structure was anticipated. This could result in the concaptamer folding or losing its optimal 3D structure, leading to a decrease in the SWV signal and, thus a negative fold change for control samples.

Taking into account these optimized parameters, the subsequent step involved utilizing them to further evaluate the assay's effectiveness in detecting cortisol.

Chapter 5 : Analytical validation and assay integration with the device.

5.1 Contribution

For this chapter, Karem Malaeb (Undergraduate summer student) took charge of designing the 3D packaging, using his skills to deliver an accessible and practical design. Habiba Abuelazm (undergraduate summer student), skilled in software engineering, was vital in developing the intuitive Android application, bridging the gap between the user and the equipment. In the realm of electronics, Dr. Kartikeya Murari, drawing from his extensive knowledge, was essential in guiding the device's electronic components to ensure its performance. Recognizing the collaborative spirit that drove the development of Captain Patch, it's essential to acknowledge the invaluable contributions of each expert who lent their specialized skills to this project.

5.2 Key research questions

As we began our investigation into the electronics and android application integrated with the Captain Patch biosensor, several essential questions guided our study. We wanted to see how this sensor works when detecting sweat's cortisol. An important aspect is its ability to differentiate cortisol from other prevalent biomolecules and its precision in detecting slight changes in cortisol concentrations. We were curious about whether its performance was sustained when exposed to the complexities of human sweat. The device's longevity and consistency were also on our mind, leading us to assess how it fares during multiple uses in one day and across longer durations like a full day. We were keen to understand the impact

of concaptamer on the quality of biosensor readings and how effectively it gauges health biomarkers when placed directly on the skin. Given the challenges with the regeneration methods on electrodes incubated with cortisol, we thought of exploring methods to regenerate concaptamers in biosensors. These crucial questions laid the groundwork for our in-depth analysis and reflections on the Captain Patch's functionality in health tracking.

5.3 Introduction

This chapter delves into the next phase in our research progression: the analytical verification of the cortisol-detecting biosensor. The purpose of such a verification procedure is to assess the performance integrity of the biosensor under varying conditions, thus ensuring its dependability for potential real-world applications.

For the initial step, the Detection Limit needs to be determined. Assessing a biosensor's response at different concentrations of the analyte is critical for determining its detection limit. The detection limit, or limit of detection (LOD), is another crucial parameter, referring to the lowest concentration of an analyte that the biosensor can reliably detect, though not necessarily quantify precisely. It's particularly important for applications requiring the detection of trace amounts, such as early disease diagnosis in clinical settings [125]. To determine the LOD, the biosensor's response is measured at decreasing cortisol concentrations in DI and artificial eccrine sweat until the detection signal is undetectable. Initially, the experiment is conducted in DI to establish the biosensor's detection range under ideal conditions, free from any chemical interference. This step is crucial for understanding the biosensor's baseline performance. The upper limit for cortisol concentration is set at 1 µM, a level considerably higher than typical physiological concentrations [40,112], to evaluate the biosensor's maximum detection capability. After gaining an initial insight into the biosensor's range in DI water, the experiment progresses to testing the biosensor in artificial sweat

containing varying concentrations of cortisol (Table 6). This phase starts with the lowest cortisol concentration that was experimentally detected in the DI water tests. The use of artificial sweat in subsequent tests introduces a more complex solution, simulating conditions where sweat with different chemical component come in contact with biosensor during the detection process. This stepwise approach helps in understanding the biosensor's capabilities and limitations in both controlled and slightly more complex settings.

Table 6: Artificial eccrine sweat composition

Component	**Amount**
Sodium Chloride (NaCl)	5 g/L
Ammonium Chloride (NH4Cl)	2.2 g/L
Sodium Hydrogen Carbonate (NaHCO3)	1 g/L
Calcium Chloride (CaCl2)	0.1 g/L
Magnesium Chloride (MgCl2)	0.1 g/L
Potassium Dihydrogen Phosphate (KH2PO4)	0.05 g/L
Disodium Hydrogen Phosphate (Na2HPO4)	0.05 g/L
pH	6.5

The dynamic range of an assay extends from zero concentration to a certain upper limit. However, in reality, assays typically cannot measure analyte concentrations accurately all the way down to zero. There must be enough analyte concentration to generate an analytical signal distinguishable from the analytical noise, which is the signal produced in the absence of the analyte. A common method used to estimate detection limits is calculation from the calibration line at low concentrations, using this equation:

$$LOD = 3.3 \times \frac{S_d}{m} \quad \text{(Equation 6)}$$

Where S_d is the standard deviation of the blank, and m is the slope of the calibration function. For 2nd order polynomial equations, this point is usually either the lowest or highest concentration point where the graph has a steep slope [125]. The estimated detection limits should be validated by analysing a suitable number of samples containing the analyte at these specific concentrations, for which a minimum of three samples should be used. Understanding these parameters is fundamental in tailoring the biosensor to specific applications. Furthermore, LODs are essential benchmarks for comparing biosensors, impacting their regulatory approval and market competitiveness [125]. Thus, evaluating a biosensor across different analyte concentrations provides invaluable insights into its operational capabilities and suitability for various applications.

For the next step, the selectivity and specificity of the assay were assessed. Evaluating a biosensor's response across various concentrations of an analyte is also vital for assessing its selectivity and specificity. Specificity refers to the biosensor's ability to exclusively respond to the target analyte. It's crucial to ensure that the biosensor's response is due to the target analyte alone and not influenced by other substances. Specificity is particularly critical in clinical diagnostics, where the presence of similar biomolecules can lead to false readings if the biosensor is not sufficiently specific. To evaluate the specificity of the biosensor, tests were conducted using other structurally similar steroid hormones, such as Testosterone and Progesterone, mixed in deionized water at a concentration of 1 µM. This approach helps determine the biosensor's ability to distinguish cortisol from other similar compounds (Figure 20). Additionally, the specificity assessment was extended to include other chemical compounds commonly found in sweat that could potentially interfere with biosensing [40,112]. In these tests, glucose and lactic acid were chosen due to their prevalence in sweat. These substances were tested at both their average physiological concentrations typically

found in sweat and the previously used concentration of 1 µM. This comprehensive specificity testing is essential to ensure that the biosensor accurately identifies cortisol in the presence of other similar or interfering substances.

Assessing the biosensor's response across these ranges of concentrations helps in understanding the limits of its specificity. Understanding these parameters ensures the biosensor can reliably detect the target analyte in the presence of other substances, thus making it a dependable tool for various analytical applications.

biomarker	Chemical Structure
Cortisol	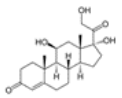
glucose	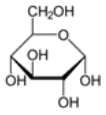
Lactic acid	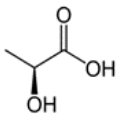
Testosterone	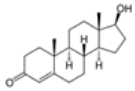
Progesterone	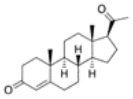

Figure 20:Chemical structure of different biomarkers assessed for specificity [126].

For the selectivity experiment, the functionalized electrodes were tested using DPV. None of the aptamer sequences had any MB modification and in order to detect cortisol levels without MBs, DPV signal was reliable. In order to test the biosensor capability, the process of subtracting the DPV signal after functionalization, from the DPV signal after target incubation, and finally dividing the resulting value from the initial DPV signal was used. In

the case of non-MB-modified aptamer, if the aptamer is specific to cortisol, the fold change should be negative since after the conformational change, the aptamer would practically block the surface of the electrode and prevent charge transfer during the DPV process.

Moving to the next assessment, the regeneration abilities of the assay were studied. Regeneration of a biosensor is a critical process that allows its repeated use for detecting the same or different analytes, essential in applications like industrial process control or environmental monitoring. This process involves restoring the biosensor to its initial state after an analyte detection event. One of the main challenges in regeneration is removing the bound analyte without damaging the bioreceptor's integrity, especially when dealing with sensitive elements like enzymes or antibodies that can be affected by environmental conditions.

Various methods are employed for biosensor regeneration. Chemical regeneration involves using solvents or chemical agents such as sodium dodecyl sulfate to dissociate the analyte from the bioreceptor. These methods, while effective, can be quite invasive and potentially damaging to the bioreceptor. Additionally, they may cause skin irritation, rendering them unsuitable for use in wearable biosensors [127].

An ideal regeneration process should present the biosensor’s signal detection before cortisol deposition over multiple cycles. However, performance degradation is often observed with each cycle, necessitating careful monitoring. Optimizing this process is therefore a pivotal aspect of biosensor development, ensuring their practical utility across various applications.

In the case of the concaptamer, UV light could be used for the regeneration. UV light can cause structural changes in DNA, including aptamers.

This UV exposure causes covalent bonds to form between adjacent bases in the concaptamer nucleotide chain, particularly at the points of their carbon-carbon double bonds. Pyrimidine

dimers are formed when thymine or cytosine bases in DNA undergo photochemical reactions. The most frequent types of UV-induced products are cyclobutane pyrimidine dimers (CPDs) and 6–4 photoproducts. The alterations are expected to induce a three-dimensional structural change in the concaptamer, which we aim to utilize for the release of cortisol through these structural transformations [128].

To test this approach, biosensors incubated with 1 µM cortisol are subjected to one hour of UV exposure, and submerged in DI water. The DI water facilitates the easier removal of cortisol. Subsequently, a signal detection reading is conducted, followed by another incubation of the biosensor with 1 µM cortisol. This cycle is repeated three times with the objective of achieving consistent signal readings and fold change across the tests.

For the next step, the reusability of the concaptamer was studied. The reusability of a biosensor refers to its capacity to be used multiple times. The reusability of a biosensor is determined by its ability to maintain functionality and performance characteristics after multiple cycles of use. High reusability is sought after as a reusable biosensor can significantly cut down on potential costs and waste associated with single-use sensors [119].

The primary issue with biosensors that utilize biological components is their tendency to degrade or denature over time through multiple electrochemical interrogations. Consequently, when exposed to more cortisol, they may fail to produce a signal higher than the previous reading, as their detection capability is impaired by this degradation.

To evaluate the biosensor's repeated usability, a concentration of 1 µM cortisol was applied to the biosensor, followed by an incubation period to observe any signal increase. This procedure was replicated five times over a three-hour period. This approach aims to determine if a single biosensor can be effectively used for at least three successive tests before

necessitating replacement, with three uses being the minimum criterion for it to be deemed reusable.

An important feature of a biosensor is their long term stability. The long-term stability of a biosensor is a critical attribute that determines its effectiveness over extended periods. This stability is essential for the sensor's reliability and is a major factor in its maintenance requirements and shelf life. Long-term stability involves the biosensor's ability to retain its functional characteristics over a prolonged period [129]. Factors influencing long-term stability include the inherent stability of the bioreceptor elements (like enzymes, antibodies, or nucleic acids), storage conditions, and the operational environment [119]. A biosensor that degrades or becomes less effective over time would be less reliable, requiring frequent replacements, which can be costly and impractical, especially in continuous or remote monitoring applications. Therefore, long-term stability is a key consideration in the design and development of biosensors for their sustainable and reliable use in various applications. In order to study this, the functionalized biosensor is left in artificial eccrine sweat for 72 hours, and the average current signal from the SWV is recorded multiple times during this period to assess if there is a signal loss over a long period of time. The biosensor's lifespan in the long term can vary. Commercial glucose biosensors usually last for up to three days on average. Therefore, the long-term stability of the biosensor was studied in the span of three days [42].

On body measurement is also essential for the biosensor assessment step. The subsequent stage concerns the assessment of the biosensor's performance when it is directly placed on the human body. The reason for this test is to see if the human skin is causing interference with the signal readings.

This process was initiated by placing distinct cortisol concentrations (0, 0.01, 0.05, 0.1, 1µM) on the electrodes. The electrodes, once prepared, were applied to human skin to facilitate the

SWV readings while directly attached to the skin. Subsequently, the cortisol-treated electrodes were integrated into a casing made of Ecoflex. This adaptation allowed the biosensor to be comfortably positioned on the skin. The intention behind this variety of cortisol levels was to simulate the array of cortisol values that could be encountered under real conditions. This foundational step was critical to verify the biosensor's capability to reliably detect a broad range of cortisol concentrations.

Desorption analysis was conducted using a UV-Vis spectrophotometer to determine the concentrations of concaptamer that were removed from the electrode surface following each SWV step. The purpose of this analysis was to evaluate the extent of biosensor degradation and the detachment of the concaptamer from the electrode surface due to the SWV interrogation. This is particularly relevant as SWV is known for its potential to dislodge bioreceptors from electrode surfaces [119].

The composition of actual human sweat can significantly impact the readings of biosensors. Real human sweat contains a variety of biological components such as electrolytes, proteins, and metabolites, and it typically has an acidic pH, often close to a value of 5 [40,112]. This acidic environment, along with the complex mixture of substances in sweat, can adversely affect the detection of cortisol by the biosensor. To replicate these conditions, real human sweat was mixed with cortisol at different concentrations to observe the biosensor's response across a range of cortisol levels. Additionally, to further emulate real-life applications, the biosensor was placed on a plastic hand, and SWV interrogations were conducted in this setup.

In the final stage of the study, the biosensor was incorporated into a standalone electronic system and subjected to testing with a 1 µM cortisol concentration. This step was primarily conducted to establish a proof of concept for the device, essentially to verify its overall functionality.

5.4 Materials and methods

5.4.1 Initial analytical performance study

The initial phase involved using functionalized corrugated electrodes and testing them using a series of cortisol (European Pharmacopoeia Hydrocortisone CRS, CAS No. 50-23-7) dilutions in DI, ranging from 1 nM to 1 µM. These electrodes were immersed in cortisol solutions of varying concentrations for 30 minutes.

Utilizing SWV (Emstat4S Potentiostat, a voltage range from 0V to -0.6V was selected for the tests. The parameters were preset to an amplitude of 0.025V and a frequency fixed at 60Hz (anodic negative). The SWV tests were conducted in a mixed solution of 25mM PBS (Sigma 10X PBS, Product No. 6505-OP) and 25mM NaCl (Sigma, CAS No. 7647-14-5), both prior to and following the introduction of cortisol to the functionalized electrode.

Moving to the next phase of assessment, to evaluate the biosensor's functionality in a more intricate medium, various concentrations of cortisol, ranging from 0 to 2µM, were prepared in artificial eccrine sweat (BIOCHEMAZONE CAS No. 7732-18-6).

For this stage, the electrodes were submerged in cortisol solutions with different concentrations for a duration of 30 minutes . For testing, SWV was employed as well, using a voltage range from 0V to -0.6V. The SWV parameters were set with an amplitude of 0.025V and a frequency of 60Hz. The SWV tests were done in a solution of 25mM PBS and 25mM NaCl, both before and after cortisol was added to the functionalized electrode.

5.4.2 Assay specificity performance evaluation

For this specificity assessment, our functionalized biosensors were exposed to several substances commonly encountered in sweat, which might potentially act as interferents. Lactic acid (Sigma, CAS No. 50-21-5), with a physiological concentration typically around

22.5mM [112], and glucose (Sigma, CAS No. 492-62-6), typically seen at concentrations of about 0.1mM [112], as well as a 1µM concentration of both were prepared in DI for this evaluation. 1µM concentration of testosterone (Sigma, CAS No. 58-22-0) and progesterone (Sigma, CAS No. 57-83-0) were also prepared in DI for the specificity test due to their structural similarity to cortisol. Functionalized electrodes were incubated with various concentrations of the previously mentioned nonspecific biomarkers for thirty minutes before being tested with SWV. Using a voltage range from 0V to -0.6V, the SWV parameters were set with an amplitude of 0.025V and a frequency of 60Hz. The SWV tests were done in a solution of 25mM PBS and 25mM NaCl, both before and after cortisol was added to the functionalized electrode.

5.4.3 Assay reusability evaluation

To assess the reusability of the biosensor, we carried out a series of repeated tests. This involved depositing 1µM cortisol solutions prepared in DI on the functionalized electrode. The electrode was then allowed to incubate for a period of thirty minutes before being interrogated using SWV. The SWV parameters were set with an amplitude of 0.025V and a frequency of 60Hz, using a voltage range from 0V to -0.6V. The SWV tests were done in a solution of 25mM PBS and 25mM NaCl, both before and after cortisol was added to the functionalized electrode.

This process of deposition, incubation, and probing was replicated five times back to back in the span of three hours on each functionalized electrode to emulate three separate measurements within a single day.

5.4.4 Assay regeneration evaluation

Biosensors that had cortisol deposits were subjected to a sequence of regeneration steps. Initially, the biosensors were submerged in DI. Subsequently, the biosensors were exposed to

a 6W UV light source (DARKBEAM) for an hour. Following UV exposure, the biosensors were washed in a solution of 25mM PBS and 25mM NaCl.

After this step, an assessment of the biosensors was performed using SWV. Spanning a potential window from 0V to -0.6V for our electrochemical assessments, and an amplitude of 0.025V, functioning at a consistent 60Hz frequency.

This entire cycle, consisting of immersion in DI, UV exposure, cleaning with the 25mM PBS/25mM NaCl Solution, and evaluation using SWV, was performed three times. All electrochemical assessments were done in 25mM PBS and 25mM NaCl solution.

5.4.5 Assay long-term repeatability evaluation

To determine the long-term repeatability of our functionalized biosensors, the biosensors were exposed to artificial eccrine sweat. The electrochemical performance of the biosensors was subsequently studied after specific time frames, such as 6, 24, 48, and 72 hours without cortisol deposition using SWV, spanning a potential window from 0V to -0.6V for electrochemical assessments. The parameters were adjusted to an amplitude of 0.025V, functioning at 60Hz frequency.

5.4.6 Assay selectivity performance evaluation

To test the selectivity of our biosensor, we conducted tests using the monomeric cortisol aptamer (no redox/concaptamer modification), the concaptamer and a mutant aptamer that lacks specificity for cortisol (Table 7). In this experimental setup, corrugated sensor electrodes were functionalized with each bioreceptor at a concentration of 1 µM later tested with 1µM cortisol solution in DI using DPV. The DPV measurements (Emstat4S potentiostat), similarly

to the SWV, were taken within a potential window of -0.4V to 0.8V, at a scan rate of 50mV/s, in a solution composed of 25mM PBS and 25mM NaCl, and 2mM Potassium hexacyanoferrate (II) trihydrate (Sigma, CAS No.14459-95-1). This DPV measurement was done both before and after the cortisol incubation step. The achieved DPV signal is later assessed for fold-change validation.

Table 7: Different aptamer sequences utilized in this study

Name	Target analyte	Aptamer sequence
Mutant aptamer	Mycoplasm	/5ThioMC6-D/TTT ACC GAC CGT GCT GGA CTC ACG TCG TCC ATT TCC TTG AAA AAG GCA CGG GTT CCA TGA ACT CAC TAT GAGC
Monomeric aptamer	Cortisol	/5ThioMC6-D/CTG CTC CAC ACC TGA GTG GTT TT
Concaptamer	Cortisol	/5ThioMC6-D/CTG CCA CAC CTG AGT GGT TTT TCC ACA CCT GAG TGG TTT TT

5.4.7. On body measurement of the biosensor

For the on-body measurement process, distinct cortisol concentrations (0, 0.01, 0.05, 0.1, 1µM) were prepared in artificial eccrine sweat and left on the electrodes.

Subsequently, the functionalized electrodes were integrated into a casing made of Ecoflex (Smooth-On, Ecoflex 00-30).

Utilizing SWV, a voltage range from 0V to -0.6V was selected for the tests. The parameters were preset to an amplitude of 0.025V and a frequency fixed at 60Hz. The SWV tests were conducted in a mixed solution of 25mM PBS and 25mM NaCl, both prior to and following the introduction of cortisol to the functionalized electrode.

After the proper assembly of the biosensor and the appropriate positioning of the electrodes, the apparatus was attached to the volunteer's skin.

Lastly, a volume of 50 microliters of the 25mM PBS/ 25mM NaCl mixture was introduced between the skin and the sensing area, acting as the electrolyte solution for the electrochemical measurement, and SWV was performed while the functionalized electrode was still in touch with the skin.

5.4.8. Desorption evaluation of the biosensor

After on-body measurement, the electrolyte used on the electrode (the previously used 25mM PBS / 25 mM NaCl solution), was gathered using a pipettor.

This investigative procedure was divided into three stages. Initially, the biosensor was tested using SWV after functionalization in a 25mM PBS and 25mM NaCl, and the electrolyte solution was taken without placing the sensor onto the skin. Following this, the biosensor was placed on the skin, and the SWV test was carried out twice. Utilizing SWV, a voltage range from 0V to -0.6V was selected for the tests. The parameters were preset to an amplitude of 0.025V and a frequency fixed at 60Hz. After every step, the 50uL of 25mM PBS / 25 mM NaCl solution applied on the biosensor as the electrolyte for the test was collected for further analysis.

The detection of any detached concaptamers in the collected solution was performed using a UV-Vis spectrophotometer (Thermo Scientific NanoDrop OneC Microvolume) to quantify the concentration of concaptamers in the collected solution.

5.4.9 Assay performance in real human sweat

In order to understand how the biosensor performs with actual human sweat, different cortisol levels would be measured when mixed with human sweat (Innovative research Inc,

IRHUSW100UL). Sweat samples were spiked with various cortisol amounts: 0µM (control), 0.1µM, 0.5µM, 1µM, and 1.5 µM. The biosensors were then incubated with these spiked sweat.

For a more realistic test scenario, we placed the incubated biosensors on a plastic hand replica.

Utilizing SWV, a voltage range from 0V to -0.6V was selected for the tests. The parameters were preset to an amplitude of 0.025V and a frequency fixed at 60Hz.

Lastly, a volume of 50 microliters of the 25mM PBS and 25mM NaCl mixture was introduced between the plastic hand and the sensing area, acting as the electrolyte solution for the electrochemical measurement, and SWV was performed while the functionalized electrode was still in touch with the hand. This SWV measurement was done both before and after the cortisol incubation step for fold change assessment.

5.4.10 Assay integration with wearable electronics

To further bolster the feasibility and applicability of the assay in the real-world context, integration with wearable electronics was prioritized. The heart of this integration rests on a designed printed circuit board (PCB) crafted with the Altium Designer software (Altium, CA). This PCB orchestrates the readout circuitry pivotal for the biosensing operations of biosensors.

The central processing capabilities of this readout circuitry are housed within the PIC18F06Q41 microcontroller (Microchip, AZ). This microcontroller includes dual 8-bit DACs, a built-in opamp, and a 12-bit ADC. To further optimize the biosensing efficiency, an LTC6079 quad opamp (Analog Devices, MA) was incorporated alongside the BM71 low-energy Bluetooth module (Microchip, AZ). The latter facilitates wireless connectivity.

To ensure stable and efficient power management, two meticulously chosen low dropout voltage regulators were integrated into the circuit. They dedicatedly cater to the power needs

of both the analog and digital components. To keep the device autonomously functional, it employs two CR2016 batteries as its power reservoir.

A setup was employed to determine the precision in waveform generation (both ramp and pulse) and to assess the accuracy of current measurements during SWV. Scanning was executed by shorting the counter and reference electrodes while connecting the working electrode to predetermined resistances. Both forward and reverse currents emerging from this setup were noted. The chosen resistances were selected to manifest nominal difference currents at five crucial points: 100nA, 333nA, 1µA, 3.3µA, and 10µA.

An Android application was designed to ensure data access and processing. It was developed in Kotlin using Android Studio.

Lastly, the packaging design for this proof-of-concept device was modeled in Autodesk Fusion 360®. Leveraging the Prusa i3 MK3s FDM 3D printer, the enclosure was 3d printed (VOXELAB 3D Printer Filament).

The device then records its response on a biosensor before and after it has been incubated in DI spiked with 1µM of cortisol.

5.5 Result and Discussion

5.5.1 Analytical performance in DI and artificial Sweat

The functional effectiveness of the biosensor was initially tested by identifying different concentrations of cortisol typically present in sweat, which is about 0.02−0.4 µM [112,113,122]. This range corresponds with the usual cortisol levels found in human perspiration.

The trial demonstrated that with an increase in cortisol concentration, there was a corresponding escalation in the detected signal. (Figure 21a-c)

Further experimentation showed that when control conditions (0 nM cortisol) and lower cortisol concentrations (1-300 nM) were tested, there was a shift in the signal. This finding implies that cortisol detection was affected by the diffusion effect on the electrode (Figure 21b).

Conversely, for elevated cortisol concentrations, the fold change in signal increased. The calibration plot shows a 2nd order polynomial relation of $y = 10^{-6}x^2 + 0.0007x - 0.2761$ between the fold change and cortisol concentration ($R^2 = 0.9461$). By calculating the slope of the graph at its steepest point (1µM), the LOD for this graph was calculated to be 219.4nM. This means that the sensor could detect cortisol concentrations as low as 220 nM. (Figure 21d)

In an effort to assess the effectiveness of the biosensor, a calibration graph showcasing the relationship between the alteration in signal and cortisol concentration was developed using artificial sweat samples spiked with cortisol. This graph also demonstrated a polynomial connection. The calibration plot shows a 2nd order polynomial relation of $y = -6*10^{-7}x^2 + 0.0022x - 0.5082$ between the fold change and cortisol concentration ($R^2 = 0.9441$). (Figure 21e)

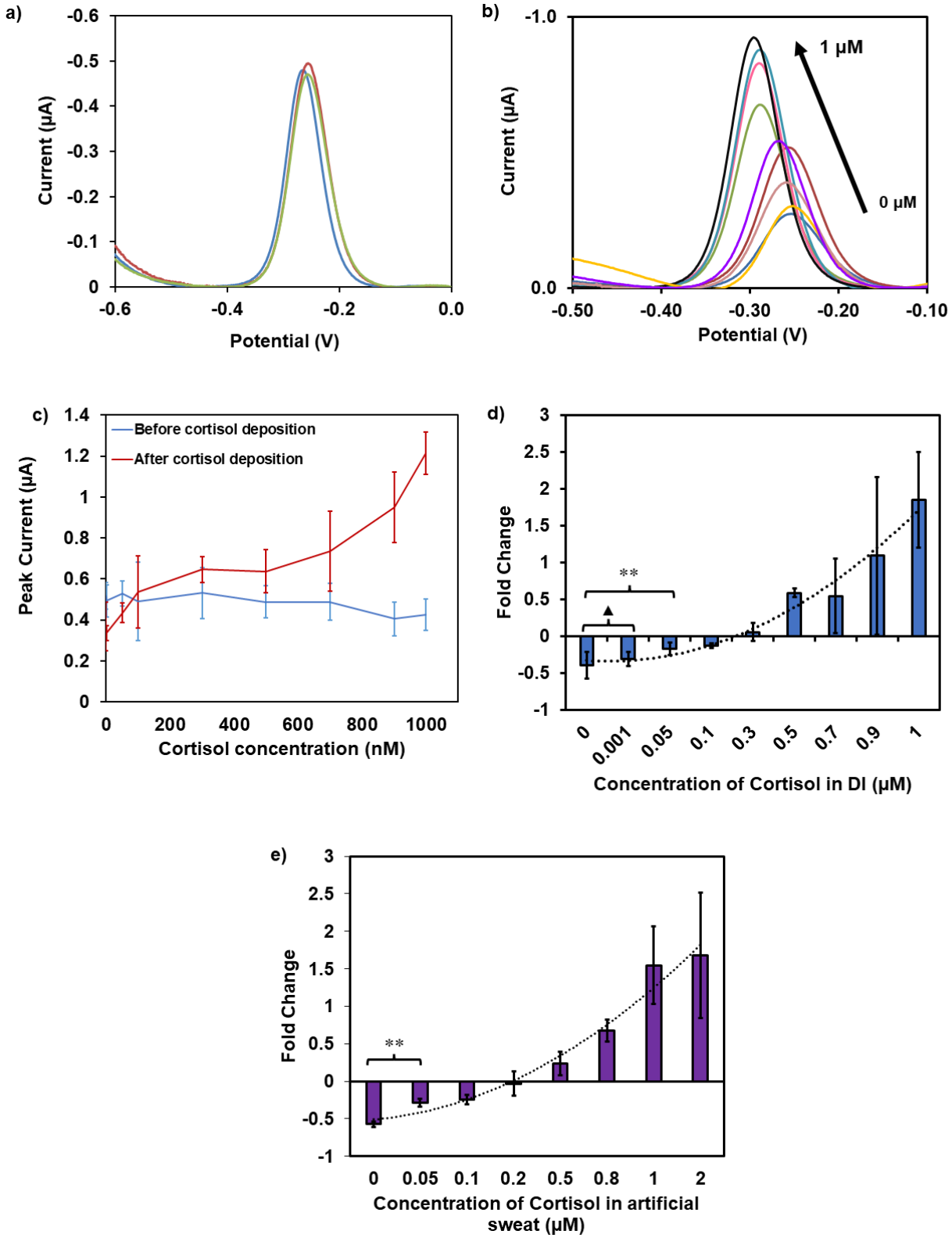

Figure 21:a) SWV signal of functionalized electrodes before cortisol addition. b) Depiction of increased SWV signal with different concentrations of cortisol. The observed shift in the peak at reduced concentrations is attributed to the diffusion effect that manifests during electrochemical interrogation. c) SWV peak current before and after cortisol deposition for different concentrations (n=3). d) The calibration plot shows a 2nd order polynomial relation of $y = 10^{-6}x^2 + 0.0007x - 0.2761$

between the fold change and cortisol concentration spiked in DI water (R^2 = 0. 9461). e) The calibration plot shows a 2nd order polynomial relation of $y = -6*10^{-7}x^2 + 0.0022x - 0.5082$ between the fold change and cortisol concentration spiked in artificial sweat (R^2 = 0.9441) (▲) represents p value > 0.05 and (**) represents p value < 0.05.

By calculating the slope of the graph at its steepest point (50nM), the LOD for this graph was calculated to be 58.1nM. This means that the sensor could detect cortisol concentrations as low as 60 nM.

5.5.2 Specificity

We compared the physiological average concentrations of possible interferent biomolecules in human sweat (22.5 mM for lactic acid and 0.1 mM for glucose) and a standard 1µM concentration for progesterone and testosterone against the biosensor's response to 1µM of cortisol and the control (0 µM). All components demonstrated only minor fluctuations in signal intensity when compared to cortisol and demonstrated a Signal-OFF compared to the distinctive Signal-ON in the fold change with cortisol (Figure 22).

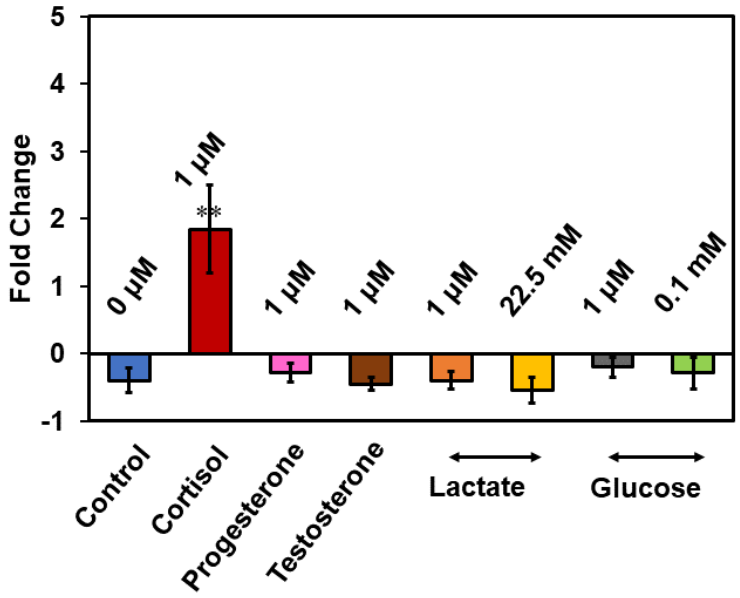

Figure 22:Specificity study of the Captain Patch in the presence of glucose and lactate (n=3). (**) represents p value < 0.05.

These findings validate the specificity of the biosensor against progesterone, testosterone, glucose and lactic acid.

5.5.3 Reusability

Upon introducing cortisol and allowing an adequate time for incubation, the biosensor demonstrated a rising trend in the fold change. It demonstrated a 0.34±0.05 fold change in the first cortisol deposition step. By the second cortisol deposition step the fold change increased to 1.14±0.22. By the third time, the fold change increased to 1.71±0.3. The fourth and fifth fold change calculations demonstrate a fold change of 2.02 ± 0.22, and 2.11 ± 0.4, respectively. This increase signals an escalation in the number of analytes securing themselves to the bioreceptors available on the electrode surface. It is important to note, however, that during the fourth and fifth measurements, the signal increase was not as pronounced as observed in the second and third trials. This pattern suggests that the biosensor may be approaching a saturated state, despite the consistent amount of cortisol added each time. An increase in the fold change is a signal indicating that it maintains its ability to identify cortisol even after being used multiple times. (Figure 23)

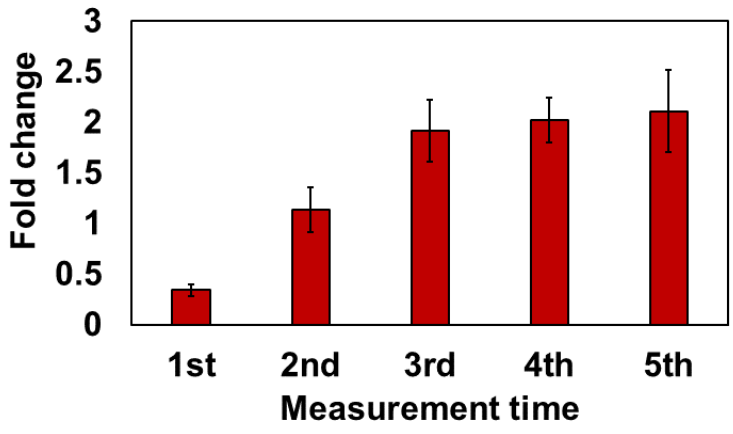

Figure 23: Assay reusability testing on functionalized electrodes using the electronics. Electrodes (n=3) were deposited with 1μM cortisol solution prepared in artificial sweat, incubated for thirty minutes, and interrogated with SWV for a total of five times in three hours.

5.5.4 Regeneration

The experiment to ascertain the viability of UV-based restoration of concaptamers involved subjecting cortisol-coated electrodes to UV light. The results indicate the ineffectiveness of the UV regeneration technique. The signal tied to cortisol detection remained unaffected after UV irradiation, suggesting that the UV light was unable to disrupt the covalent bond between the cortisol and the aptamers through the creation of pyrimidine dimers. (Figure 24)

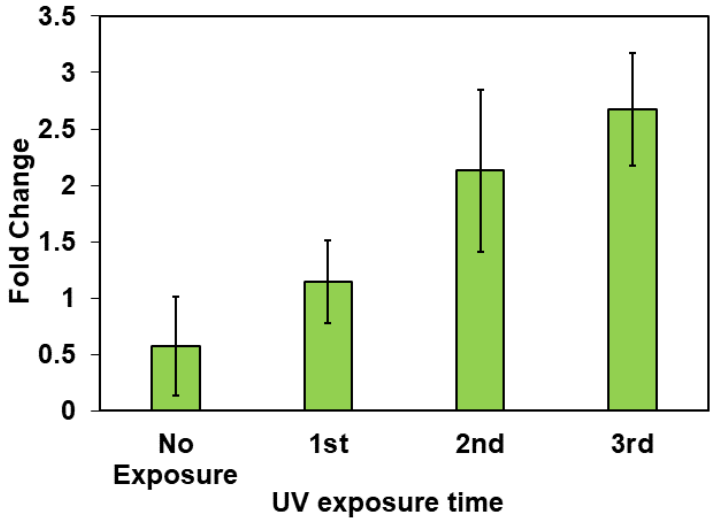

Figure 24: Regeneration effect of one-hour UV exposure with the assay. Electrodes were dipped in DI, exposed to UV for an hour, interrogated with SWV, incubated with 1µM Cortisol and tested with SWV once more before the next cycle.

In fact, the cortisol detection signal saw an escalation with every additional cortisol application on the electrodes. The fold-change for the first cortisol deposition without UV exposure was 0.57±0.43. After exposing the electrodes to UV for an hour and incubating them with cortisol again, the fold change increased to 1.44±0.36. By repeating this cycle for the second and third time, the fold change increased to, 2.12±0.71, and 2.67±0.50 respectively. This suggested that the concaptamers were not restored to their original non-bound state post UV treatment.

It's crucial to note that the observed increase in the cortisol detection signal is not indicative of successful concaptamer regeneration. In a successful restoration process, the cortisol detection signal should drop post UV exposure (due to the unbinding of cortisol) and rise only upon the introduction of fresh cortisol (signifying the bonding of regenerated concaptamers).

5.5.5 Long-term repeatability

The biosensor’s repeatability efficiency was put to the test through an extended usage trial, which took place over the course of three days with SWV measuring intervals of 6, 24, 48, 72 hours, operating in an environment of artificial sweat.

Findings from this test revealed a decline in the sensor's SWV signal, with the strength diminishing to about half by the third day's end. These results hint at the fact that the concaptamer undergoes a gradual decay when exposed to artificial sweat over an extended timeframe and without cortisol exposure.

Even with the degradation seen over the three-day span, it is of important to note that the biosensor manages to retain performance for up to a 12-hour period, displaying only a minor fluctuation in signal between 5-10%. (Figure 25)

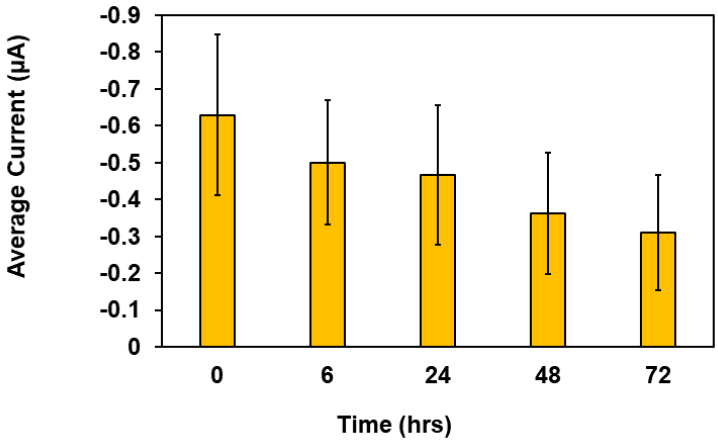

Figure 25:Long-term repeatability test of the assays in the artificial sweat performed over a period of 3 days (n=3). All measurements were done with standard Ag/AgCl reference electrode and Pt counter electrode.

5.5.6 Selectivity

Through this section, the functionalized electrodes were tested using DPV. The results demonstrated that concatenating the cortisol aptamer does not alter its capability to detect its target. The cortisol specific aptamer and concaptamer demonstrated a negative fold-change of -0.1±0.03 and -0.08±0.05 respectively, while the non-cortisol-specific aptamer showed a positive fold change of 0.07±0.02. Other control samples also demonstrated a positive fold change as previously expected. (Figure 26)

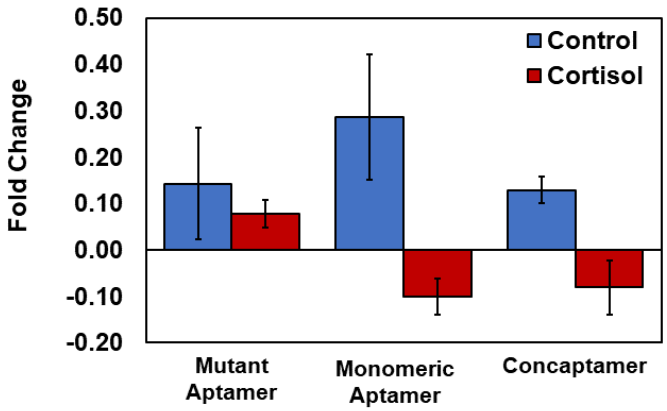

Figure 26:Selectivity analysis using the mutant aptamer, the monomeric cortisol aptamer, and concatenated Aptamer (cortisol concentration: control = 0µM, cortisol = 1µM, n=3).

5.5.7 On-body measurements

For the on-body evaluation section, the biosensor was able to detect the diverse cortisol levels. The fold change shows a polynomial relation of $y = -3*10^{-6}x^2 + 0.0039x - 0.5845$ with the cortisol concentration ($R^2 = 0.8396$). The calculated LOD based on the slope of the graph at the lowest detectable concentration (10nM) is 30nM, although it is important to note that this value is not accurate at all since the R^2 is lower than 0.9, meaning that the 2nd degree polynomial trendline does not properly fit the data. (Figure 27)

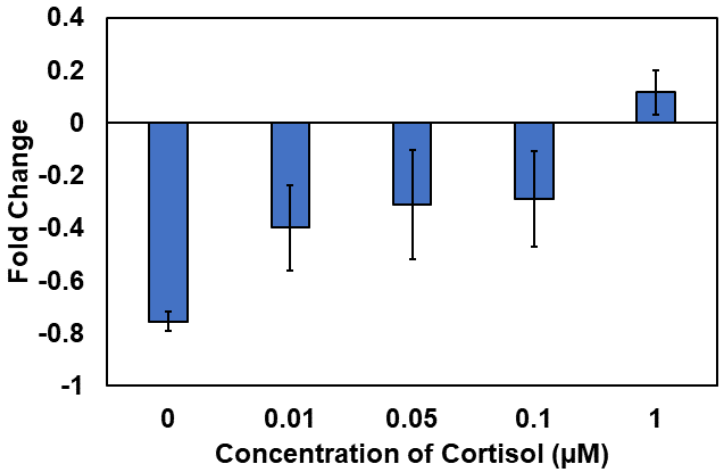

*Figure 27:On-body measurements with biosensor's internal gold electrodes on human skin (n=3). The fold change shows a polynomial relation of y = -3*10-6x2 + 0.0039x - 0.5845 with the cortisol concentration ($R^2 = 0.8396$).*

However, it's essential to point out a difference. Even though the biosensor demonstrated its capability to differentiate various cortisol levels from blank (0 µM), the extent of change was not as marked as seen in experiments involving artificial sweat and DI water supplemented with cortisol. For example, in the experiment with the 1µM spiked artificial sweat, the fold change was close to 1.54±0.52, while the fold change for the same concentration in this experiment is 0.11±0.08. This lesser fold-change could be a consequence of the challenges associated with placing the sensor directly on the skin. Elements like skin conductivity, the intricate blend of internal and external agents on the dermal surface, and the skin's uneven

features might bring about shifts, possibly affecting the electric readings gathered through SWV.

5.5.8. Desorption evaluation

The data derived from the assessment of desorption highlight that some amount of concaptamer separation is witnessed after each SWV interrogation. These insights are not unique and echo the conclusions from various other research works, indicating that the use of SWV methods often results in a certain degree of desorption [119].

Specifically, these insights pinpoint that the SWV measurement right after functionalization phase is where this impact is most prominent. The concentration of the detached concaptamer in this stage was 0.12±0.02μM. The detached concaptamer concentration was reduced in the second and third stage to 0.05±0.01μM and 0.03±0.01μM. (Figure 28)

Nevertheless, it's crucial to clarify that, while desorption does occur, its influence wanes following the first measurement and doesn't notably impair the cortisol detection ability. Thus, even with desorption occurring to some extent, the biosensor remains a dependable instrument for cortisol tracking.

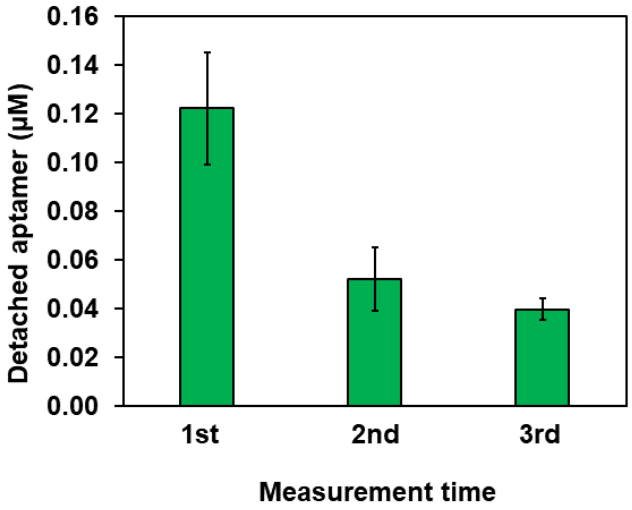

Figure 28:Detached concaptamer concentrations after the first, post functionalization measurement, second, post cortisol deposition measurements, and third, another post cortisol measurement (n=3).

5.5.9 Biosensor performance in human sweat and, wearable electronics and Android application

In order to assess the potential of the biosensor for human sweat examination, a series of tests were performed using combined human sweat samples spiked with different concentrations of cortisol. Upon review of the gathered data, a decline in the biosensor's sensitivity became apparent when it was exposed to this fluid. Notably, even though there was a rise in fold-change, pointing to the detection of cortisol to the concaptamer, a negative fold change persisted across the spectrum, even at heightened cortisol concentrations, as depicted in Figure 29.

Considering the fold change and the cortisol concentrations, a polynomial relation of $y = -0.0346x^2 + 0.1929x - 0.3714$ exists ($R^2 = 0.9743$). Considering the slope at the lowest detectable concentration (100 nM), the LOD was calculated to be 1098nM.

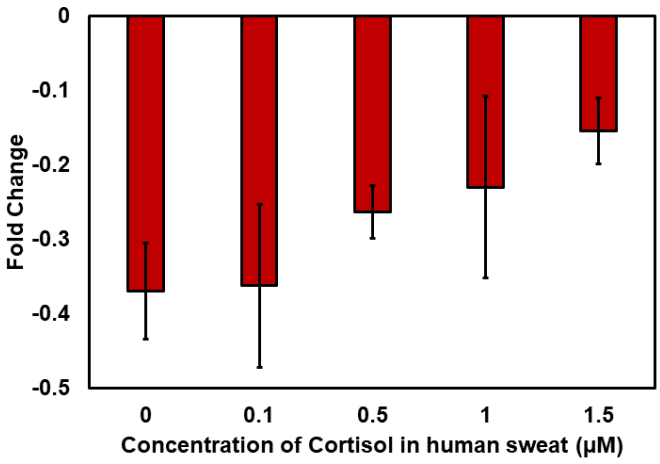

Figure 29: Fold change measurement of different cortisol concentrations in human sweat. a polynomial relation of $y = -0.0346x^2 + 0.1929x - 0.3714$ *between the fold change and cortisol concentration exist* ($R^2 = 0.9743$).

Such findings deviate from what we observed in the experiments involving artificial sweat samples, which were devoid of complex biological materials like proteins and other minute compounds, presenting an entirely different interaction profile with the biosensor.

For the electronics and the integration of the biosensor with the said electronics, at its core, the readout circuitry incorporates functionalities that blend both the digital and analog worlds. Specifically, the digital to analog converter (DAC) ensures the generation of SWV waveform. Meanwhile, the potentiostat facilitates the electrochemical sensor's driving force. Amplifying and digitizing these signals are the roles of the current to voltage amplifier and the analog to digital converter (ADC), respectively, before the Bluetooth module transmits the digitized data wirelessly.

Central to the function of this process is the PIC18F16Q41 microcontroller. This microcontroller's trait is its capacity to minimize the reliance on numerous discrete integrated circuits, capitalizing instead on its analog peripheral capabilities (Figure 30a). In terms of waveform precision, the two DACs work in synergy with the internal opamp and one of the

LTC6079 opamps to construct a high-resolution DAC. This configuration ensures the voltage changes are captured, specifically at 128 uV LSB, for precise SWV waveforms.

The signal processing, is managed on the microcontroller. The architecture allows for a microcontroller general-purpose input-output (GPIO) controlled feedback network. Consequently, the firmware drives the DACs to undertake eight ADC acquisitions for every current sample, both in reverse and forward directions. This data undergoes on-chip analysis, where the voltage amplifier gain is adjusted. All the resultant current values throughout the sweep are stored in memory before their wireless transmission through the BM71 Bluetooth module. These electronics derive their power from two CR2016 batteries, filtered through two low-dropout regulators to ensure stability (Figure 30b).

When benchmarked against the Emstat4S potentiostat, the biosensor electronics showcase analogous SWV measurement results (Figure 30c). This is further validated in Figure 30d, where the biosensor's current measurements consistently align with those documented by the Emstat4S potentiostat across varying resistance parameters.

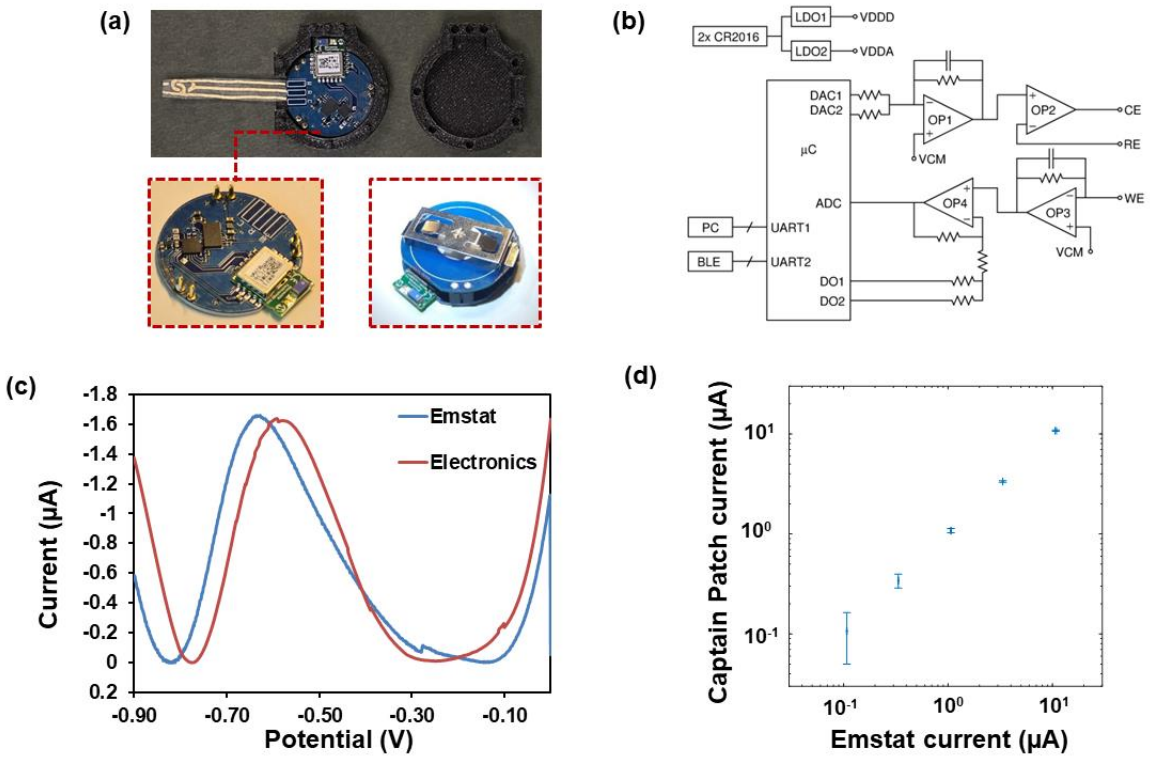

Figure 30: (a) Picture of Electronics with the 3d printed packaging and circuit board. The battery unit is mounted on top of the Electronics and CAPTAIN Patch. (b) The Electronics circuit block diagram. For the block diagram, UART: universal asynchronous receiver transmitter, µC: microcontroller, OP: opamp, LDO: low drop-out voltage regulator, VDDD/VDDA: digital and analog supply, CR2016: battery, PC: computer (wired interface), BLE: Bluetooth low energy module (wireless interface), DAC: digital to analog controller, ADC: analog to digital controller, DO: digital output, VCM: common mode voltage, and CE/RE/WE: potentiostat electrodes. (c) Comparison between the current produced in standard Emstat4S Potentiostat and the in-house developed electronics. (d) Comparison between the measured current for the Emstat4S Potentiostat and the electronics by shorting the counter and reference electrode and connecting the working electrode to different resistors.

From a design perspective, the biosensor and its accompanying electronics are housed within a 3D printed package. This enclosure, measuring 25.2 mm in diameter and 5 mm in height (Figure 31), employs a two-layer click-together mechanism. The Biosensor is seamlessly integrated through a slit, ensuring optimal contact with the PCB's bond pads.

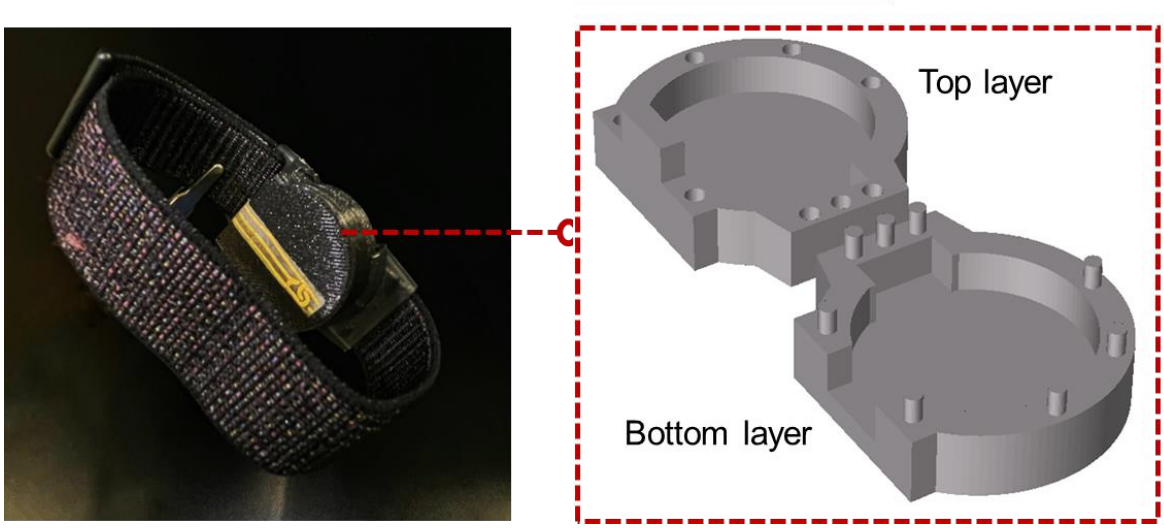

Figure 31: 3D printed packaging design for the electronics consisting of two layers to secure electronics and Captain Patch.

The 'Breather' Android application enhances the user experience by providing an intuitive interface for cortisol level monitoring (Figure 32). Apart from live data visualization, 'Breather' facilitates user data storage, helping users to share their medical records with healthcare professionals. Despite these capabilities, it's imperative to note that the current version of 'Breather' isn't endorsed for data sharing beyond the research spectrum.

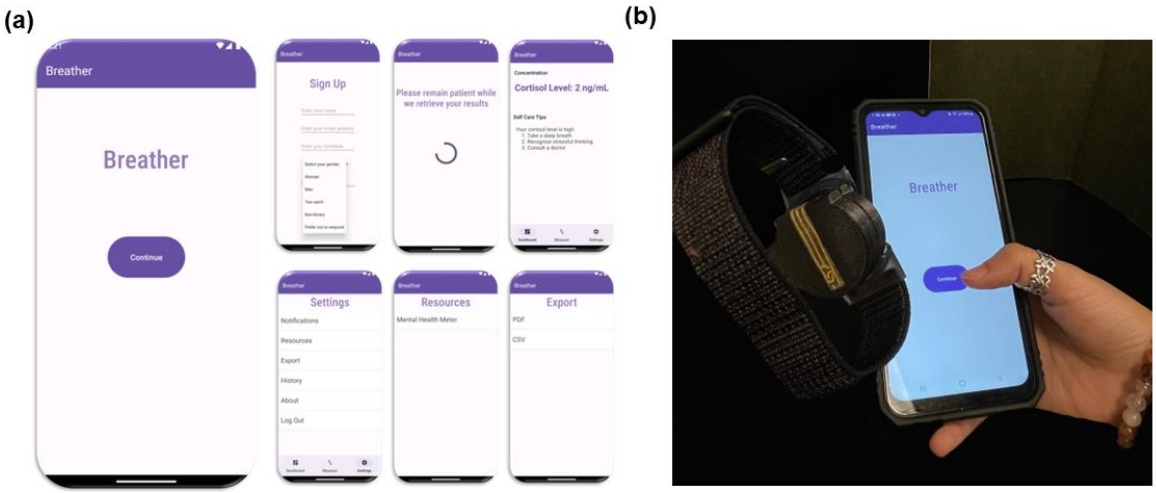

Figure 32: (a) Breather: An Android application to record and display measured cortisol levels. Developed using Kotlin within the Android Studio integrated development environment, this application offers an accessible and user-friendly platform for users to gauge their unique stress thresholds. Boasting key features including a streamlined user registration module, efficient data export functionality, and seamless integration with external resources to enhance assessment

capabilities, Breather embodies a comprehensive approach to stress management and well-being assessment. (b) Picture of a prototype wearable consisting of Captain Patch, electronics, 3D printed packaging and an App.

This system, including biosensors, electronics, and a mobile application, is captured in Figure 33a. On-body tests with Captain Patch and its integrated electronics corroborate findings from the previous results tests, revealing a 'Signal On' surge in currents during cortisol detection, especially evident between 0 and 1µM cortisol concentrations, as depicted in Figure 33b.

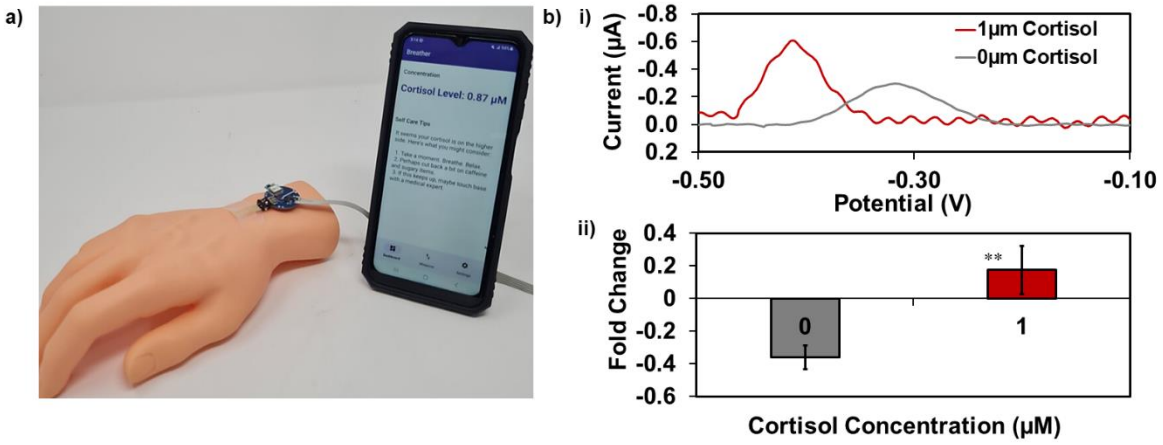

Figure 33: a) Connecting Breather app to Electronics through the imbedded Bluetooth module. The Electronics in this setup are connected to a power outlet. b) Measurement of cortisol spiked artificial sweat using electronics integrated biosensor, (i) data of the measurement in the presence and absence of the cortisol performed using a wired configuration of the prototype, (ii) fold change in the signal corresponding to the on-body measurements (n=3). (**) represents p value < 0.05.

5.6 Conclusion

The biosensor's functionality was first evaluated by detecting cortisol concentrations typically found in human sweat. Trials indicated an increase in the detected signal with rising cortisol levels. A calibration plot was added using a 2nd order polynomial equation, indicating an LOD of 219.4nM for cortisol solutions made in DI and 58.1nM, for cortisol solutions made in artificial sweat. This result implies the biosensor's ability to detect cortisol levels as low as 220 nM and 60 nM.

The study assessed the specificity of the biosensor by comparing its response to cortisol at a concentration of 1μM with that of common interferent biomolecules in human sweat – specifically, 22.5 mM lactic acid, 0.1 mM glucose, and standard concentrations of 1μM for progesterone and testosterone. The results indicated only minor signal intensity variations for these substances compared to cortisol, with all showing a Signal-OFF contrasted with the distinctive Signal-ON in response to cortisol.

For reusability assessment, upon introducing cortisol to the biosensor and allowing time for incubation, an increase in fold change was noted. The first cortisol deposition showed a fold change of 0.34±0.05, which escalated to 1.14±0.22 in the second cortisol deposition and then to 1.71±0.3 in the third. Subsequent fold changes for the fourth and fifth depositions were recorded at 2.02 ± 0.22 and 2.11 ± 0.4, respectively. This trend indicates more analytes binding to the bioreceptors on the electrode surface. However, the increase in signal during the fourth and fifth measurements was less compared to the second and third, suggesting the biosensor might be reaching a saturated state. Despite this, the fold change continued to rise, showing the biosensor's ability to detect cortisol repeatedly.

The experiment evaluating UV light as a method for regenerating concaptamers on cortisol-coated electrodes demonstrated that this approach was ineffective. Despite UV exposure, the cortisol detection signal did not change, indicating that UV light did not disrupt the cortisol-aptamer bond. Subsequent tests showed an increasing fold change in cortisol detection after each application, contrary to expectations for successful regeneration, where the signal should decrease post UV exposure and rise only upon introducing new cortisol. This pattern suggests that the concaptamers did not return to their original state after UV treatment.

The long-term repeatability of the biosensor was evaluated over a three-day period using SWV measurements at intervals of 6, 24, 48, and 72 hours, in an artificial sweat environment.

Results indicated a reduction in the sensor's SWV signal, decreasing by about half by the end of the third day. This suggested a gradual degradation of the concaptamer in artificial sweat over time without cortisol exposure. Despite this decline, the biosensor maintained functionality for up to 12 hours, exhibiting only a minor 5-10% fluctuation in signal.

During the selectivity test, it was observed that the concaptamer, similar to the original non-concatenated aptamer, exhibited selectivity in detecting cortisol. Conversely, when a mutant aptamer lacking specificity to cortisol was used, there was no indication of cortisol detection.

In the on-body evaluation, the biosensor detected different cortisol levels, showing a polynomial relationship between fold change and cortisol concentration, with a calculated LOD of 30nM. However, this LOD may not be entirely accurate due to a lower R^2 value. The biosensor's response on the skin was less pronounced compared to tests in artificial sweat, with a notably lower fold change for the same cortisol concentration. This difference is likely due to factors like skin conductivity and surface irregularities affecting the SWV readings.

The desorption evaluation data indicated that concaptamer separation occurred after each SWV interrogation. The effect was most significant immediately after the functionalization phase, with a concaptamer detachment concentration of 0.12±0.02µM, decreasing in subsequent stages to 0.05±0.01µM and 0.03±0.01µM. Its impact lessens after the first measurement and does not significantly affect the biosensor's ability to detect cortisol.

Tests using combined human sweat samples spiked with varying cortisol concentrations were conducted to evaluate the biosensor's effectiveness in human sweat analysis. Data analysis revealed a decrease in the biosensor's sensitivity in this medium. Despite an increase in fold-change indicating cortisol detection by the concaptamer, a consistent negative fold change was observed across all cortisol levels, with an LOD calculated to be 1098nM.

Chapter 6 : Conclusion and future recommendations

6.1 Overview

This chapter concludes the project by reviewing all steps undertaken, evaluating the biosensor's features, and comparing its characteristics with other studies in this field. The limitations of the fabrication section, assay preparation, and testing will be discussed. Each experiment's significance and limitations, based on the gathered data, will be examined, along with potential improvements.

6.2 Electrode design and production phase

In the initial phase of biosensor development, PVDF was utilized as the substrate for the bilayer electrode, designed to create controllable surface modifications through wrinkles. The bilayer structure was successfully produced using the sputtering technique, adaptable for various biosensor designs involving two or three electrode surfaces. The effectiveness of the electrode cleaning process was evaluated by analyzing the gap between oxidation and reduction peaks and their reversibility. Among the methods tested, plasma cleaning proved most effective in cleaning the electrodes. Basic mechanical tests confirmed the bilayer electrodes' flexibility, and further electrochemical analysis validated the device's suitability for the intended application.

Heat treatment using a convection oven emerged as a practical approach to induce shrinking near the electrodes' melting points, resulting in wrinkles with a wavelength of about 50µm. While these steps were critical in the biosensor's development, it's also essential to acknowledge some shortcomings in the design and this experimental phase as a whole.

6.2.1 Limitations and issues on the design of the electrodes

It should be noted that some phases of this project encountered challenges. Specifically, the surface area consistency of the UC logo electrode after shrinking, proved to be challenge for electrochemical applications. The primary issue lies in the inconsistent three-dimensional structure production on the surface for the electrodes after the heating process. Although the total available surface area remained consistent after heat shrinking, the specific structure of wrinkles on each electrode could vary based on individual heat shrinking process. This consideration becomes crucial when both the reference and counter electrodes are also heat treated. Despite initial electrochemical analyses using CV and ferrocyanide indicating minimal performance differences between non-corrugated and corrugated reference electrodes, the situation may change when the working electrode is functionalized with concaptamers for detecting low concentrations of biomarkers. This could lead to inconsistencies in the results. This variability in the electrode surface for electrochemical reaction complicates electrochemical measurements, undermining the consistency of charge transfer between the electrodes and analytes [130].

The electromechanical tests conducted were not based on established standards. The chosen methods, involving 180-degree twisting and bending in half for 10 minutes, were selected on the assumption that these mechanical forces were extreme, but they are not considered as such by any standard measure.

Additionally, the size of the electrodes was a factor considered during the design phase. While the working electrode was sized for standard concaptamer immobilization, no standards were applied to the dimensions of the working electrode, reference electrode, or counter electrode.

Regarding the heating process, the optimization was achieved through trial and error. Temperatures varied by 10℃ increments for each sample, and durations ranged from 5 to 30 minutes. A more detailed analysis might be needed on the material engineering aspects of

PVDF-Au, particularly to determine if slight changes in temperature and duration could impact the wrinkling process. The heating regimen's effect was primarily assessed to check for crack propagation in the samples. While it was successful in reducing cracks, this regimen should also be applied to the electrodes under a similar variety of temperatures and durations to evaluate whether the heating process can be further optimized.

The issue of crack propagation in the electrodes extends beyond initial concerns. The size of the electrodes influences their susceptibility to cracks during the heat shrinking process. Larger materials tend to face more challenges since a greater number of atoms need to move during heat transfer within the material. Given that the PVDF-Au electrode is particularly prone to cracking, this poses considerable difficulties in adapting the electrode for different designs or future applications that may require alternative configurations.

The use of PTFE felt during the heating process also presents challenges. While necessary for applying heat close to the melting point of the PVDF to the PVDF-Au substrate, and despite the substrate being effectively sandwiched between PTFE felts, this approach detracts from the predictability of the wrinkling process. Ideally, the thickness of the gold and PVDF, along with their specific mechanical properties, would aid in predicting the wrinkling wavelength. However, sandwiching the substrate in PTFE, though advantageous for managing the near-liquid polymer due to its non-sticking properties, may lead to unforeseen changes. For instance, in the optimized heating samples, wrinkles with a waveform of 32.6±5.6μm were observed, whereas a 1um wavelength was theoretically expected, indicating that the heating process may not be as predictable as initially thought. Furthermore, heating the PVDF-Au well above its melting point (190°C) resulted in more intense wrinkling with a wavelength of 10um, which was not effective for the electrochemical measurements.

An additional challenge arises with the cleaning process. Of the three methods attempted, only one proved effective for the electrodes. This restricts the versatility of cleaning options,

especially when compared to other electrodes, such as those made from PET polymer, which can be cleaned using various techniques [117]. This suggests that PVDF-Au electrodes may have inherent limitations in terms of their cleanability.

6.2.2 Suggestion for future experiments and electrode design

Future experiments should focus on significantly modifying the electrode pattern to ensure consistent distance between the counter and working electrodes. Adopting standard electrode configurations like the ring-disk pattern, commonly used in commercial glucose systems, could be more effective. Ring-disk electrodes feature a central disk electrode encircled by a ring electrode, where the disk usually functions as the working electrode, and the ring serves as the counter electrode [130].

In biosensing, the size of ring-disk electrodes plays a crucial role in their performance. The trend in modern biosensors leans towards miniaturization, which offers benefits like reduced reagent consumption, decreased waste production, and suitability for portable or wearable devices. The central disk electrode in a ring-disk setup is typically designed to be small, often in the micrometer range, enhancing sensitivity due to a higher current density for a given total current. The width of the ring electrode and its distance from the disk are critical design aspects. The ring should be positioned close enough to effectively collect species generated at the disk yet maintain sufficient distance to avoid direct electrical interference, typically ranging from a few micrometers to several millimeters [130].

For the mechanical testing of the PVDF-Au substrate, aligning with specific standards, such as those provided by ASTM International, would ensure more accurate and reliable results. For instance, ASTM D412, which focuses on the tensile properties of elastomers, and ASTM D624, dealing with the tear strength of rubber, are relevant standards that could be applied.

The heating process of the substrate requires substantial optimization. A preliminary step could involve conducting tests like Differential Scanning Calorimetry (DSC) or Thermogravimetric Analysis (TGA) to better understand the material's transition temperature from solid to liquid. This information would facilitate finding the optimal heating temperature more efficiently. Additionally, employing a detailed heating regimen for electrode production might eliminate the need to sandwich the substrate with Teflon felt.

Post-optimization, the samples obtained should undergo SEM analysis to measure the wavelength of the wrinkles and compare them to theoretical expectations. Despite some challenges with PVDF material, another cleaning option is the use of a 3:1 piranha solution, a mixture of 99% pure sulfuric acid and 35% hydrogen peroxide. However, due to its highly reactive nature, it's essential to ensure this solution does not damage the PVDF substrate. Piranha solution has previously been used for cleaning gold and semiconductor surfaces.

6.3 Assay optimization phase

In this section, the assay deposition process was fine-tuned to determine how various parameters influence the biosensor's performance in detecting a standard cortisol concentration of 1uM. Given the critical role of MgCl2 concentration in the binding buffer relative to Tris-HCl and NaCl concentrations, the MgCl2 concentration was optimized. It was discovered that a concentration of 1mM MgCl2 effectively detects 1uM cortisol. Additionally, the incubation time was established at 30 minutes, as this duration yielded a significantly high fold change compared to blank samples.

It is important to note a consistent negative fold change of -0.4 was observed in these blank samples. This may be attributed to the lack of necessary salt concentrations in the blank solution during incubation on the electrode. The absence of these salts potentially leads to the loss of the concaptamer's optimal 3D structure, which is crucial for the desired conformational change.

The CD experiment revealed that the concatenated cortisol possesses a structure akin to the original aptamer. Upon the addition of cortisol, a conformational change was evident, as indicated by alterations in the intensity of the CD peaks. The functionalization of the electrode with 1µM concaptamer emerged as the most effective approach for detecting 1µM cortisol, in terms of both fold change and the signal-to-blank ratio. When 1µM concaptamer was deposited on both planar and corrugated electrodes, it was found that approximately 1013 concaptamers were attached to the electrode, a quantity comparable to other studies quantifying nucleic acid bioreceptors. Notably, the corrugated electrodes enhanced the biosensor's ability to detect 1µM cortisol fold change better compared to the planar electrodes.

6.3.1 Limits and issues with the assay optimization phase

A notable issue in this section was the range of concaptamer concentrations tested. The experiment used three concentrations: 0.5, 1, and 1.5µM. While this range aligns with those used in other studies, and the 1µM concentration appeared adequate (in case of their fold change), a broader spectrum of concentrations, such as 0.6, 0.7, 0.8 up to 1.5µM, could have been more informative. This approach might have identified a concentration with even better performance.

Although the corrugated electrode outperformed the planar one, it's critical to recognize that all optimization steps in the project were based on detecting a relatively high cortisol concentration (1µM) to simplify the visualization of changes. However, focusing the optimization process on lower cortisol concentrations, rather than a high one, might have been more advantageous and representative of real-world applications.

Crucially, both the cortisol and blank solutions were prepared in DI water, which could impact the biosensor's accuracy in later stages. This is because the biosensor was primarily optimized for performance in this medium, rather than in a more complex biofluid.

6.3.2 Future experiments for assay optimization

In future experiments, rather than concentrating on optimizing the biosensor for detecting 1µM cortisol in DI, it would be more beneficial to focus on optimizing the detection process for lower, physiologically relevant cortisol concentrations. Additionally, the medium for preparing the cortisol solution should be reconsidered. Using artificial sweat or even real human sweat could yield more accurate and relevant results compared to DI water. Finally, for a comprehensive understanding, it would be advantageous to test the biosensor across a broader range of concentrations rather than limiting the experiments to a few specific values.

6.4 Assay performance analysis phase

In the final stage of biosensor development, its performance was evaluated. The biosensor's response was initially tested across a range of cortisol concentrations prepared in DI and artificial sweat. By analyzing the fold change and applying a 2nd degree polynomial relation to the graph with various concentrations, the LOD was determined to be 220nM for DI and 59nM for artificial sweat. The biosensor's specificity was also tested against physiologically relevant concentrations of potential interferents found in sweat, such as glucose and lactic acid, as well as structurally similar hormones like progesterone and testosterone. The results confirmed that the concaptamer specifically responded to cortisol, with no false positive signals triggered by other biomarkers.

The reusability of the assay was evaluated by repeatedly incubating the biosensor with 1µM cortisol to observe any changes in fold change upon each deposition. This process spanned 3 hours, during which five SWV measurements were conducted. The results indicated that an increase in fold change occurred for up to three measurements with 1µM cortisol, although some increase was also noted in the fourth and fifth depositions.

The biosensor's stability was assessed in an artificial sweat medium over a period of 72 hours. The initial SWV signal was measured and then compared with SWV signals recorded in each

specific hour. The biosensor demonstrated effective stability for the first 6 hours; however, a significant decline in the SWV signal was observed after 72 hours.

The regeneration strategy using UV light proved to be ineffective. A comparison of the concaptamer's performance with the original aptamer and a non-cortisol specific aptamer confirmed that selective detection of cortisol was occurring and was not arbitrary. Nonetheless, the analyses conducted on the body and in human sweat were found to be less effective compared to those performed in DI and artificial sweat.

6.4.1 Discussing the results of this work – limitations and issues with the biosensor in general

When examining the LOD results and comparing them with other studies, it becomes evident that the biosensor's performance is suboptimal. A primary factor is the short incubation time. (Table 8)

Table 8: Comparison between recent studies on cortisol detection.

Electrode	Measurement time (min)	LOD (pM)	range (nM)	References
Anti-cortisol antibody/functionalised-polyethylene glycol/screen-printed electrode	30	110	0.5–200	[131]
Anti-cortisol antibody/denatured bovine serum albumin/reduced graphene oxide/quartz substrate electrode	40	10	0.01–100	[132]
Anti-cortisol antibody/gold nanoparticles-multi walled carbon nanotubes-n-octylpyridinium hexafluoro phosphate-ionic liquid microsized paste electrode	45	41.38	0.27–27.60	[133]

Biotin-antibody/functionalised-magnetic reduced graphene oxide-nafion/glassy carbon electrode	60	140	0.28–2758.62	[134]
In_2O_3 FET on polyamide with tape-based microfluidics	40	0.001	0.001-10	[52]
Platinum-Graphene Extended gate electrode	30	0.2	1-2000	[76]
Wrinkled PVDF-Au electrodes	30	59	100-1000	This work

While a shorter incubation time for the biosensor is not inherently problematic, it could contribute to its less-than-optimal performance due to a lack of diffusion time for the cortisol molecules in the medium. The biosensor's effectiveness is primarily gauged based on its LOD, and when compared to other studies, both nucleic acid-based and antibody-based, this biosensor's LOD is not as competitive. Specifically, the range of cortisol tested was somewhat similar to the physiological range (0.02nM to 0.4nM) [40,112], but the concentrations used in the tests were not comprehensive. For instance, between 1000nM and 100nM, cortisol concentrations were tested in steps of 200nM, and below 100nM, only a limited number of concentrations were examined. This approach resulted in a suboptimal LOD, even in ideal testing conditions like DI and artificial sweat. The performance further deteriorates when testing the device on the body and in pooled human sweat.

In both on-body testing and pooled human sweat scenarios, the device failed to produce a positive fold change. This issue, coupled with the suboptimal performance reflected in the LOD graph, highlights the biosensor's overall inefficiency.

Additionally, the number of samples tested for each concentration was quite low. Using only three samples per concentration is insufficient to accurately determine a specific fold change, even in ideal conditions with DI and artificial sweat, leading to large statistical error bars in the LOD graph.

This becomes more apparent when we compare the standard deviation percentage derived from the fold change at the lowest concentration in DI. The calculated standard deviation percentage for 1nM concentration is 30.29%. When compared to other research that attempted to detect analytes at lower concentrations, where they reported a standard deviation percentage of 16.13%, this value is significantly higher [135]. This elevated standard deviation could be attributed to several factors, such as a limited number of sample groups or inconsistencies in the electrode functionalization step.

Additionally, when examining the standard deviation percentage for both the before cortisol deposition SWV signal and post-cortisol signal, a further contributor to the high error margin becomes evident. For instance, the standard deviation percentage for the 700nM cortisol in DI before cortisol deposition measurement is 18.70%, which escalates to 26.52% for the post-cortisol measurement. This increase in the standard deviation percentage also accounts for the observed enlargement of the error bars.

When comparing the percentage standard deviation for the CV reduction peak signal from the optimized wrinkled electrode, there is a notable 15.45% for the standard deviation percentage. This percentage could also be a contributing factor to the heightened error bars observed in the data.

Another potential source for the high error margin could be related to the heat shrinking of both the reference and counter electrodes. As previously mentioned, while the corrugation of the reference and counter electrodes might not have shown any significant effect during the

electrochemical tests with ferrocyanide, it could substantially impact the cortisol detection process, especially when the working electrode is functionalized. This inconsistency contributes to less reliable fold change signals, further impacting the biosensor's effectiveness.

The development of this device reveals its unsuitability as a wearable biosensor. Initially conceptualized as a wrist-mounted watch for detecting cortisol in sweat, the device faces practical limitations. Although the biosensor can distinguish between three depositions of 1µM cortisol over three hours, it might be mistakenly assumed that it could perform three cortisol measurements in this duration. The idea of changing the electrode every three hours to enable continuous, real-time monitoring throughout the day is not feasible, given the biosensor's current capabilities.

The human body contains up to 4 million eccrine sweat glands, but the wrist area, where the device is intended to be mounted, only has about 200 glands per square centimeter [40,112,136,137,137]. With the working electrode covering just 5mm², this area would encompass roughly 10 eccrine sweat glands. Considering the body's total sweat production rate of 0.8 liters per hour, this small area would produce only about 10µL of sweat per hour. The SWV technique used requires a minimum of 50µL of electrolyte solution to function, and all incubation steps with varying cortisol concentrations in this project were performed with 10µL of cortisol solution in a humid chamber. Collecting 10µL of sweat for a 30-minute incubation on the working electrode, while accounting for evaporation, is impractical.

It is essential to recognize that the biosensor's stability, limited to a maximum of 6 hours, is significantly impacted by the skin's acidic pH environment. This limitation is a major obstacle to its development as a wearable biosensor for continuous cortisol monitoring.

Even assuming sufficient sweat collection on the working electrode area, the biosensor has not performed well on the skin, even under ideal conditions using 6.5 pH artificial sweat, or

when cortisol diluted in pooled sweat was tested. The suboptimal performance in these scenarios is attributed to several factors, including the sensitivity of MB to pH changes, potential obstruction of the working electrode's surface by biological entities, and the electroconductivity of human skin. The sweat's acidic pH of around 5 could lead to the degradation of MB. Furthermore, proteins and bacteria present on human skin could block the electrode surface, leading to a ‘fouling’ phenomenon. The skin's conductivity may also interfere with the charge transfer between the working and counter electrodes, potentially causing a short circuit and impacting SWV measurement accuracy.

Cortisol solutions were prepared and incubated on the electrode in a humid chamber in controlled conditions, not directly on the skin. Testing on skin or a plastic hand presented additional challenges; pressing the concaptamer-immobilized surface against another could result in displacement or scraping off the concaptamers, complicating the biosensor's practical use.

The biosensor was unable to regenerate effectively using only 6W UV light. Even partial regeneration might compromise the aptamer's detection capabilities, as the primary release mechanism for cortisol involves damage to the aptamer through the formation of CPDs and nucleotide cross-linking, which could alter the aptamer's functionality.

Another limitation is the biosensor's inability to distinguish between old and new sweat, as it cannot effectively remove previously bound cortisol. Although it performed well in artificial sweat, the biosensor's testing range suggests it might only be applicable in scenarios where high cortisol levels are present, such as in patients with stress disorders or PTSD. However, even this application is questionable, as the LOD in tests using human sweat, even without skin contact, is close to 1.2µM.

Given these various issues, the concept of a wristwatch design for detecting cortisol in sweat is not viable as a wearable biosensor.

6.4.2 Future suggestions for the biosensor development

The PVDF-Au electrode, modified with MB and the concaptamer, successfully detected high concentrations of cortisol. However, subsequent modifications necessitate further testing across a broader range of cortisol concentrations, especially those closer to physiological levels, tailored to specific patient conditions. It is critical for the biosensor to effectively differentiate between lower cortisol concentrations, thereby demonstrating high resolution at these levels. The cortisol solutions used for testing should be representative of this requirement. For a more realistic assessment, the medium used in the testing and optimization phases should ideally be pooled human sweat to simulate complex real-world scenarios better.

The sensitivity of MB to pH necessitates the use of alternative redox reporters or, their complete removal if possible. When designing the biosensor, it's important to consider the concentration of sweat glands in various body parts, ensuring that the biosensor's sweat requirements align with the amount produced in the targeted area, as well as the cortisol levels present there.

Incorporating a microfluidic system could enhance the biosensor's performance by facilitating the collection of larger liquid volumes. This approach also prevents direct contact between the biosensor and skin, allowing for the addition of electrolyte solutions through alternate channels or pre-treatment of the sweat to simplify the biosensing process. For instance, adjusting the pH of the sweat could reduce MB degradation, or providing a binding buffer could help maintain the bioreceptor's optimal 3D structure while on standby.

Additionally, employing an anti-fouling layer on the working electrode could repel other biological entities that might obstruct the electrode surface, further improving the biosensor's efficacy.

The optimization of incubation time, relevant to earlier phases of the study, should be extended, as other studies typically employ at least two hours for sample incubation. A longer incubation period could enhance cortisol diffusion and provide more time for effective bonding with concaptamers, potentially improving the signal-to-blank ratio.

In light of the data from the reusability tests, it appears that the biosensor can detect cortisol effectively up to three times under ideal conditions. However, this finding also needs to be verified in pooled sweat to confirm the biosensor's efficacy in more realistic scenarios.

For regeneration, alternative techniques involving chemical agents such as SDS or IPA washing could be employed. In the context of concaptamers, UV light has been known to induce DNA lesions, resulting in structural changes that may alter the concaptamer's binding affinity to its target molecule. However, if the use of UV for regeneration remains a consideration, an approach involving the integration of photoresponsive azobenzene moieties into the DNA chain of the concaptamer could be explored. Exposure to UV light would cause the azobenzene moiety to alternate between trans and cis conformations, inducing a conformational change in the concaptamer that could potentially dissociate it from its target molecule [50].

References

1. Janghorban, M.; Aradanas, I.; Kazemi, S.; Ngaju, P.; Pandey, R. Recent Advances, Opportunities, and Challenges in Developing Nucleic Acid Integrated Wearable Biosensors for Expanding the Capabilities of Wearable Technologies in Health Monitoring. *Biosensors* **2022**, *12*, 986, doi:10.3390/bios12110986.
2. Wood, C.S.; Thomas, M.R.; Budd, J.; Mashamba-Thompson, T.P.; Herbst, K.; Pillay, D.; Peeling, R.W.; Johnson, A.M.; McKendry, R.A.; Stevens, M.M. Taking Connected Mobile-Health Diagnostics of Infectious Diseases to the Field. *Nature* **2019**, *566*, 467–474, doi:10.1038/s41586-019-0956-2.
3. Jeong, J.-W.; Yeo, W.-H.; Akhtar, A.; Norton, J.J.S.; Kwack, Y.-J.; Li, S.; Jung, S.-Y.; Su, Y.; Lee, W.; Xia, J.; et al. Materials and Optimized Designs for Human-Machine Interfaces Via Epidermal Electronics. *Adv. Mater.* **2013**, *25*, 6839–6846, doi:10.1002/adma.201301921.
4. Pusta, A.; Tertiș, M.; Cristea, C.; Mirel, S. Wearable Sensors for the Detection of Biomarkers for Wound Infection. *Biosensors* **2021**, *12*, 1, doi:10.3390/bios12010001.
5. Davies, E.H.; Johnston, J.; Toro, C.; Tifft, C.J. A Feasibility Study of mHealth and Wearable Technology in Late Onset GM2 Gangliosidosis (Tay-Sachs and Sandhoff Disease). *Orphanet Journal of Rare Diseases* **2020**, *15*, 199, doi:10.1186/s13023-020-01473-x.
6. Cappon, G.; Acciaroli, G.; Vettoretti, M.; Facchinetti, A.; Sparacino, G. Wearable Continuous Glucose Monitoring Sensors: A Revolution in Diabetes Treatment. *Electronics* **2017**, *6*, 65, doi:10.3390/electronics6030065.
7. Wang, B.; Zhao, C.; Wang, Z.; Yang, K.-A.; Cheng, X.; Liu, W.; Yu, W.; Lin, S.; Zhao, Y.; Cheung, K.M.; et al. Wearable Aptamer-Field-Effect Transistor Sensing System for Noninvasive Cortisol Monitoring. *Sci. Adv.* **2022**, *8*, eabk0967, doi:10.1126/sciadv.abk0967.
8. Kim, J.; Sempionatto, J.R.; Imani, S.; Hartel, M.C.; Barfidokht, A.; Tang, G.; Campbell, A.S.; Mercier, P.P.; Wang, J. Simultaneous Monitoring of Sweat and Interstitial Fluid Using a Single Wearable Biosensor Platform. *Advanced science (Weinheim, Baden-Wurttemberg, Germany)* **2018**, *5*, 1800880, doi:10.1002/advs.201800880.
9. Mannoor, M.S.; Tao, H.; Clayton, J.D.; Sengupta, A.; Kaplan, D.L.; Naik, R.R.; Verma, N.; Omenetto, F.G.; McAlpine, M.C. Graphene-Based Wireless Bacteria Detection on Tooth Enamel. *Nature Communications* **2012**, *3*, doi:10.1038/ncomms1767.
10. Yao, H.; Shum, A.J.; Cowan, M.; Lähdesmäki, I.; Parviz, B.A. A Contact Lens with Embedded Sensor for Monitoring Tear Glucose Level. *Biosensors and Bioelectronics* **2011**, *26*, 3290–3296, doi:10.1016/j.bios.2010.12.042.
11. Lee, H.; Hong, Y.J.; Baik, S.; Hyeon, T.; Kim, D.-H. Enzyme-Based Glucose Sensor: From Invasive to Wearable Device. *Advanced Healthcare Materials* **2018**, *7*, 1701150, doi:10.1002/adhm.201701150.
12. Sonawane, A.; Manickam, P.; Bhansali, S. Stability of Enzymatic Biosensors for Wearable Applications. *IEEE Reviews in Biomedical Engineering* **2017**, *10*, 174–186, doi:10.1109/RBME.2017.2706661.
13. Li, M.; Yin, F.; Song, L.; Mao, X.; Li, F.; Fan, C.; Zuo, X.; Xia, Q. Nucleic Acid Tests for Clinical Translation. *Chem. Rev.* **2021**, *121*, 10469–10558, doi:10.1021/acs.chemrev.1c00241.

14. Khan, S.; Burciu, B.; Filipe, C.D.M.; Li, Y.; Dellinger, K.; Didar, T.F. DNAzyme-Based Biosensors: Immobilization Strategies, Applications, and Future Prospective. *ACS Nano* **2021**, *15*, 13943–13969, doi:10.1021/acsnano.1c04327.
15. Moore, A.R.; Holland-Winkler, A.M.; Ansley, J.K.; Boone, E.D.H.; Schulte, M.K.O. Reliability and Diagnostic Performance of a New Blood Ketone and Glucose Meter in Humans. *Journal of the International Society of Sports Nutrition* **2021**, *18*, 6, doi:10.1186/s12970-020-00404-2.
16. Bonaventura, J.M.; Sharpe, K.; Knight, E.; Fuller, K.L.; Tanner, R.K.; Gore, C.J. Reliability and Accuracy of Six Hand-Held Blood Lactate Analysers. *J Sports Sci Med* **2015**, *14*, 203–214.
17. Li, S.; Lin, L.; Chang, X.; Si, Z.; Plaxco, K.W.; Khine, M.; Li, H.; Xia, F. A Wrinkled Structure of Gold Film Greatly Improves the Signaling of Electrochemical Aptamer-Based Biosensors. *RSC Adv.* **2021**, *11*, 671–677, doi:10.1039/D0RA09174J.
18. Nimjee, S.M.; Rusconi, C.P.; Sullenger, B.A. Aptamers: An Emerging Class of Therapeutics. *Annu. Rev. Med.* **2005**, *56*, 555–583, doi:10.1146/annurev.med.56.062904.144915.
19. Zheng, H.; GhavamiNejad, A.; GhavamiNejad, P.; Samarikhalaj, M.; Giacca, A.; Poudineh, M. Hydrogel Microneedle-Assisted Assay Integrating Aptamer Probes and Fluorescence Detection for Reagentless Biomarker Quantification. *ACS Sensors* **2022**, doi:10.1021/acssensors.2c01033.
20. Wang, M.; Zhai, S.; Ye, Z.; He, L.; Peng, D.; Feng, X.; Yang, Y.; Fang, S.; Zhang, H.; Zhang, Z. An Electrochemical Aptasensor Based on a TiO_2 /Three-Dimensional Reduced Graphene Oxide/PPy Nanocomposite for the Sensitive Detection of Lysozyme. *Dalton Transactions* **2015**, *44*, 6473–6479, doi:10.1039/C5DT00168D.
21. Wu, P.; Hwang, K.; Lan, T.; Lu, Y. A DNAzyme-Gold Nanoparticle Probe for Uranyl Ion in Living Cells. *Journal of the American Chemical Society* **2013**, *135*, 5254–5257, doi:10.1021/ja400150v.
22. Pali, M.; Jagannath, B.; Lin, K.C.; Upasham, S.; Sankhalab, D.; Upashama, S.; Muthukumar, S.; Prasad, S. CATCH (Cortisol Apta WATCH): 'Bio-Mimic Alarm' to Track Anxiety, Stress, Immunity in Human Sweat. *Electrochimica Acta* **2021**, *390*, doi:10.1016/j.electacta.2021.138834.
23. Ganguly, A.; Lin, K.C.; Muthukumar, S.; Prasad, S. Autonomous, Real-Time Monitoring Electrochemical Aptasensor for Circadian Tracking of Cortisol Hormone in Sub-Microliter Volumes of Passively Eluted Human Sweat. *ACS Sensors* **2021**, *6*, 63–72, doi:10.1021/acssensors.0c01754.
24. Mugo, S.M.; Alberkant, J.; Bernstein, N.; Zenkina, O.V. Flexible Electrochemical Aptasensor for Cortisol Detection in Human Sweat. *Analytical Methods* **2021**, *13*, 4169–4173, doi:10.1039/d1ay01233a.
25. Sadighbayan, D.; Hasanzadeh, M.; Ghafar-Zadeh, E. Biosensing Based on Field-Effect Transistors (FET): Recent Progress and Challenges. *TrAC - Trends in Analytical Chemistry* **2020**, *133*, doi:10.1016/J.TRAC.2020.116067.
26. Gao, J.; Gao, Y.; Han, Y.; Pang, J.; Wang, C.; Wang, Y.; Liu, H.; Zhang, Y.; Han, L. Ultrasensitive Label-Free MiRNA Sensing Based on a Flexible Graphene Field-Effect Transistor without Functionalization. *ACS Applied Electronic Materials* **2020**, *2*, 1090–1098, doi:10.1021/acsaelm.0c00095.
27. An, J.E.; Kim, K.H.; Park, S.J.; Seo, S.E.; Kim, J.; Ha, S.; Bae, J.; Kwon, O.S. Wearable Cortisol Aptasensor for Simple and Rapid Real-Time Monitoring. *ACS Sensors* **2022**, *7*, 99–108, doi:10.1021/acssensors.1c01734.
28. Arroyo-Currás, N.; Scida, K.; Ploense, K.L.; Kippin, T.E.; Plaxco, K.W. High Surface Area Electrodes Generated via Electrochemical Roughening Improve the Signaling of

Electrochemical Aptamer-Based Biosensors. *Anal. Chem.* **2017**, *89*, 12185–12191, doi:10.1021/acs.analchem.7b02830.
29. Hauke, A.; Kumar, L.S.S.; Kim, M.Y.; Pegan, J.; Khine, M.; Li, H.; Plaxco, K.W.; Heikenfeld, J. Superwetting and Aptamer Functionalized Shrink-Induced High Surface Area Electrochemical Sensors. *Biosensors and Bioelectronics* **2017**, *94*, 438–442, doi:10.1016/j.bios.2017.03.024.
30. Saha, S.K.; Soleymani, L. Developing Wrinkled Surface to Achieve Low-Cost Photoelectrochemical Biosensor and Study the Interplay between LSPR of Nanoparticles and Semiconductive Quantum Dots. *Meet. Abstr.* **2018**, *MA2018-01*, 2141–2141, doi:10.1149/MA2018-01/36/2141.
31. Li, W.; Gao, T.; Lou, C.; Wang, H.; Liu, Y.; Cao, A. Biotinylated Au Nanoparticle-Based Artificial Antibody for Detection of Lysozyme by the Lateral Flow Immunoassay and Enzyme-Linked Immunosorbent Assay. *ACS Appl. Nano Mater.* **2022**, *5*, 12571–12581, doi:10.1021/acsanm.2c02268.
32. Lu, M.; Zhu, H.; Bazuin, C.G.; Peng, W.; Masson, J.-F. Polymer-Templated Gold Nanoparticles on Optical Fibers for Enhanced-Sensitivity Localized Surface Plasmon Resonance Biosensors. *ACS Sens.* **2019**, *4*, 613–622, doi:10.1021/acssensors.8b01372.
33. Lu, M.; Zhu, H.; Hong, L.; Zhao, J.; Masson, J.-F.; Peng, W. Wavelength-Tunable Optical Fiber Localized Surface Plasmon Resonance Biosensor *via* a Diblock Copolymer-Templated Nanorod Monolayer. *ACS Appl. Mater. Interfaces* **2020**, *12*, 50929–50940, doi:10.1021/acsami.0c09711.
34. Labuda, J.; Brett, A.M.O.; Evtugyn, G.; Fojta, M.; Mascini, M.; Ozsoz, M.; Palchetti, I.; Paleček, E.; Wang, J. Electrochemical Nucleic Acid-Based Biosensors: Concepts, Terms, and Methodology (IUPAC Technical Report). *Pure and Applied Chemistry* **2010**, *82*, 1161–1187, doi:10.1351/PAC-REP-09-08-16.
35. Demuru, S.; Kim, J.; El Chazli, M.; Bruce, S.; Dupertuis, M.; Binz, P.-A.; Saubade, M.; Lafaye, C.; Briand, D. Antibody-Coated Wearable Organic Electrochemical Transistors for Cortisol Detection in Human Sweat. *ACS Sens.* **2022**, *7*, 2721–2731, doi:10.1021/acssensors.2c01250.
36. Morales, M.A.; Halpern, J.M. Guide to Selecting a Biorecognition Element for Biosensors. *Bioconjugate Chemistry* **2018**, *29*, 3231–3239, doi:10.1021/acs.bioconjchem.8b00592.
37. Bradbury, A.R.M.; Trinklein, N.D.; Thie, H.; Wilkinson, I.C.; Tandon, A.K.; Anderson, S.; Bladen, C.L.; Jones, B.; Aldred, S.F.; Bestagno, M.; et al. When Monoclonal Antibodies Are Not Monospecific: Hybridomas Frequently Express Additional Functional Variable Regions. *mAbs* **2018**, *10*, 539–546, doi:10.1080/19420862.2018.1445456.
38. *Enzyme Biocatalysis Principles and Applications*; Illanes, A., Ed.; Springer, 2008;
39. KVASSMAN, J.; PETTERSSON, G. Effect of pH on Coenzyme Binding to Liver Alcohol Dehydrogenase. *European Journal of Biochemistry* **1979**, *100*, 115–123, doi:10.1111/j.1432-1033.1979.tb02039.x.
40. Sato, K.; Kang, W.H.; Saga, K.; Sato, K.T. Biology of Sweat Glands and Their Disorders. I. Normal Sweat Gland Function. *Journal of the American Academy of Dermatology* **1989**, *20*, 537–563, doi:10.1016/S0190-9622(89)70063-3.
41. Wang, L.; Sun, Y. Engineering Organophosphate Hydrolase for Enhanced Biocatalytic Performance: A Review. *Biochemical Engineering Journal* **2021**, *168*, 107945, doi:10.1016/j.bej.2021.107945.
42. Yoo, E.-H.; Lee, S.-Y. Glucose Biosensors: An Overview of Use in Clinical Practice. *Sensors* **2010**, *10*, 4558–4576, doi:10.3390/s100504558.

43. Kim, J.; Campbell, A.S.; Ávila, B.E.-F. de; Wang, J. Wearable Biosensors for Healthcare Monitoring. *Nature biotechnology* **2019**, *37*, 389–406, doi:10.1038/s41587-019-0045-y.
44. Wang, F.; Li, P.; Chu, H.C.; Lo, P.K. Nucleic Acids and Their Analogues for Biomedical Applications. *Biosensors* **2022**, *12*, 93, doi:10.3390/bios12020093.
45. Bora, U. Nucleic Acid Based Biosensors for Clinical Applications. *Biosensors Journal* **2013**, *02*, doi:10.4172/2090-4967.1000104.
46. Khorana, H.G. Nucleic Acid Synthesis. *Pure and Applied Chemistry* **1968**, *17*, 349–382, doi:10.1351/pac196817030349.
47. Yang, Y.; Yang, D.; Schluesener, H.J.; Zhang, Z. Advances in SELEX and Application of Aptamers in the Central Nervous System. *Biomolecular Engineering* **2007**, *24*, 583–592, doi:10.1016/j.bioeng.2007.06.003.
48. Wang, Z.; Hao, Z.; Yu, S.; Huang, C.; Pan, Y.; Zhao, X. A Wearable and Deformable Graphene-Based Affinity Nanosensor for Monitoring of Cytokines in Biofluids. *Nanomaterials* **2020**, *10*, 1–9, doi:10.3390/nano10081503.
49. Hao, Z.; Wang, Z.; Li, Y.; Zhu, Y.; Wang, X.; Moraes, C.G.D.; Pan, Y.; Zhao, X.; Lin, Q. Measurement of Cytokine Biomarkers Using an Aptamer-Based Affinity Graphene Nanosensor on a Flexible Substrate toward Wearable Applications. *Nanoscale* **2018**, *10*, 21681–21688, doi:10.1039/c8nr04315a.
50. Zhang, X.; Song, C.; Yang, K.; Hong, W.; Lu, Y.; Yu, P.; Mao, L. Photoinduced Regeneration of an Aptamer-Based Electrochemical Sensor for Sensitively Detecting Adenosine Triphosphate. *Anal. Chem.* **2018**, *90*, 4968–4971, doi:10.1021/acs.analchem.7b05442.
51. Hasegawa, H.; Taira, K.; Sode, K.; Ikebukuro, K. Improvement of Aptamer Affinity by Dimerization. *Sensors* **2008**, *8*, 1090–1098, doi:10.3390/s8021090.
52. Liu, Q.; Zhao, C.; Chen, M.; Liu, Y.; Zhao, Z.; Wu, F.; Li, Z.; Weiss, P.S.; Andrews, A.M.; Zhou, C. Flexible Multiplexed In2O3 Nanoribbon Aptamer-Field-Effect Transistors for Biosensing. *iScience* **2020**, *23*, doi:10.1016/j.isci.2020.101469.
53. Wang, Z.; Hao, Z.; Wang, X.; Huang, C.; Lin, Q.; Zhao, X.; Pan, Y. A Flexible and Regenerative Aptameric Graphene–Nafion Biosensor for Cytokine Storm Biomarker Monitoring in Undiluted Biofluids toward Wearable Applications. *Advanced Functional Materials* **2021**, *31*, doi:10.1002/adfm.202005958.
54. Wang, B.; Zhao, C.; Wang, Z.; Yang, K.-A.; Cheng, X.; Liu, W.; Yu, W.; Lin, S.; Zhao, Y.; Cheung, K.M.; et al. *A P P L I E D S C I E N C E S A N D E N G I N E E R I N G Wearable Aptamer-Field-Effect Transistor Sensing System for Noninvasive Cortisol Monitoring*; 2022; Vol. 8, p. 967;.
55. Zea, M.; Bellagambi, F.G.; Halima, H.B.; Zine, N.; Jaffrezic-Renault, N.; Villa, R.; Gabriel, G.; Errachid, A. Electrochemical Sensors for Cortisol Detections: Almost There. *TrAC Trends in Analytical Chemistry* **2020**, *132*, 116058, doi:10.1016/j.trac.2020.116058.
56. Singh, N.K.; Chung, S.; Sveiven, M.; Hall, D.A. Cortisol Detection in Undiluted Human Serum Using a Sensitive Electrochemical Structure-Switching Aptamer over an Antifouling Nanocomposite Layer. *ACS Omega* **2021**, *6*, 27888–27897, doi:10.1021/acsomega.1c03552.
57. Pandey, R.; Chang, D.; Smieja, M.; Hoare, T.; Li, Y.; Soleymani, L. Integrating Programmable DNAzymes with Electrical Readout for Rapid and Culture-Free Bacterial Detection Using a Handheld Platform. *Nature Chemistry* **2021**, *13*, 895–901, doi:10.1038/s41557-021-00718-x.

58. Müller, S.; Strohbach, D.; Wolf, J. Sensors Made of RNA: Tailored Ribozymes for Detection of Small Organic Molecules, Metals, Nucleic Acids and Proteins. *IEE Proceedings - Nanobiotechnology* **2006**, *153*, 31, doi:10.1049/ip-nbt:20050047.
59. Yao, C.; Zhu, T.; Qi, Y.; Zhao, Y.; Xia, H.; Fu, W. Development of a Quartz Crystal Microbalance Biosensor with Aptamers as Bio-Recognition Element. *Sensors* **2010**, *10*, 5859–5871, doi:10.3390/s100605859.
60. Gao, Y.; Nguyen, D.T.; Yeo, T.; Lim, S.B.; Tan, W.X.; Madden, L.E.; Jin, L.; Long, J.Y.K.; Aloweni, F.A.B.; Liew, Y.J.A.; et al. *A Flexible Multiplexed Immunosensor for Point-of-Care in Situ Wound Monitoring*; 2021; Vol. 7;.
61. Vorobyeva, M.; Vorobjev, P.; Venyaminova, A. Multivalent Aptamers: Versatile Tools for Diagnostic and Therapeutic Applications. *Molecules* **2016**, *21*, 1613, doi:10.3390/molecules21121613.
62. Stojanovic, M.N.; Kolpashchikov, D.M. Modular Aptameric Sensors. *J. Am. Chem. Soc.* **2004**, *126*, 9266–9270, doi:10.1021/ja032013t.
63. Schoukroun-Barnes, L.R.; Macazo, F.C.; Gutierrez, B.; Lottermoser, J.; Liu, J.; White, R.J. Reagentless, Structure-Switching, Electrochemical Aptamer-Based Sensors. *Annual Rev. Anal. Chem.* **2016**, *9*, 163–181, doi:10.1146/annurev-anchem-071015-041446.
64. Yang, B.; Kong, J.; Fang, X. Bandage-like Wearable Flexible Microfluidic Recombinase Polymerase Amplification Sensor for the Rapid Visual Detection of Nucleic Acids. *Talanta* **2019**, *204*, 685–692, doi:10.1016/j.talanta.2019.06.031.
65. Damborský, P.; Švitel, J.; Katrlík, J. Optical Biosensors. *Essays in Biochemistry* **2016**, *60*, 91–100, doi:10.1042/EBC20150010.
66. Sadighbayan, D.; Hasanzadeh, M.; Ghafar-Zadeh, E. Biosensing Based on Field-Effect Transistors (FET): Recent Progress and Challenges. *TrAC Trends in Analytical Chemistry* **2020**, *133*, 116067, doi:10.1016/j.trac.2020.116067.
67. Pali, M.; Jagannath, B.; Lin, K.-C.; Upasham, S.; Sankhalab, D.; Upashama, S.; Muthukumar, S.; Prasad, S. CATCH (Cortisol Apta WATCH): 'Bio-Mimic Alarm' to Track Anxiety, Stress, Immunity in Human Sweat. *Electrochimica Acta* **2021**, *390*, 138834, doi:10.1016/j.electacta.2021.138834.
68. Wu, Y.; Ghoraani, B. Biological Signal Processing and Analysis for Healthcare Monitoring. *Sensors (Basel, Switzerland)* **2022**, *22*, doi:10.3390/s22145341.
69. Nguyen, P.Q.; Soenksen, L.R.; Donghia, N.M.; Angenent-Mari, N.M.; de Puig, H.; Huang, A.; Lee, R.; Slomovic, S.; Galbersanini, T.; Lansberry, G.; et al. Wearable Materials with Embedded Synthetic Biology Sensors for Biomolecule Detection. *Nat Biotechnol* **2021**, *39*, 1366–1374, doi:10.1038/s41587-021-00950-3.
70. Yang, B.; Kong, J.; Fang, X. Bandage-like Wearable Flexible Microfluidic Recombinase Polymerase Amplification Sensor for the Rapid Visual Detection of Nucleic Acids. *Talanta* **2019**, *204*, 685–692, doi:10.1016/j.talanta.2019.06.031.
71. Kong, M.; Li, Z.; Wu, J.; Hu, J.; Sheng, Y.; Wu, D.; Lin, Y.; Li, M.; Wang, X.; Wang, S. A Wearable Microfluidic Device for Rapid Detection of HIV-1 DNA Using Recombinase Polymerase Amplification. *Talanta* **2019**, *205*, 120155, doi:10.1016/j.talanta.2019.120155.
72. Hao, Z.; Wang, Z.; Li, Y.; Zhu, Y.; Wang, X.; De Moraes, C.G.; Pan, Y.; Zhao, X.; Lin, Q. Measurement of Cytokine Biomarkers Using an Aptamer-Based Affinity Graphene Nanosensor on a Flexible Substrate toward Wearable Applications. *Nanoscale* **2018**, *10*, 21681–21688, doi:10.1039/C8NR04315A.
73. Sedki, M.; Shen, Y.; Mulchandani, A. *Nano-FET-Enabled Biosensors: Materials Perspective and Recent Advances in North America*; 2020;

74. Nakatsuka, N.; Yang, K.-A.; Abendroth, J.M.; Cheung, K.M.; Xu, X.; Yang, H.; Zhao, C.; Zhu, B.; Rim, Y.S.; Yang, Y.; et al. *Aptamer-Field-Effect Transistors Overcome Debye Length Limitations for Small-Molecule Sensing*;
75. Zhang, A.; Lieber, C.M. Nano-Bioelectronics. *Chem. Rev.* **2016**, *116*, 215–257, doi:10.1021/acs.chemrev.5b00608.
76. Sheibani, S.; Capua, L.; Kamaei, S.; Akbari, S.S.A.; Zhang, J.; Guerin, H.; Ionescu, A.M. Extended Gate Field-Effect-Transistor for Sensing Cortisol Stress Hormone. *Communications Materials* **2021**, *2*, doi:10.1038/s43246-020-00114-x.
77. Rafat, N.; Satoh, P.; Worden, R.M. Electrochemical Biosensor for Markers of Neurological Esterase Inhibition. *Biosensors* **2021**, *11*, doi:10.3390/bios11110459.
78. Mamun, M.A.; Wahab, Y.A.; Hossain, M.A.M.; Hashem, A.; Johan, M.R. Electrochemical Biosensors with Aptamer Recognition Layer for the Diagnosis of Pathogenic Bacteria: Barriers to Commercialization and Remediation. *TrAC Trends in Analytical Chemistry* **2021**, *145*, 116458, doi:10.1016/j.trac.2021.116458.
79. Elgrishi, N.; Rountree, K.J.; McCarthy, B.D.; Rountree, E.S.; Eisenhart, T.T.; Dempsey, J.L. A Practical Beginner's Guide to Cyclic Voltammetry. *J. Chem. Educ.* **2018**, *95*, 197–206, doi:10.1021/acs.jchemed.7b00361.
80. Bagotskiĭ, V.S. *Fundamentals of Electrochemistry*; 2nd ed.; Wiley-Interscience: Hoboken, N.J., 2006; ISBN 978-0-471-74198-5.
81. Chen, A.; Shah, B. Electrochemical Sensing and Biosensing Based on Square Wave Voltammetry. *Anal. Methods* **2013**, *5*, 2158, doi:10.1039/c3ay40155c.
82. Liao, W.-C.; Ho, J.A. Attomole DNA Electrochemical Sensor for the Detection of *Escherichia Coli* O157. *Anal. Chem.* **2009**, *81*, 2470–2476, doi:10.1021/ac8020517.
83. Lee, J.; Suh, H.N.; Park, H.; Park, Y.M.; Kim, H.J.; Kim, S. Regenerative Strategy of Gold Electrodes for Long-Term Reuse of Electrochemical Biosensors. *ACS Omega* **2023**, *8*, 1389–1400, doi:10.1021/acsomega.2c06851.
84. Zamani, M.; Klapperich, C.M.; Furst, A.L. Recent Advances in Gold Electrode Fabrication for Low-Resource Setting Biosensing. *Lab Chip* **2023**, *23*, 1410–1419, doi:10.1039/D2LC00552B.
85. Gabardo, C.M.; Hosseini, A.; Soleymani, L. A New Wrinkle in Biosensors: Wrinkled Electrodes Could Be a Breakthrough for Lab-on-a-Chip Devices. *IEEE Nanotechnology Mag.* **2016**, *10*, 6–18, doi:10.1109/MNANO.2016.2539999.
86. Tan, Y.; Hu, B.; Song, J.; Chu, Z.; Wu, W. Bioinspired Multiscale Wrinkling Patterns on Curved Substrates: An Overview. *Nano-Micro Lett.* **2020**, *12*, 101, doi:10.1007/s40820-020-00436-y.
87. Schweikart, A.; Horn, A.; Böker, A.; Fery, A. Controlled Wrinkling as a Novel Method for the Fabrication of Patterned Surfaces. In *Complex Macromolecular Systems I*; Müller, A.H.E., Schmidt, H.-W., Eds.; Advances in Polymer Science; Springer Berlin Heidelberg: Berlin, Heidelberg, 2009; Vol. 227, pp. 75–99 ISBN 978-3-642-12875-2.
88. Lanzalaco, S.; Molina, B.G. Polymers and Plastics Modified Electrodes for Biosensors: A Review. *Molecules* **2020**, *25*, 2446, doi:10.3390/molecules25102446.
89. Zhang, Y.; Yao, Y.; Guang, Z.; Xue, J.; Wang, Q.; Gong, J.; Ali, Z.; Yang, Z. A High-Sensitivity Fiber Biosensor Based on PVDF-Excited Surface Plasmon Resonance in the Terahertz Band. *Photonics* **2023**, *10*, 1159, doi:10.3390/photonics10101159.
90. Kamel, N.A. Bio-Piezoelectricity: Fundamentals and Applications in Tissue Engineering and Regenerative Medicine. *Biophys Rev* **2022**, *14*, 717–733, doi:10.1007/s12551-022-00969-z.
91. Fakhr, M.H.; Beshchasna, N.; Balakin, S.; Carrasco, I.L.; Heitbrink, A.; Göhler, F.; Rösch, N.; Opitz, J. Cleaning of LTCC, PEN, and PCB Au Electrodes towards

Reliable Electrochemical Measurements. *Sci Rep* **2022**, *12*, 20431, doi:10.1038/s41598-022-23395-3.
92. Kerman, K.; Saito, M.; Tamiya, E.; Yamamura, S.; Takamura, Y. Nanomaterial-Based Electrochemical Biosensors for Medical Applications. *TrAC Trends in Analytical Chemistry* **2008**, *27*, 585–592, doi:10.1016/j.trac.2008.05.004.
93. Wang, J. Electrochemical Biosensors: Towards Point-of-Care Cancer Diagnostics. *Biosensors and Bioelectronics* **2006**, *21*, 1887–1892, doi:10.1016/j.bios.2005.10.027.
94. Beer, F.P. *Mechanics of Materials*; Seventh edition.; McGraw-Hill Education: New York, NY, 2015; ISBN 978-0-07-339823-5.
95. Ren, B.; Cho, H.; Lissenden, C. A Guided Wave Sensor Enabling Simultaneous Wavenumber-Frequency Analysis for Both Lamb and Shear-Horizontal Waves. *Sensors* **2017**, *17*, 488, doi:10.3390/s17030488.
96. Rose, T.K.; Merloc, W.T. *The Metallurgy of Gold: With Application to Mining and Mineral Processing*; 6th ed. / rev. by William Thomas Merloc.; Wexford Press: LaVergne, Tenn., 2008; ISBN 978-1-934939-24-6.
97. Tsukahara, K. The Relationship Between Wrinkle Depth and Dermal Thickness in the Forehead and Lateral Canthal Region. *Arch Dermatol* **2011**, *147*, 822, doi:10.1001/archdermatol.2011.158.
98. Yang, Z.; Cheng, D.; Su, B.; Ji, C.; Huang, J.; Li, H.; Zhang, K. Study on the Optimization of Temperature Uniformity in the Oven under the Forced Convection Mode. *Sci Rep* **2023**, *13*, 12486, doi:10.1038/s41598-023-39317-w.
99. Columb, M.; Atkinson, M. Statistical Analysis: Sample Size and Power Estimations. *BJA Education* **2016**, *16*, 159–161, doi:10.1093/bjaed/mkv034.
100. Mackintosh, S.A.; Rodgers, J.I.; Blythe, S.P. Modeling an Enzyme Based Electrochemical Blood Glucose Sensor.
101. Chen, Y.; Liao, X.; Zhao, W.; Yang, P.; Xiao, H.; Liu, Y.; Chen, X. Post-Wrinkling Behaviors of a Bilayer on a Soft Substrate. *International Journal of Solids and Structures* **2021**, *214–215*, 74–79, doi:10.1016/j.ijsolstr.2021.01.002.
102. Bharathi, S.J.; Thilagar, S.H.; Jayasurya, V. Design and Modeling of Electrochemical Sensor for Determining ION Concentration. In Proceedings of the 2019 IEEE 1st International Conference on Energy, Systems and Information Processing (ICESIP); IEEE: Chennai, India, July 2019; pp. 1–5.
103. Li, L.-D.; Zhao, H.-T.; Chen, Z.-B.; Mu, X.-J.; Guo, L. Aptamer Biosensor for Label-Free Impedance Spectroscopy Detection of Thrombin Based on Gold Nanoparticles. *Sensors and Actuators B: Chemical* **2011**, *157*, 189–194, doi:10.1016/j.snb.2011.03.048.
104. Huang, Y.; Zhang, Y.-L.; Xu, X.; Jiang, J.-H.; Shen, G.-L.; Yu, R.-Q. Highly Specific and Sensitive Electrochemical Genotyping via Gap Ligation Reaction and Surface Hybridization Detection. *J. Am. Chem. Soc.* **2009**, *131*, 2478–2480, doi:10.1021/ja808700d.
105. Sharma, V.; Sharma, T.K.; Kaur, I. Electrochemical Detection of Cortisol on Graphene Quantum Dots Modified Electrodes Using a Rationally Truncated High Affinity Aptamer. *Appl Nanosci* **2021**, *11*, 2577–2588, doi:10.1007/s13204-021-02086-x.
106. Durst, R.A.; Staples, B.R. Tris/Tris·HCl: A Standard Buffer for Use in the Physiologic pH Range. *Clinical Chemistry* **1972**, *18*, 206–208, doi:10.1093/clinchem/18.3.206.
107. Omidinia, E.; Shadjou, N.; Hasanzadeh, M. Aptamer-Based Biosensor for Detection of Phenylalanine at Physiological pH. *Appl Biochem Biotechnol* **2014**, *172*, 2070–2080, doi:10.1007/s12010-013-0656-6.
108. Vu; Chen Field-Effect Transistor Biosensors for Biomedical Applications: Recent Advances and Future Prospects. *Sensors* **2019**, *19*, 4214, doi:10.3390/s19194214.

109. Yang, K.A.; Chun, H.; Zhang, Y.; Pecic, S.; Nakatsuka, N.; Andrews, A.M.; Worgall, T.S.; Stojanovic, M.N. High-Affinity Nucleic-Acid-Based Receptors for Steroids. *ACS Chemical Biology* **2017**, *12*, 3103–3112, doi:10.1021/acschembio.7b00634.
110. Zhang, Q.; Jiang, D.; Xu, C.; Ge, Y.; Liu, X.; Wei, Q.; Huang, L.; Ren, X.; Wang, C.; Wang, Y. Wearable Electrochemical Biosensor Based on Molecularly Imprinted Ag Nanowires for Noninvasive Monitoring Lactate in Human Sweat. *Sensors and Actuators, B: Chemical* **2020**, *320*, doi:10.1016/j.snb.2020.128325.
111. Wang, M.; Zhang, S.; Ye, Z.; Peng, D.; He, L.; Yan, F.; Yang, Y.; Zhang, H.; Zhang, Z. A Gold Electrode Modified with Amino-Modified Reduced Graphene Oxide, Ion Specific DNA and DNAzyme for Dual Electrochemical Determination of Pb(II) and Hg(II). *Microchimica Acta* **2015**, *182*, 2251–2258, doi:10.1007/s00604-015-1569-6.
112. Baker, L.B. Physiology of Sweat Gland Function: The Roles of Sweating and Sweat Composition in Human Health. *Temperature* **2019**, *6*, 211–259, doi:10.1080/23328940.2019.1632145.
113. Scott, S.M.; Watterberg, K.L. Effect of Gestational Age, Postnatal Age, and Illness on Plasma Cortisol Concentrations in Premature Infants. *Pediatr Res* **1995**, *37*, 112–116, doi:10.1203/00006450-199501000-00021.
114. Di Dalmazi, G.; Fanelli, F.; Zavatta, G.; Ricci Bitti, S.; Mezzullo, M.; Repaci, A.; Pelusi, C.; Gambineri, A.; Altieri, P.; Mosconi, C.; et al. The Steroid Profile of Adrenal Incidentalomas: Subtyping Subjects With High Cardiovascular Risk. *The Journal of Clinical Endocrinology & Metabolism* **2019**, *104*, 5519–5528, doi:10.1210/jc.2019-00365.
115. Liu, Q.; Liu, Y.; Wu, F.; Cao, X.; Li, Z.; Alharbi, M.; Abbas, A.N.; Amer, M.R.; Zhou, C. Highly Sensitive and Wearable In $_2$ O $_3$ Nanoribbon Transistor Biosensors with Integrated On-Chip Gate for Glucose Monitoring in Body Fluids. *ACS Nano* **2018**, *12*, 1170–1178, doi:10.1021/acsnano.7b06823.
116. Wang, Q.; Wang, J.; Huang, Y.; Du, Y.; Zhang, Y.; Cui, Y.; Kong, D. Development of the DNA-Based Biosensors for High Performance in Detection of Molecular Biomarkers: More Rapid, Sensitive, and Universal. *Biosensors and Bioelectronics* **2022**, *197*, 113739, doi:10.1016/j.bios.2021.113739.
117. Nguyen, P.Q.; Soenksen, L.R.; Donghia, N.M.; Angenent-Mari, N.M.; Puig, H. de; Huang, A.; Lee, R.; Slomovic, S.; Galbersanini, T.; Lansberry, G.; et al. Wearable Materials with Embedded Synthetic Biology Sensors for Biomolecule Detection. *Nature Biotechnology* **2021**, *39*, 1366–1374, doi:10.1038/s41587-021-00950-3.
118. Steel, A.B.; Herne, T.M.; Tarlov, M.J. Electrochemical Quantitation of DNA Immobilized on Gold. *Anal. Chem.* **1998**, *70*, 4670–4677, doi:10.1021/ac980037q.
119. Shaver, A.; Arroyo-Currás, N. The Challenge of Long-Term Stability for Nucleic Acid-Based Electrochemical Sensors. *Current Opinion in Electrochemistry* **2022**, *32*, 100902, doi:10.1016/j.coelec.2021.100902.
120. Radi, A.-E.; Abd-Ellatief, M.R. Electrochemical Aptasensors: Current Status and Future Perspectives. *Diagnostics* **2021**, *11*, 104, doi:10.3390/diagnostics11010104.
121. Contreras Jiménez, G.; Eissa, S.; Ng, A.; Alhadrami, H.; Zourob, M.; Siaj, M. Aptamer-Based Label-Free Impedimetric Biosensor for Detection of Progesterone. *Anal. Chem.* **2015**, *87*, 1075–1082, doi:10.1021/ac503639s.
122. Kypr, J.; Kejnovska, I.; Renciuk, D.; Vorlickova, M. Circular Dichroism and Conformational Polymorphism of DNA. *Nucleic Acids Research* **2009**, *37*, 1713–1725, doi:10.1093/nar/gkp026.
123. Chang, D.; Zakaria, S.; Sahar, +; Samani, E.; Chang, Y.; Filipe, C.D.M.; Soleymani, L.; Brennan, J.D.; Liu, M.; Li, Y. Functional Nucleic Acids for Pathogenic Bacteria Detection. *Acc. Chem. Res* **2021**, *54*, 3540–3549, doi:10.1038/s41557-021.

124. Steel, A.B.; Herne, T.M.; Tarlov, M.J. Electrochemical Quantitation of DNA Immobilized on Gold. *Anal. Chem.* **1998**, *70*, 4670–4677, doi:10.1021/ac980037q.
125. Shrivastava, A.; Gupta, V. Methods for the Determination of Limit of Detection and Limit of Quantitation of the Analytical Methods. *Chron Young Sci* **2011**, *2*, 21, doi:10.4103/2229-5186.79345.
126. *Harper's Illustrated Biochemistry*; 31st ed.; Lange medical book McGraw Hill education: New York, 2018; ISBN 978-1-259-83793-7.
127. Sun, L.; Shen, K.; Zhang, J.; Wan, W.; Cao, W.; Wang, Z.; Guo, C. Aptamer Based Surface Plasma Resonance Assay for Direct Detection of Neuron Specific Enolase and Progastrin-Releasing Peptide (31-98). *RSC Adv.* **2021**, *11*, 32135–32142, doi:10.1039/D1RA05041A.
128. Goodsell, D.S. The Molecular Perspective: Ultraviolet Light and Pyrimidine Dimers. *The Oncologist* **2001**, *6*, 298–299, doi:10.1634/theoncologist.6-3-298.
129. Takaloo, S.; Zand, M.M. Wearable Electrochemical Flexible Biosensors: With the Focus on Affinity Biosensors. *Sensing and Bio-Sensing Research* **2021**, *32*, 100403, doi:10.1016/j.sbsr.2021.100403.
130. Kalita, N.; Gogoi, S.; Minteer, S.D.; Goswami, P. Advances in Bioelectrode Design for Developing Electrochemical Biosensors. *ACS Meas. Sci. Au* **2023**, acsmeasuresciau.3c00034, doi:10.1021/acsmeasuresciau.3c00034.
131. Liu, J.; Xu, N.; Men, H.; Li, S.; Lu, Y.; Low, S.S.; Li, X.; Zhu, L.; Cheng, C.; Xu, G.; et al. Salivary Cortisol Determination on Smartphone-Based Differential Pulse Voltammetry System. *Sensors* **2020**, *20*, 1422, doi:10.3390/s20051422.
132. Kim, K.S.; Lim, S.R.; Kim, S.-E.; Lee, J.Y.; Chung, C.-H.; Choe, W.-S.; Yoo, P.J. Highly Sensitive and Selective Electrochemical Cortisol Sensor Using Bifunctional Protein Interlayer-Modified Graphene Electrodes. *Sensors and Actuators B: Chemical* **2017**, *242*, 1121–1128, doi:10.1016/j.snb.2016.09.135.
133. Yamaguchi, M.; Yoshikawa, S.; Tahara, Y.; Niwa, D.; Imai, Y.; Shetty, V. Point-of-Use Measurement of Salivary Cortisol Levels. In Proceedings of the 2009 IEEE Sensors; IEEE: Christchurch, New Zealand, October 2009; pp. 343–346.
134. Vabbina, P.K.; Kaushik, A.; Pokhrel, N.; Bhansali, S.; Pala, N. Electrochemical Cortisol Immunosensors Based on Sonochemically Synthesized Zinc Oxide 1D Nanorods and 2D Nanoflakes. *Biosensors and Bioelectronics* **2015**, *63*, 124–130, doi:10.1016/j.bios.2014.07.026.
135. Ye, C.; Wang, M.; Min, J.; Tay, R.Y.; Lukas, H.; Sempionatto, J.R.; Li, J.; Xu, C.; Gao, W. A Wearable Aptamer Nanobiosensor for Non-Invasive Female Hormone Monitoring. *Nat. Nanotechnol.* **2023**, doi:10.1038/s41565-023-01513-0.
136. Bariya, M.; Li, L.; Ghattamaneni, R.; Ahn, C.H.; Nyein, H.Y.Y.; Tai, L.-C.; Javey, A. Glove-Based Sensors for Multimodal Monitoring of Natural Sweat. *Sci. Adv.* **2020**, *6*, eabb8308, doi:10.1126/sciadv.abb8308.
137. Bariya, M.; Nyein, H.Y.Y.; Javey, A. Wearable Sweat Sensors. *Nature Electronics* **2018**, *1*, 160–171, doi:10.1038/s41928-018-0043-y.